TWDB Report

Developing a Multi-model Simulation System for Estimation and Prediction of Freshwater Inflow to Matagorda Bay

By Yu Zhang, Ph. D
Md. Arifur Rahman
Mohammadvaghef Ghazvinian
DongJun Seo, Ph. D
University of Texas at Arlington

DRAFT Final Report: Developing a Multi-model Simulation System for Estimation and Prediction of Freshwater Inflow to Matagorda Bay

TWDB Contract Number 1800012276

This page is intentionally blank.

Table of Contents

List of Tables

List of Figures

List of Acronyms

ASOS	Automated Surface Observing Systems
AWS	Amazon Web Service
CRP	Corpus Christi Radar
COOP	Cooperative Observer
DPA	Digital Precipitation Array
EDNT2	Lavaca River at Edna
ET	Evapotranspiration
GHCN	Global Historical Climate Network
HGX	Houston-Galveston Radar
HL-RDHM	Hydrology Lab- Research Distributed Hydrologic Model
HRAP	Hydrologic Rainfall Analysis Project
HTST2	Navidad River above Hallettsville
MAP	Mean Areal Precipitation
MAP-G	Mean Areal Precipitation based on gauge obervations
MAP-X	Mean Areal Precipitation based on radar or multisensor products
MMIPS	Multimodel Inflow Prediction System
MPE	Multisensor Precipitation Estimates
MTPT2	Tres Palacios River near Midfield
NCEP	National Centers for Environmental Predictions
NGCT2	Garcitas Creek near Inez
NEXRAD	Next Generation Weather Radar
NHD-Plus	National Hydrographic Database-Plus
NLCD	National Land Cover Database
NLDAS	North American Land Data Assimilation System

NWM	National Water Model
NWS	National Weather Service
OWP	Office of Water Prediction (NWS)
PB	Percentage Bias
PLPT2	Placedo Creek near Placedo
PPS	Precipitation Processing System
RFC	River Forecast Center
RMSE	Root-mean squared error
SAC-SMA	Sacramento Soil Moisture Accounting
SCS	Soil Conservation Service
SHEF	Standard Hydrologic Exchange Format
SMA	Soil Moisture Accounting
SSURGO	Soil Survey Geographic Database
TWDB	Texas Water Development Board
TxRR	Texas Rainfall Runoff Model
USACE	US Army Corps of Engineers
USGS	US Geological Survey
UTA	University of Texas at Arlington
WGRFC	West-Gulf River Forecast Center

1   Executive Summary

The Texas Water Development Board (TWDB) produces estimates of freshwater inflow to major bays and estuaries along the Texas coast at both monthly and daily increments. A central element of the system for producing such estimates is Texas Rainfall-Runoff (TxRR) model, a simple, parsimonious hydrologic model that calculates runoff on a continuous basis for ungauged bay watersheds. TxRR currently ingests gauge-interpolated precipitation data, and it implements a simple water balance scheme that lumps evapotranspiration and percolation-related losses. The structural simplicity of TxRR, on one hand, makes the model computationally efficient, and yet, it may on the other hand hinder the model's ability in representing inter-event and inter-annual variations in runoff.

To address the potential limitations of the existing TxRR-based inflow estimation system, the TWDB contracted University of Texas at Arlington (UTA) to undertake an effort to augment this system by introducing new products and modeling systems, and to assess the potential impacts of the augmentation on the inflow estimates for Matagorda Bay, an estuary system situated in the central Texas coast. The assessment focuses on five gauged watersheds and eleven ungauged bay watersheds that drain to Matagorda Bay. There are four specific tasks in this project. The major results for each of the tasks are summarized below.

Task 1: The UTA team introduced the National Weather Service (NWS) Multisensor Precipitation Estimates (MPE) product as a potential replacement for the current gauge-interpolated data as the input to TxRR. The project team created a suite of tools for ingesting the MPE data to produce mean areal precipitation series for TxRR, and shared these tools and documentations with TWDB. The team also compared the MPE and gauge-based precipitation products, and performed parallel, experimental TxRR simulations using the MPE and existing gauge-based data set as input forcing for 11 ungauged watersheds that drain to Matagorda Bay. Notable observations are summarized as follows:

1. MPE features broadly higher precipitation amounts across the ungauged watersheds. The differences are appreciably wider over the eastern portion of the bay.

2. Using MPE as the input to TxRR yields larger runoff volumes across all bay watersheds, and the contrasts in simulated runoff are more pronounced than those in precipitation. This magnification of contrasts is likely because the increases in precipitation amounts are distributed primarily during time windows with wetter surface conditions and higher runoff efficiency.

3. TxRR runoff simulations driven by MPE show higher incidence of large daily runoff volumes.

It remains unresolved whether the contrasting runoff volumes from MPE and gauge-based TxRR simulations indeed point underrepresentation of runoff in the latter simulations, or are simply artifacts of distorted parameter values due to the use of gauge data in model calibration. Additional validation is needed to determine the need of model re-calibration before routine use of MPE data for TxRR simulations.

Task 2: In this task, the UTA team introduced three widely known hydrologic models as potential complements to TxRR. These are the HEC-HMS by the US Army Corps of Engineers, the Hydrology-Laboratory Research Distributed Hydrologic Model (HL-RDHM) maintained by the NWS and University of Texas at Arlington, and the National Water Model (NWM) that is running operationally at the NWS. Among these models, HEC-HMS and TxRR are lumped models, whereas HL-RDHM and NWM are considered distributed models[1]. These four models form the skeleton of the Multi-model inflow prediction system (MMIPS).

The team compared the performance of the four models for the period of 2003-2017 for five gauged watersheds, with each model driven by the forcings from the North American Land Data Assimilation System-2 (NLDAS-2), which include, but are not limited to precipitation, temperature, wind speed, and net radiation[2]. HEC-HMS and HL-RDHM were calibrated for 2004-2012. Key observations include:

1) TxRR performs favorably for the largest watershed (Lavaca River at Edna) over the period of 2004-2012, whereas for 2013-2017 HEC-HMS consistently outperforms other models.

2) Large biases are observed in the simulations of TxRR and NWM for both periods.

3) Performance of different models in capturing seasonal and interannual variations is mixed. NWM performs slightly better in capturing the interannual variations, and TxRR has major issues in reproducing the seasonal variation of flow for Navidad River above Hallettsville.

4) Three alternative models, namely HEC-HMS, HL-RDHM, and NWM, tend to inflate the baseflow for Lavaca River at Edna.

5) Performance of models varies widely across major historical storm events. All models tend to overproduce runoff for the 2011 drought.

Task 3: The team performed a detailed assessment of the biases in NWM simulations over gauged coastal watersheds. The biases of NWM simulations are rather large and highly variable across the five gauged watersheds. For the two largest watersheds, i.e., Lavaca River at Edna, and Navidad River above Hallettsville, NWM simulations exhibit pronounced positive biases. The project team developed a table of multi-basin averaged monthly bias factors based on the simulations for 2003-2017 that can be used for mitigating the biases.

Task 4: The team configured a prototype of MMIPS for the 11 bay watersheds, and produced an ensemble of simulated inflow series using this for 2003-2017 with NLDAS-2 forcings. The ensemble members include the series based on simulations of HEC-HMS and HL-RDHM

---

[1] Lumped models commonly use basins, subbasins, or hydrologic response units as the basic units, whereas distributed models rely on regular or irregularly shaped cells as the units. Distributed models often use topography-based flow direction to identify and connect upstream and downstream units.

[2] TxRR and HL-RDHM only uses precipitation as input.

configured for the bay watersheds, streamflow retrieved for bay inlets from NWM v1.2 reanalysis that underwent bias correction, and TxRR simulations. The team compared the flow simulations from the four models, and the results point to a dichotomy between the lumped (TxRR and HEC-HMS) and distributed models (NWM and HL-RDHM), with the latter producing smaller volumes for a majority of smaller bay watersheds. This contrast is rooted in the differing representations of drainage areas by the two groups of models. The lumped models compute runoff using for the entirety of each TWDB watershed, whereas the distributed models route only the runoff generated over a subset of grid pixels within each watershed that are hydrologically connected to bay inlets. The analysis underscores potential limitations in both set of models in representing flow paths over the low gradient zone. There is a distinct possibility that lumped models inflate the runoff because of their inclusion of areas that are not hydrologically connected to the bay. On the other hand, distributed models may underrepresent inflow due to the errors in the topography-based flow paths on which these models were built, as well as due to the exclusion of contributions from small, ephemeral streams.

On the basis of the findings, this report offers a set of specific recommendations for further improving the MMIPS, and transitioning to the new paradigm of ensemble freshwater inflow estimation and prediction.   The report further offers perspectives on the potential of using MMIPS to address the challenges related to flood forecasting, mitigation and planning that are confronting the state of Texas. It also outlines the resources needed in order for the TWDB to adopt the current MMIPS prototype and to extend its coverage to other bays and estuaries along the Texas coast.

2 Introduction

Freshwater inflow to bays and estuaries is arguably one of the most critical variables that maintains the function of coastal ecosystems (Russell et al., 2006; Kim and Montagna; 2009). Inadequate freshwater inflow has been demonstrated to be a major cause for the diminishing freshwater wetlands and aggravated saltwater intrusion, which in turn threaten the habitats of a variety of species residing in the bays and estuaries. By contrast, excessive inflow during extreme flooding events can serve as a barrier that inhibits the influx of oxygen and thereby induces hypoxia beneath (Rabalias et al., 1998).

In the state of Texas, modeling and monitoring freshwater inflow has been an important mission of the Texas Water Development Board (TWDB). At present, the TWDB produces both monthly and daily estimates of freshwater inflow to major bays and estuaries along the Texas coast. As many of the coastal streams are ungauged, the TWDB's estimation mechanism relies on a combination of observed discharge at upstream gauging stations and model simulations of runoff in the ungauged watersheds. The resulting discharge then undergoes adjustments to account for water use and withdrawal, and the finalized inflow estimates thus produced are then disseminated to stakeholders through a web portal. The TWDB also applies the inflow estimates as boundary conditions for the TWDB's 2-D estuary model (TxBLEND) that is run on a daily basis to create maps of salinity distribution in the bays and estuaries (Schoenbaechler et al. 2011).

To date, the agency has been relying on the Texas Rainfall-Runoff (TxRR) model, a simple, lumped, continuous rainfall-runoff model developed within the TWDB, to perform rainfall-runoff calculations for the ungauged basins. A schematic of the TxRR model is shown in Fig. 2-1.
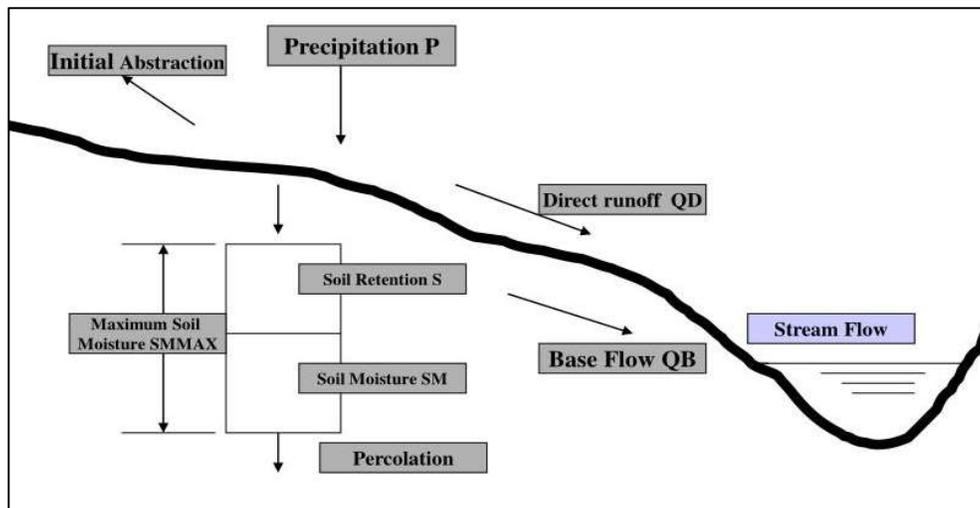
Figure 2-1   **Schematic of Texas Rainfall-Runoff (TxRR) model. Source: the TWDB.**

The TxRR uses the Soil Conservation Service (SCS) method for calculating initial abstraction and direct runoff, and combines this with prescribed, seasonally-varying baseflow to determine total runoff to the stream. As in the SCS method, the initial abstraction and direct runoff are computed using a storage factor, which is determined by the averaged curve number of a watershed. In order to account for the change in storage related to loss of soil water between storms, TxRR implements a simple, 1-layer water accounting scheme that allows soil water to percolate to deeper layers underneath (Fig. 2-1).

In this scheme, the maximum soil moisture (SMMAX) is divided into soil retention (S), which represents the soil moisture deficit, and actual soil moisture (SM). Soil retention (S) determines the initial abstraction and runoff via the SCS equation

$$Q = \frac{(P-I_a)^2}{(P-I_a)+S} \qquad\qquad (2\text{-}1)$$

Where P is the precipitation, and I_a is the initial abstraction. TxRR deviates slightly from SCS by relating I_a to soil retention S through a tunable abstraction parameter "abst".

SM controls the rate of percolation (depletion). In TxRR, the depletion is modeled via a simple exponentially decaying function.

$$SM(t_2) = SM(t_1)e^{-a_m(t_2-t_1)} \qquad\qquad (2\text{-}2)$$

where a_m is the depletion constant for month m.

The soil moisture accounting scheme further allows replenishment of SM by rainfall excess F:

$$SM(t_2) = SM(t_1) + F(t_2) \qquad\qquad (2\text{-}3)$$

Where F is defined as the difference between rainfall, initial abstraction I_a and runoff Q:

$$F = P - I_a - Q \qquad\qquad (2\text{-}4)$$

TxRR combines the direct runoff Q with baseflow to generate the total streamflow, where baseflow under dry conditions is assumed to follow an exponential decay function.

$$Q_B(t_2) = Q_B(t_1)K^{t_2-t_1} \qquad\qquad (2\text{-}5)$$

where K is a decay constant. During a precipitation event, the baseflow is elevated by an increment that is related to either the amount of precipitation or infiltration.

For daily simulation, TxRR employs the SCS dimensionless unit hydrograph to route the direct runoff Q. The parameter lag time in the unit hydrograph model T_l is estimated from drainage area A via an empirical relationship:

$$T_l = \beta A^{0.6} \qquad\qquad (2\text{-}6)$$

where coefficient β is treated as a calibration parameter.

TxRR's major strength lies in its structural simplicity and parsimony in parameterization. The model only incorporates four parameters that need to be adjusted during calibration, namely maximum storage SMMAX, soil moisture depletion constant $a_{m.}$, baseflow recession constant K, and the coefficient β that relates lag time with drainage area. This parsimony facilitates model calibration. Yet, in the meantime, the oversimplified structure most likely distorts the physical processes of runoff generation, and this distortion would manifest as errors in model simulations for events and for basins where the runoff mechanisms differ from the cases included in the calibration. The primary mechanistic limitations of TxRR include

1. A lack of an explicit way of modeling evapotranspiration (ET), and the resulting inability to account for the impacts of varying meteorological conditions on ET-related loss;

2. A lack of a routing mechanism that would factor in changes in the shape of the discharge hydrograph along channels;

3. The somewhat arbitrary way of calculating baseflow with no regard to the fact that baseflow is often governed by shallow subsurface flow, which may not respond instantaneously to rainfall input;

4. The relatively simplistic depiction of hillslope process without any differentiation of surface and interflow which typically differ in response time;

5. The inability of the model structure to represent spatial distribution of rainfall

While some of these limitations can be mitigated through changes in the model structure, such changes are costly to implement and test. Alternatively, one could employ contemporary, widely used hydrologic models with more sophisticated runoff mechanisms in place as potential complementary modeling systems. For example, the recently operational National Water Model (NWM) at the National Weather Service (NWS) incorporates representations of a wide range of physical processes; being a distributed model, it is able to account for spatial rainfall variability and impacts of land surface and channel features on discharge. Nevertheless, as past efforts, and in particular the Distributed Model Intercomparison Projects (DMIP; Reed et al. 2004; Smith et al. 2012) illustrate, spatially distributed, process-based models are not immune to under or misrepresentation of runoff processes, and their performance can be compromised by the uncertainties in parameterization and associated difficulty in calibration. The outcome of DMIP also points to the potential of enhancing model prediction by harnessing the complementary strengths of different models through a model ensemble approach (Georgakakos et al. 2004).

Aside from the aforementioned structural limitations, TxRR currently employs interpolated gauge observations whose accuracy is constrained by the density of gauge networks. In a previously published TWDB report (Schoenbaechler et al., 2011), it is shown that some of the sharp drop-offs in salinity in Matagorda Bay were not captured by the TxBLEND Model, and one of the potential causes is inaccuracy in precipitation input along the coast that led to underestimation of inflow volume by TxRR (Schoenbaechler et al. 2011).

Building on the lessons accumulated through research performed within the NWS Hydrology Laboratory (now the National Water Center) over the past few decades, the UTA team undertook an effort to augment the TWDB's freshwater inflow estimation process. The effort comprises

13

two major thrusts. The first focuses on developing tools for integrating gauge-radar blended precipitation products produced by NWS as future forcing inputs to TxRR (Task 1). The second entails creating a prototype multi-model simulation system capable of producing ensemble inflow simulations by leveraging the complementary strengths of contemporary hydrologic models (Tasks 2, 3, and 4). At present the system consists of TxRR and three additional models, namely NWM, HEC-HMS, and Hydrology Lab – Research Distributed Hydrologic Model (HL-RDHM; NWS, 2008; Zhang et al. 2011a, 2017). Included in the second thrust is the effort to postprocess the streamflow analysis of NWM to mitigate the biases in the latter's analysis (Task 3). Implementation and testing of the new modeling systems and forcings are done for a cluster of watersheds that drain to Lavaca-Colorado Estuary System, a major estuary system along the southeast portion of the Texas coast.

This report details steps involved in the execution of each task, methods of implementation and evaluation, and outcomes of validation and comparisons; it also offers a set of recommended actions to be undertaken to address limitations in the multi-model framework. The remainder of the report will be divided into five sections accordingly. Section 2 introduces the study settings and common rainfall and streamflow data sets. Section 3 describes the creation of the mean areal precipitation from Multi-sensor Precipitation Estimates (MPE) and summarizes the comparisons of the precipitation series based on gauge and MPE, and resulting TxRR inflow simulations driven by the two data sets. Sections 4 reviews the National Water Model and its streamflow products, presents the implementations of HL-RDHM and HEC-HMS, and summarizes the results from the streamflow calibration-validation experiments. Section 5 summarizes the tasks and findings, outlines further actions for improving the MMIPS, and discusses steps and resources needed to operationalize MMIPS and to expand its coverage to the remaining bays and estuaries along the Texas coast.

3 Study Setting

Situated along the central portion of the Texas coast, the Lavaca-Colorado Estuary System is a cluster of bays and estuaries (Schoenbaechler et al. 2011), the largest among which is Matagorda Bay. Freshwater flows into Matagorda Bay mainly through Lavaca River over the north, Colorado River over the northeast, and a number of smaller streams (Fig. 3-1).
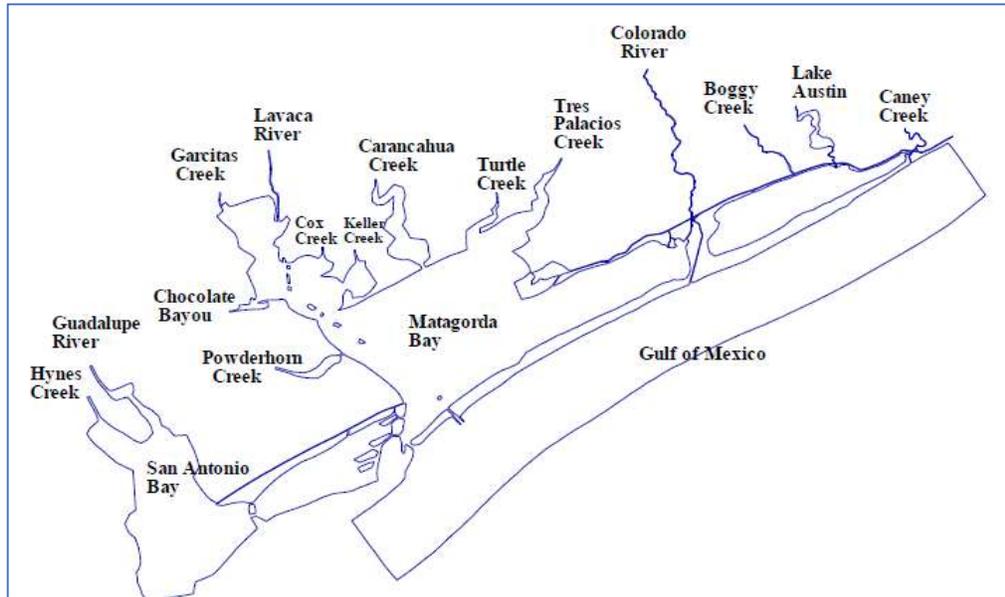
Figure 3-1   **Streams contributing to inflows to Lavaca-Colorado Estuary System, which includes Matagorda Bay. Source: Schoenbaechler et al. (2011).**

The TWDB identified eleven major streams with inlets to Matagorda Bay. Table 3-1 summarizes the ungauged watersheds associated with each inlet.

Table 3-1.   **Ungauged watersheds with inlets to Matagorda Bay**

Ungauged Watershed	Inflow Point	Drainage Area [mi^2]	Upstream USGS Gauges
17070	Powderhorn Ck	162	
17060	Chocolate Bayou	151	08164800
17010	Garcitas Ck	37	
17030	Garcitas Ck	273	08164600
17050	Garcitas Ck	50	
16008	Lavaca River	88	08164000, 08164525
15060	Cox Creek	63	
15050	Carancahua Ck	384	
15040	Turtle Ck	107	
15030	Tres Palacios Ck	94	08162600
15010	Oyster Bayou	149	

Note that we exclude the Colorado River in the modeling effort and instead focus on the Matagorda watershed, because of the interest the US Army Corps of Engineers (USACE) Galveston District had in setting up a HEC-HMS model for this region. The locations and extents of both gauged and ungauged watersheds that contribute to Matagorda Bay are shown in Fig. 3-2, where the gauging stations used in validation are highlighted in red.
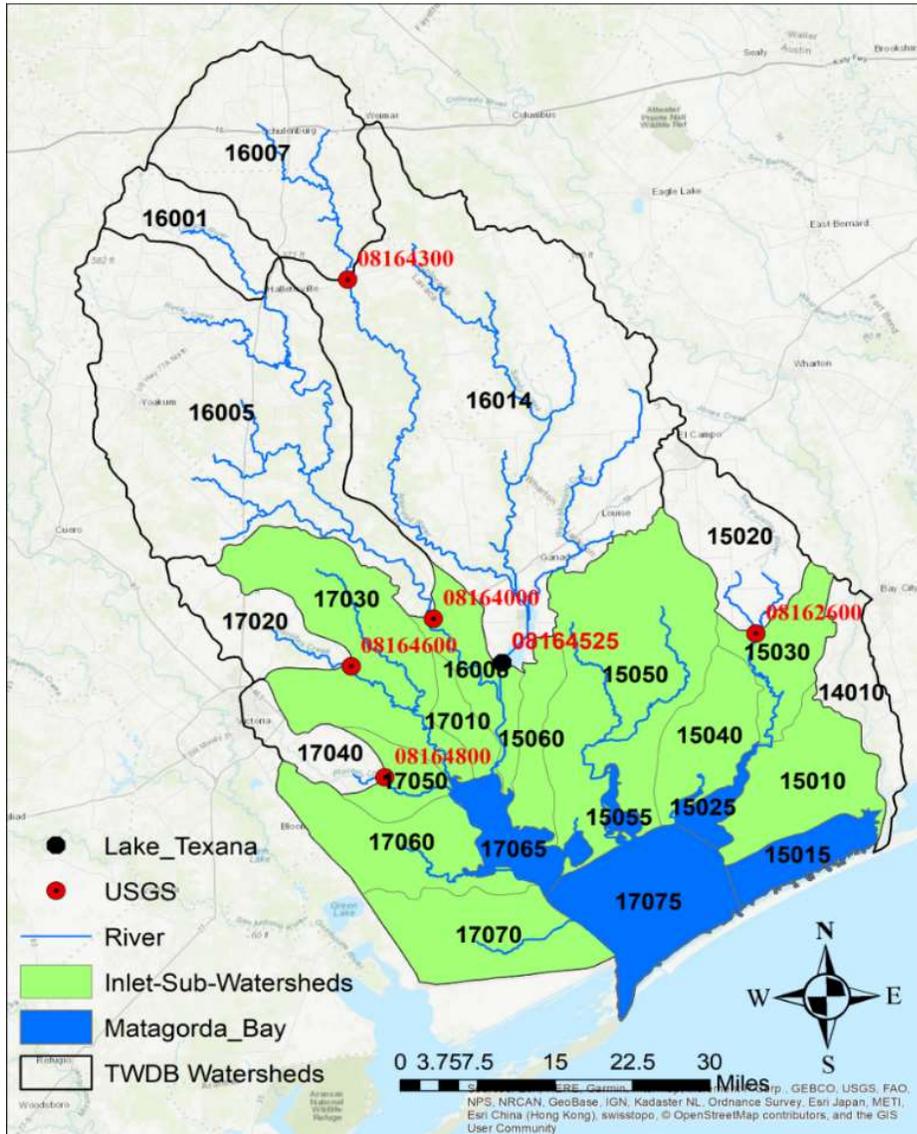
Figure 3-2   **Gauged and ungauged watersheds that drain to Matagorda Bay. The locations of USGS gauging stations and identifiers are marked in red. The outlet for Lake Texana is highlighted in black.**

16

Evaluation of model performance involves streamflow records for five gauged catchments. Information about each catchment, including size, US Geological Survey (USGS) station identifier for the outlet, and NWS code can be found in Table 3-2. For all catchments real-time (15-minute) USGS flow observations are available since 1991. Daily observations went back further and the length of record varies among sites (Table 3-2). Three additional USGS stations provide gauge height readings in the region, namely, 08163500 (Lavaca River at Hallettsville), 08164370 (Navidad River at Morales) and 08164525 (Lake Texana near Edna; marked in black in Fig. 3-2). The data from the former two are limited in duration and therefore are not used in this project. The third station only provides gauge height and we instead use the archived daily outflow estimates from the Lavaca-Navidad River Authority.

Table 3-2.   **USGS Stations in Lavaca River Basin with long-term streamflow records**

USGS ID	Station Name	NWS SHEF ID*	Drainage Area [mi^2]	Availability of daily flow
08164300	Navidad River above Hallettsville	HTST2	332	1938-present
08164000	Lavaca River near Edna	EDNT2	817	1961-present
08162600	Tres Palacios River near Midfield	MTPT2	156	1970-present
08164600	Garcitas Creek near Inez	NGCT2	107	1970-present
08164800	Placedo Creek near Placedo	PLPT2	71	1970-present

*SHEF stands for Standard Hydrologic Exchange Format used by National Weather Service

In this project, we acquired the USGS National Hydrography Dataset – Plus (NHD-Plus), including the digital elevation model (DEM), flow direction, and stream links. The DEM and flow direction data served as the basis in establishing the modeling systems, and stream segment identifier was used for retrieving the NWM v1.2 reanalysis[1]. We also obtained the boundaries of ungauged watersheds from the TWDB in Shapefile format. For model implementation and assessments, we acquired two precipitation data sets, i.e., the NWS MPE product produced by West Gulf River Forecast Center (WGRFC), and the North America Land Data Assimilation System (NLDAS) forcings created by NWS National Centers for Environmental Prediction, which include meteorological variables such as precipitation, radiation, temperature, etc. The latter data set was used because the reanalysis of NWM, a member of the multi-model system, was based on the NLDAS forcings. Both data sets use radar and gauge observations, and the primary difference is that NLDAS is created by disaggregating the daily gauge totals using radar-based estimates, whereas the MPE data set blends radar and gauge data. Additional details about the data sets will be provided in later sections.

---

[1] Reanalysis refers to simulations performed using a frozen version of the model for a designated historical window.

4   Enhancing Precipitation Estimates for TxRR

The primary motivation of Task 1 is to adopt high resolution (hourly and 4-km), extensively validated, and widely used MPE product as a replacement for the current daily gauge-interpolated product. It is anticipated that this transition will help improve the accuracy of precipitation estimates over the bay watersheds and thus the inflow estimates. In addition, the adoption of the MPE data will enhance interoperability with NWS, the USACE, and state river authorities which all have adopted the MPE product for operational hydrologic prediction. The section documents and discusses the differences between MPE and gauge-based precipitation products, and those between TxRR simulations driven by the two products.

In this report, we use the term MPE to loosely refer to the operational products created at the NWS River Forecast Centers (RFCs) on an hourly basis by blending radar-only precipitation data with rain gauge reports. These include the early radar-gauge blended product created using the legacy Stage III algorithm which was first introduced in the 1990s and in use until 2003, and the subsequent products generated using the Multisensor Precipitation Estimator suite (Seo 1998a,b; Seo et al. 1999; Seo and Breidenbach 2002; Kitzmiller et al. 2013; Seo et al. 2013). The MPE products until 2014 were created based on radar-only Digital Precipitation Array (DPA) produced through the Next Generation Weather Radar (NEXRAD) Precipitation Processing System (PPS; Fulton et al. 1998; Kitzmiller et al. 2011). Since circa 2014, most RFCs have switched from the DPA product to the radar-only products of the Multi-radar multi-sensor (MRMS) system maintained by the National Severe Storm Laboratory. The MRMS and its predecessor Q2 algorithm package were described in Zhang et al. (2011), Kitzmiller et al. (2011), and later by Zhang et al. (2016); it featured a number of enhancements to the NEXRAD PPS such as automatic bright-band detection, selection of reflectivity-rain rate (Z-R) relation, and correction for the vertical profile of reflectivity. A few RFCs, including the West Gulf River Forecast Center (WGRFC), also incorporate limited satellite-based precipitation estimates in creating the MPE, primarily to fill gaps in radar and gauge coverages along the US-Mexico border (Zhang et al., 2013; He et al. 2018).

Zhang et al. (2011a) offered a detailed overview of the process through which MPE products are created at RFCs. In a series of studies (e.g., Zhang et al. 2011a; 2017), the MPE data, at least those from the mid-2000, were shown to be advantageous to gauge-interpolated product for their ability to capture the spatially variation of precipitation systems while avoiding large biases as a result of gauge-based bias correction. These studies also underscored issues in the quality of early MPE data, one of which is the presence of a truncation error in the NEXRAD PPS that artificially reduces precipitation accumulations in both radar-only and multisensor products (Fulton et al. 2004; Zhang et al. 2011a). The quality of MPE products has steadily improved after the correction of the error in 2003 (Zhang et al. 2011a). At present, most NWS RFCs, including WGRFC, are using MPE as the forcing to its streamflow prediction system. In the state of Texas; MPE is also the standard forcing input for modeling systems maintained by organizations including the USACE and Lower Colorado River Authority.

In this project, we acquired the MPE product from the WGRFC over the period of 1998-2017. The data set is in the Hydrologic Rainfall Analysis Project (HRAP) coordinate system (Greene and Hudlow 1983; Reed 1999), with its grid mesh roughly 4km in size over the mid-latitude. The gridded MPE data are converted to hourly time series of Mean Areal Precipitation-MPE

(henceforth referred to as MAP-X) using watershed masks derived from the watershed boundaries provided by the TWDB. The detailed steps and software packages involved in creating the MAP-X series are outlined in **Appendix A**.

Two sets of runoff simulations[1] are conducted using TxRR. The first, or baseline, was driven by the MAP series supplied by the TWDB, which were created by interpolating the daily accumulations reported by stations in the Global Historical Climate Network (GHCN). This MAP series is henceforth referred to as the MAP-G series. The second simulation was done using a hybrid rainfall series that combines the MAP-G series for 1940-1997 and the MAP-X series for 1998-2017. The practice guarantees that the model is properly warmed up and that the two runs share identical initial conditions. The two sets of simulations over the latter period (1998-2017) are compared to assess the impacts of replacing the MAP-G by MAP-X.

The comparisons on a mean annual basis are shown in Table 4-1 and Fig. 4-1. MPE-based MAP is on average higher than the corresponding gauge products across the watersheds, with the highest percentage difference (relative to MAP-G) of 17% for WS15040 (Turtle Creek). Correspondingly, the TxRR simulated runoff driven by MAP-X are systematically higher than those based on the gauge product. It is also worth noting that the differences in runoff estimates tend to be much wider than that in the precipitation forcing. Take WS15010 (Oyster Bayou) for example: MAP-X is only 9% higher than MAP-G, but the TxRR simulation driven by the former is 26% higher. This amplified contrast can be possibly explained by nonlinearity in runoff response as modeled by TxRR – it is possible that the additional precipitation takes place disproportionately over time periods when soil moisture is at or near capacity, and therefore the additional rainfall introduced by the MPE efficiently turns into runoff.

Table 4-1   **Mean areal precipitation based on gauge data and MPE and simulated runoff**

Watershed ID/Group		Precipitation			TxRR Runoff		
		MAP-G [in/year]	MAP-X [in/year]	% Diff	MAP-G [10³af/year]	MAP-X [10³af/year]	%Diff
15010	East	43	47	9	119	150	26
15030	East	45	49	8	76	100	32
15040	East	41	47	15	84	108	29
15050	East	42	45	5	246	313	28
15060	West	41	42	2	40	42	3
16008	West	42	43	1	65	72	10
17010	West	41	43	4	23	28	21
17030	West	42	43	5	136	179	32
17050	West	41	42	2	28	32	13
17060	West	41	43	3	103	116	12
17070	West	41	42	3	113	122	8

---

[1] Throughout this paper, we use "runoff" to describe runoff generated locally in each watershed, and "inflow" to describe the aggregate of local runoff and upstream flow that passes through a bay watershed. These two terms are equivalent for watersheds without upstream contributions.
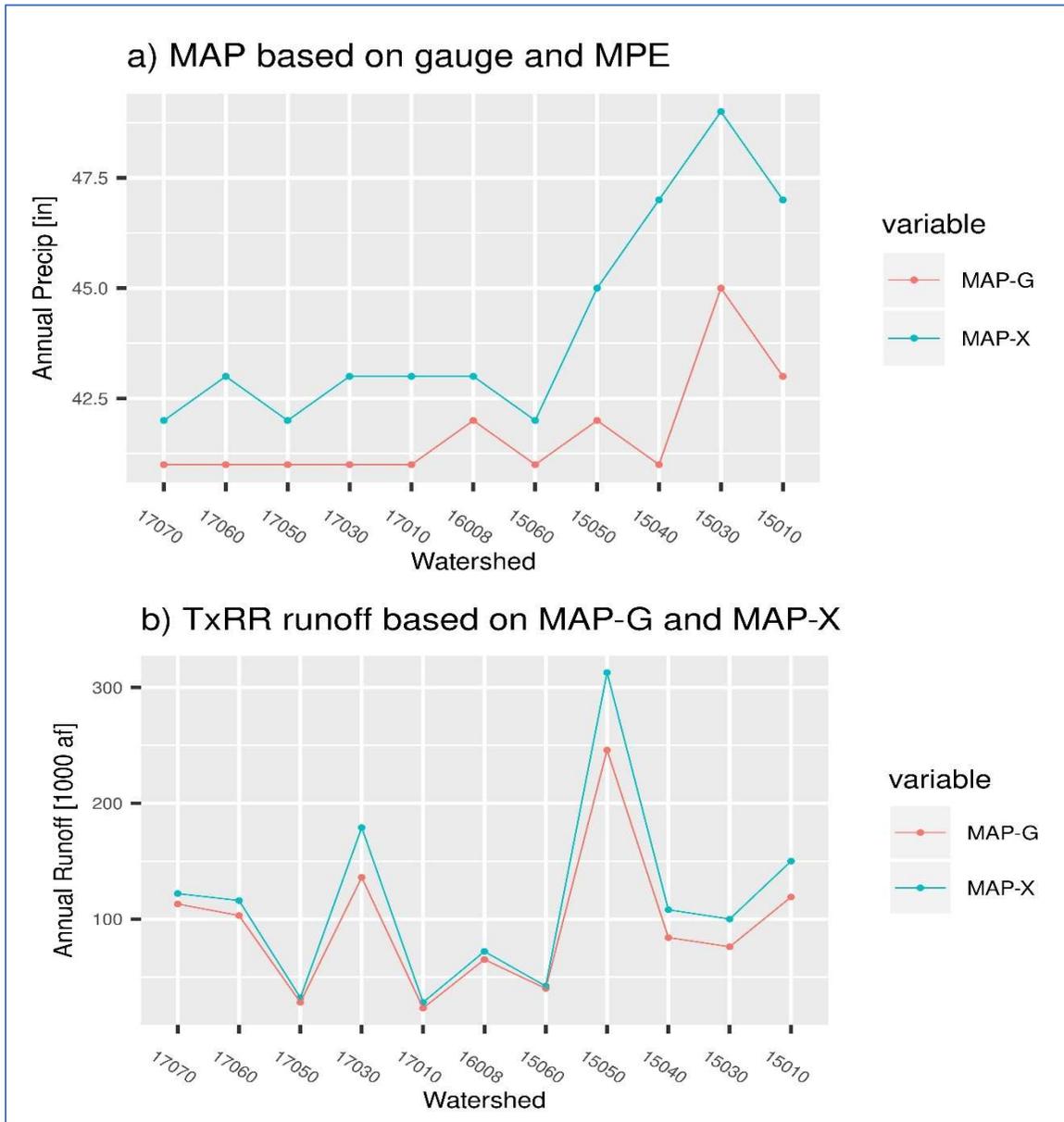
Figure 4-1   **Differences between a) mean annual MAPs based on gauge (MAP-G) and MPE data (MAP-X), and b) simulated inflows using respective data sets for each ungauged watershed that drains to Matagorda Bay. The watersheds are sorted roughly from the west to east. Note that the differences in MAPs tend to be larger toward the east where annual precipitation is higher.**

Another noteworthy feature in Fig. 4-1 is that the differences in rainfall estimates are more pronounced for a group of watersheds over the east (15010, 15030, 15040, and 15050) where annual precipitation is higher. Hence, we designate these four watersheds over the east as Group East, and the remainder watersheds as Group West. For each group, the quantiles for MAP and

20

TxRR-based inflow series are computed by lumping the series for all watersheds in respective group, and the results for the gauge and MPE-based series are compared in Fig. 4-2.
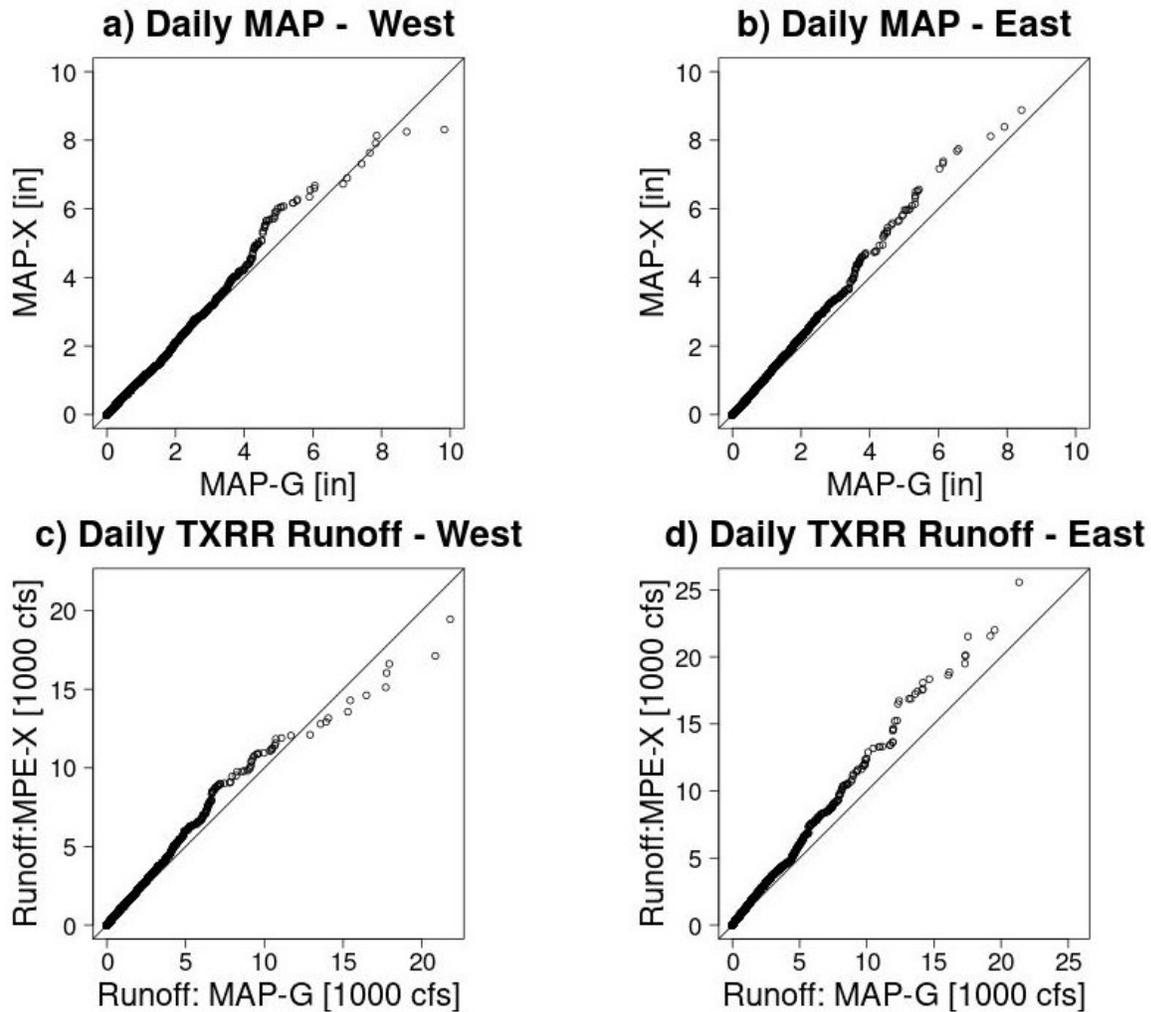
Figure 4-2   **Quantile-quantile plots of daily MAP and corresponding daily TxRR simulated runoff coastal watersheds located over the west and east portion of the bay. The list of watersheds for each group can be found in Table 4-1.**

For Group West, the quantiles of MAP-X are higher in the range of 4-6 inches, whereas the peak rainfall amounts (highest quantiles) are in fact lower than those based off the MAP-G (Fig. 4-2a). Correspondingly, higher quantiles for daily inflows based on MAP-X are in fact lower (Fig. 4-2c), despite that the simulated inflow rate is on average higher when MAP-X is used as the forcing. By contrast, for Group East, quantiles for MAP-X and associated inflow are systematically higher across the entire range of values (Figs. 4-2b and d), and particularly so at the peak of inflow rates (Fig. 4-2d). Evidently, for the western portion of the bay watershed, MPE features overall higher daily amounts but lower incidence of anomalously large amounts (>

8 in); whereas, over the east, MPE-based amounts are consistently higher across the spectrum of precipitation amounts. These differences in the MAP data sets tend to be amplified in the TxRR model simulations.

Fig. 4-3 illustrates the overall impacts of replacing the gauge-based by MPE-based precipitation inputs on the temporal distribution and interannual variation of runoff. From Fig. 4-3a, it is clear that the daily inflow driven by MAP-X exhibits a slightly heavier tail, with a larger fraction of daily inflow exceeding 10^4af. This contrast is reminiscent of the quantile difference in precipitation and streamflow for the Group East as illustrated in Figs. 4-2b and d, respectively. As precipitation is relatively higher over the east part of the region, the differences in terms of precipitation and runoff over this region tend to dominate those for the averaged total runoff across the 11 watersheds.
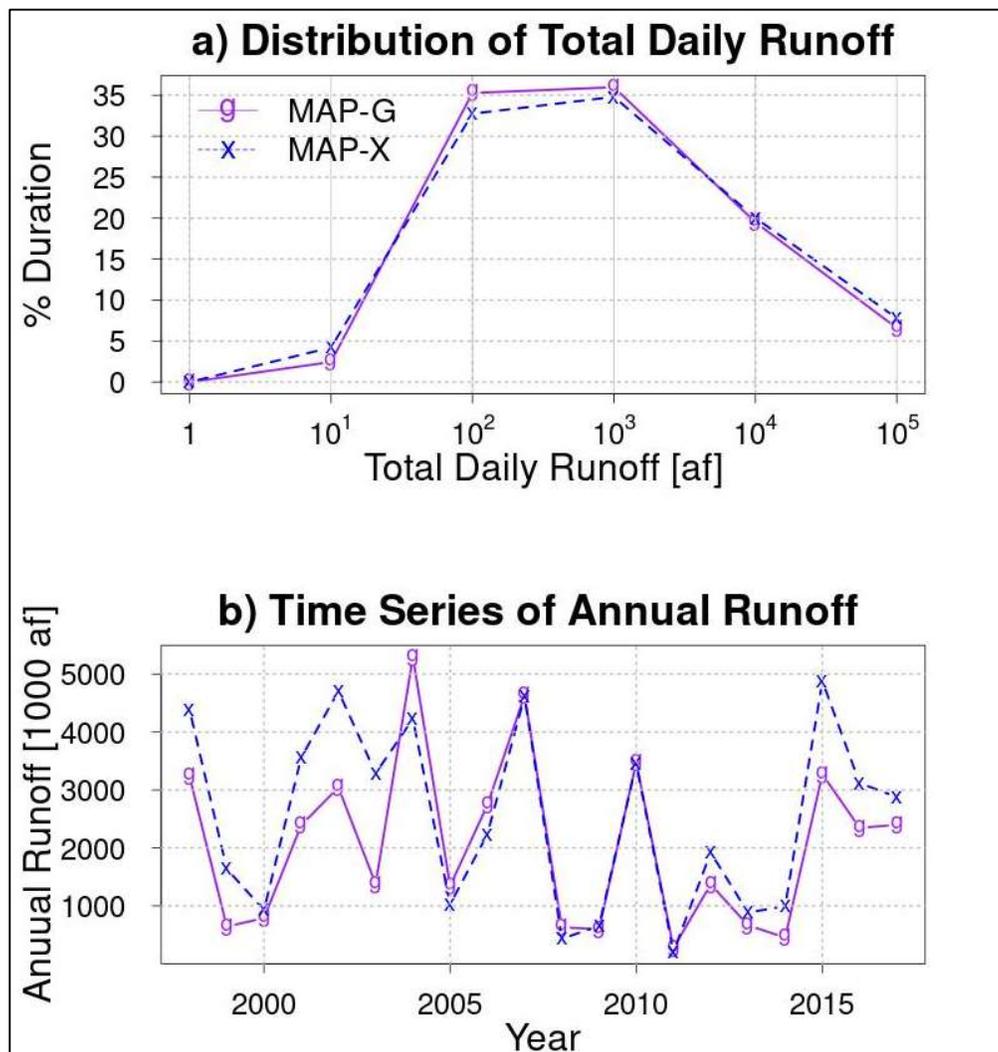
Figure 4-3   **Comparisons of TxRR simulated total inflow to Matagorda Bay driven by gauge (MAP-G) and MPE (MAP-X) rainfall products: a) temporal distribution of inflow (percentage duration of flow in a specific category, say between 102 and 103 af/day); and b) time series of mean annual inflow.**

22

As Fig. 4-3b shows, the contrast between the two sets of inflow simulation varies over the 20-year window, but there is no clear trend. It appears that the streamflow based on MAP-X is mostly higher, and sometimes significantly so, in the earlier and later portions of the time window (1998-2003 and 2012-2017, respectively). For example, in 2015, driving TxRR using MAP-X results in 4.88×10^6af of runoff, nearly 50% higher than 3.27×10^6af when MAP-G is used. For the rest of the years, however, the two sets of results are comparable. The difference over the earlier period (1998-2003) is interesting, as it is known that the early MPE data was often biased low due to the presence of a truncation error in the NEXRAD PPS. Zhang et al. (2011a) showed that this bias indeed affects the inflow simulations over a cluster of Mid-Atlantic basins. Such a feature, however, is absent in the present results. The precise causes of these differences over the earlier years are difficult to pinpoint without a close scrutiny of the GHCN gauge reports used in creating the two data sets, but several plausible explanations exist. These include i) a sparse gauge network that failed to resolve rainfall intensity over major historical storm events; and ii) quality issues in the earlier MPE data which introduces positive biases and offsets the impacts of the truncation error. Investigating the contributions from each factor is an effort well beyond the scope of the present study and is left for future efforts.

The overall higher amounts from the MPE over the later period (i.e., 2012-2017) are consistent with the observations from earlier investigations (Zhang et al. 2011a; 2016). Interpolated gauge products are often unable to fully depict heavy rainfall cells that fall between gauges, and therefore tend to exhibit severe negative bias at larger precipitation amounts. This phenomenon, commonly referred to as the Type II conditional bias, was closely examined by Seo (2013), among other authors. Weather radar relies on volume scans for precipitation detection and estimation, and its ability to resolve spatial variation of rainfall intensity makes its product less susceptible to Type-II bias arising from spatial representation errors.

It is interesting to note that the gauge, rather than MPE product in fact features higher rainfall maximums over the western portion of the bay (Fig. 4-3a), whereas the opposite is true for the watersheds over the east. One possible cause of this east-west contrast is the presence of two NEXRAD units, namely the Houston-Galveston unit (HGX) and the Corpus Christi unit (CRP), with overlapping coverage of the region (Fig. 4-4). The software package that WGRFC uses to produce MPE relies on beam height and range (distance to radar installation) are the primary variables to determine the radar unit whose product will be employed when overlapping coverages from multiple units are present. It is likely that the observations from HGX/CRP were the predominant source of input in MPE creation over eastern/western portion of the bay. If so, any differences between the two units in terms of radar calibration, beam height, and reflectivity-rain rate relation could have contributed to the east-west contrast. Though biases in radar products are mitigated through bias correction, the effectiveness of bias correction depends on the quantity and quality of gauge reports. A close differentiation of various contributing factors is needed in future analysis.

For practical purposes, we would consider it prudent to use MPE data from 2003 onward as the forcing to the TxRR model, as the data has demonstrable accuracy across the nation and over Texas (Zhang et al. 2011a; He et al. 2018). Zhang et al. (2011a), for example, noted that the bias of the MPE data was much improved after 2003 as a result of correction of the truncation error, the expanded gauge database, and the introduction of more robust bias correction schemes. For the earlier Stage III and MPE data, it is recommended that a more comprehensive assessment be

conducted to determine their bias characteristics and possible mitigation measures. In case the effect of truncation error is pronounced, the retrospective correction scheme described in Zhang et al (2011a) can be employed. This scheme entails adjusting the MPE data so that its monthly totals match those from monthly gauge products (e.g., the PRISM product by Oregon State University; https://prism.oregonstate.edu/). Note that the efficacy of this scheme is again predicated on a presence of a sufficiently dense gauge network. Therefore, a detailed comparison of PRISM, Stage III, and the gauge data set on which the TWDB MAP-G was based is warranted to ascertain the applicability of this measure.
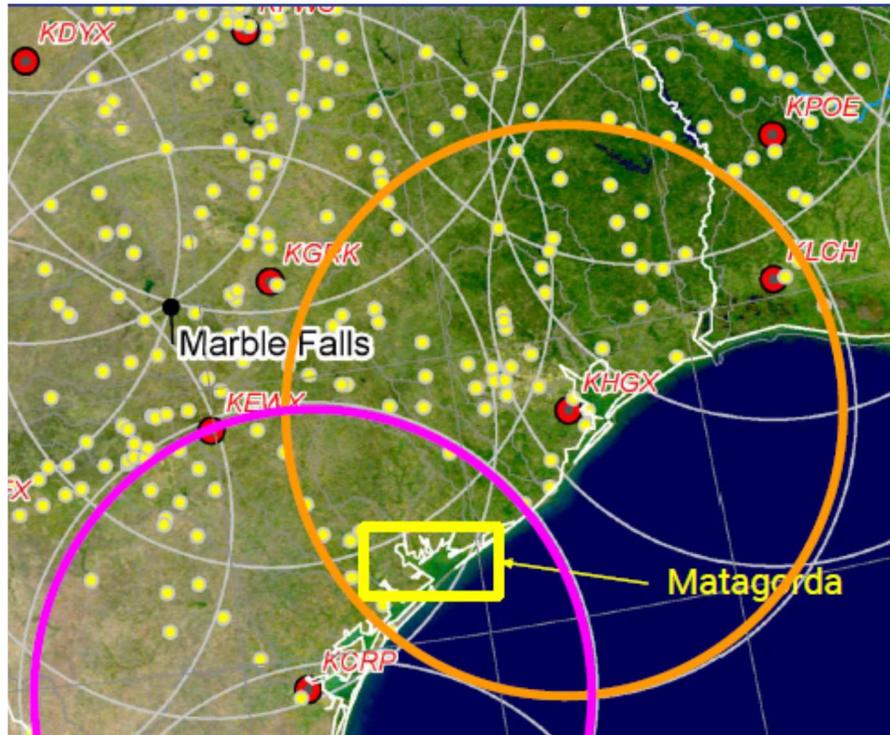
Figure 4-4 **Locations of NEXRAD units in central and south Texas. The shaded rectangle highlights the region where Matagorda Bay is situated. Note it is under the overlapping coverage of both CRP and HGX radar units.**

The magnification of the bias through TxRR simulation is a feature that requires further analysis. The rather large increase in the historical runoff volumes produced through the TxRR may NOT necessarily be an indication of underestimation of runoff by the TxRR using the default, gauge-interpolated precipitation, because the model was calibrated using this very product and the bias may have been compensated by adjustments of parameter values. A potentially useful way of determining the biases in the two sets of inflow simulation is through validation of the streamflow simulations over upstream, gauged locations. This is beyond the scope of the present project but is recommended prior to the transition from the gauge product to MPE.

24

5 The Multi-model Inflow Prediction System (MMIPS)

The structure of the multi-model inflow prediction system (MMIPS) is illustrated in Fig. 5-1. The system is initially set up to comprise four models, three running internally at the TWDB, namely the TxRR, HEC-HMS, HL-RDHM, and one running externally (i.e., NWM). The system will ingest a common set of forcing variables, including precipitation, temperature, wind speed, radiation, for the three models to produce daily and monthly inflow simulations. It will also include a module that retrieves and adjusts the real-time analysis of NWM produced at NWS for specific segments along Matagorda Bay. This section focuses on the features and implementations of alternative models, namely HEC-HMS, HL-RDHM and NWM, comparisons of model performance, and demonstration of the ensemble inflow estimates produced by MMIPS over bay inlets. The section is structured as follows: Section 5.1 offers an overview of structure and implementation of models; Section 5.2 describes the performance assessments and comparisons; and Section 5.3 presents example outputs from the system and discusses the differences among member model simulations.
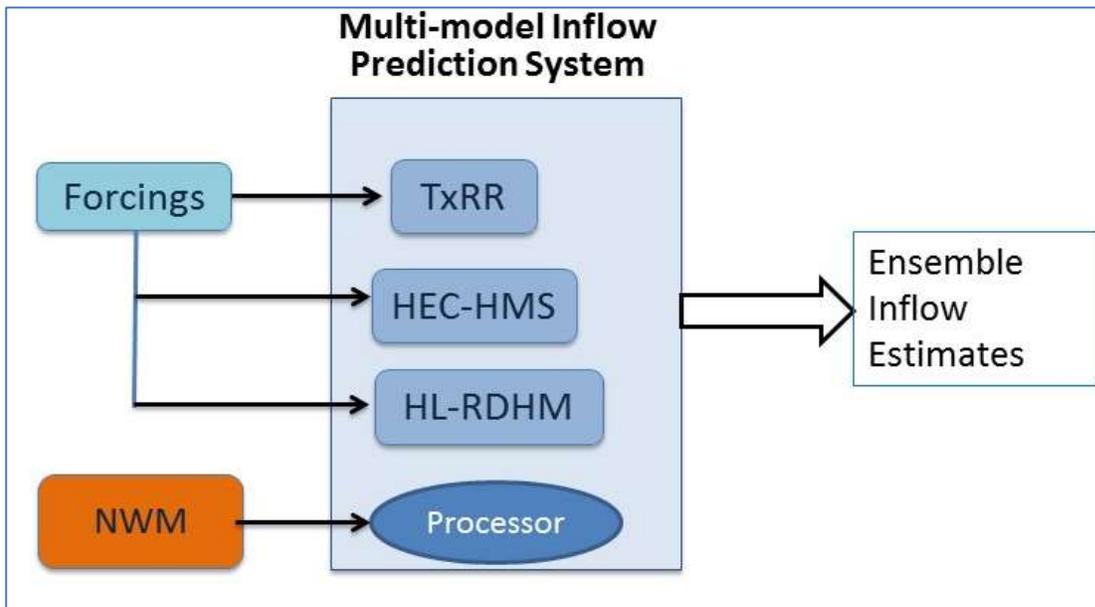
Figure 5-1   **Schematic of the multi-model inflow prediction system.**

5.1 Structure and implementation of member models

The features and implementation of each model are summarized in Table 5-1. The default TxRR model has been described in Section 1 and will not be elaborated here. Note that among the four models, both TxRR and HEC-HMS are 'lumped' in the sense that each uses watersheds or sub-watersheds as the basic units. For these models, areal means of forcing variables, in particular precipitation, are used. HL-RDHM and NWM, on the other hand, are grid-based, or "distributed" models.

25

Table 5-1   **Member models in the multi-model inflow prediction system**

Model	TxRR	NWM	HL-RDHM	HEC-HMS
Model Unit	Basin	Grid (1-km)	Grid (4-km)	Sub-basin
Evapotranspiration	Depletion	Evaporation (soil/vegetation) + plant transpiration	Static monthly PET with adj. factors	Penman-Monteith
Runoff generation	Surface+ baseflow	Surface, exfiltration interflow, baseflow	Surface runoff, interflow, baseflow	Surface runoff + baseflow
Overland routing	N/A	2-D diffusive wave	2-D kinematic wave	N/A
Channel routing	Linear reservoir	Muskingum-Cunge	Kinematic wave	Muskingum

All models except NWM will be implemented at the TWDB and run locally. For NWM, the plan is to ingest its real-time streamflow analysis distributed at NWS. Since NWM real-time analysis is available only for a limited time window, we instead use the NWM version 1.2 reanalysis (https://registry.opendata.aws/nwm-archive/) for validation and demonstration. This reanalysis was generated using a frozen NWM model configuration (v1.2) and forcings of the North American Land Data Assimilation System-Phase 2 (NLDAS-2; Xia et al. 2012), which features numerous enhancements from NLDAS-1 (Cosgrove et al. 2003). The NLDAS-2 product is available hourly on a 1/8 degree grid mesh in the geographic coordinate system from a ftp portal (ftp://ldas.ncep.noaa.gov/nldas2/). Its precipitation product is created by first interpolating daily gauge observations and then disaggregating the results using the Stage II national mosaic radar precipitation product [1], whereas its other variables are derived from either surface observations, or the North American Regional Reanalysis (Mesinger et al. 2006), or a combination of both. NLDAS-2 precipitation data can be considered as a proxy of the MPE, though its accuracy is widely seen as being inferior to MPE owing to its method of creation, data feed, and spatial resolution.

In order to gauge the performance of member models, a split-sample calibration-validation experiment is set up with 2004-2012 as the calibration window and 2013-2017 as the validation window. The year of 2003 is used for model spin-up. Note that only HEC-HMS and HL-RDHM undergo calibration, whereas TxRR simulations and NWM reanalysis are validated alongside the results of the former two models.   In order to maintain consistency in forcing input among the models, we chose to use the NLDAS-2 forcing data, which was used in creating the NWM reanalysis, as the input to TxRR, HEC-HMS, and HL-RDHM. Note that TxRR and the HL-RDHM implementation only require the precipitation products from NLDAS-2.   Details concerning the physics and implementation of HEC-HMS, HL-RDHM and NWM are provided below.

---

[1] Stage II data is a national mosaic of hourly rainfall products from NEXRAD units in the US created using an older version of PPS.

5.1.1   HEC-HMS

The Hydrologic Engineering Center-Hydrologic Modeling System (HEC–HMS), developed by the Hydrologic Engineering Center of USACE, is a hydrological modeling system widely used in engineering practice (Scharffenberg et al. 2010). Typically, an HEC-HMS model implementation consists of two components, namely the basin model and the meteorological model (Agrawal 2005). The basin model contains the specifications of the watershed configuration, water balance model, and channel routing method, whereas the meteorological model specifies precipitation and the method of calculating ET demand. The schematic of the HEC-HMS model for the Lavaca River and bay watersheds is shown in Fig. 5-1. In this model, the subbasins are specified in such a way that each USGS station or bay inlet is situated at the outlet of a subbasin (Fig. 5-2). Each subbasin serves as the basic unit on which runoff is calculated from mean areal precipitation. In order to perform continuous simulation, we implement the Soil Moisture Accounting (SMA) model as the loss scheme, and enable ET calculation using the Penman-Monteith method. Table 5-2 provides a comprehensive list of model components and the methods of choice, and a step-by-step guide on model set up and calibration is offered in **Appendix B**.

Figure 5-2   **Schematic of HEC-HMS model for gauged and ungauged watersheds that drain to Matagorda Bay.**

Table 5-2   Components of HEC-HMS Model for Watersheds draining to Lavaca-Colorado Estuary

Component	Surface	Canopy	Loss	Transform	Baseflow	Channel Routing	ET
Method	Simple Surface	Simple Canopy	SMA	SCS UH	Linear Reservoir	Muskingum	Penman-Monteith

The SMA is one of the few "loss modules" in HEC-HMS that permit continuous simulations, and it has been used in various contexts around the world (De Silva et al. 2014; Singh and Jain, 2015). A brief overview of the HEC-HMS SMA is provided here whereas readers are referred to Bennett and Peters (2000) for a more comprehensive description of various components of the model. In brief, the HEC-HMS SMA can be considered as a simplified version of the Sacramento Soil Moisture Accounting Model (SAC-SMA) being used in the HL-RDHM and the lumped prediction system running at NWS RFCs. As shown in Fig. 5-3, the model features an upper zone where soil water is further divided into free and tension storages, and two groundwater layers beneath that contribute baseflow. Water is allowed to percolate from the upper zone to the shallow groundwater layer, and from the latter to the deep groundwater layer. The ET calculation first produces the ET demand, whereas the actual ET depends on both the ET demand, the availability of water remaining on canopy and surface, and the water in the upper zone tension storage once the surface storages are depleted. The streamflow in HEC-HMS is calculated by combining the surface runoff generated over impervious surface or over pervious surface of watersheds where upper zone is saturated, and baseflow from the groundwater layers. The runoff generated from an upstream subbasin is routed downstream using the Muskingum scheme.   Table 5-3 offers a comprehensive list of model parameters and methods of estimation.
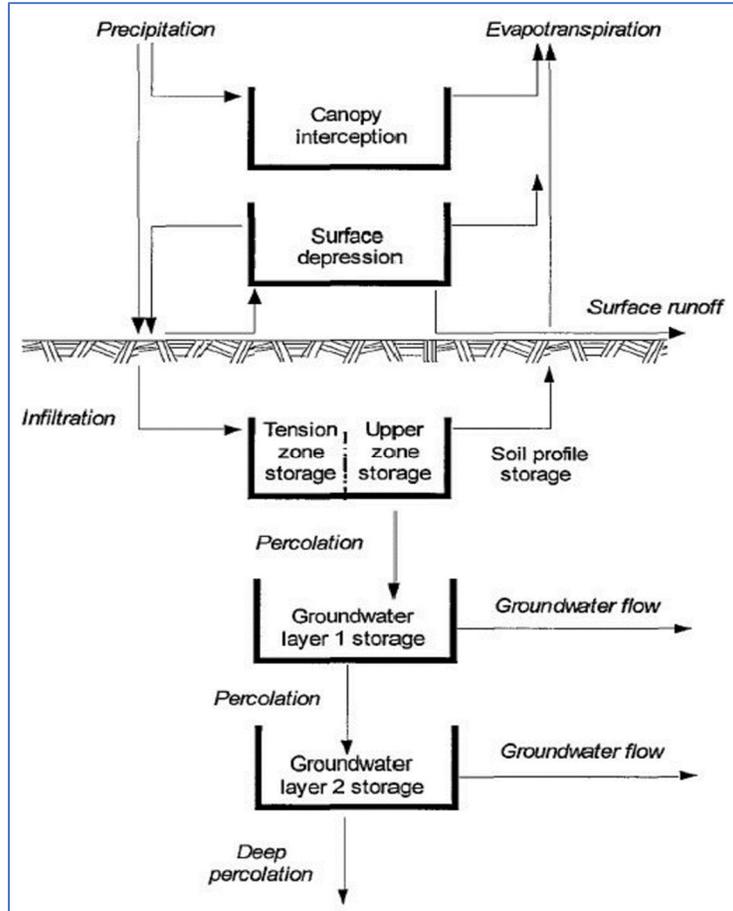
Figure 5-3   **Schematic of HEC-HMS surface and loss models. Note the Soil Moisture Accounting is chosen as the loss model for this implementation.**

Table 5-3   **HEC-HMS Model Parameters and Method of Estimation**

Types	Initial Estimate	Source of Initial Estimate
Canopy		**Simple Canopy**
Initial Storage (%)	0.00	Assuming dry canopy
Maximum Storage(in)	0.05	From land cover
Surface		**Simple Surface**
Initial Storage (%)	0.00	Assuming dry surface
Maximum Storage (in)	0.3	From soil survey (SSURGO)
Routing Method		**Muskingum**
Muskingum K (h)	12	Via NRCS velocity method
Muskingum X	0.25	Used the average value of X (0-0.5)
Transformed method		**Clark Unit Hydrograph**
Time of Concentration (h)	6.5	From Manning's equation
Storage Coefficient (h)	11.5	Based on observed hydrographs
Baseflow Method		**Linear Reservoir**
GW1 initial (cfs)	6.5	HEC-HMS default
GW2 initial (cfs)	6.5	HEC-HMS default
Loss		**Method of estimation**
Initial Soil Storage (%)	0.00	Assuming dry initial condition
Initial Groundwater 1 Storage (%)	0.00	Assuming dry initial condition
Initial Groundwater 2 Storage (%)	0.00	Assuming dry initial condition
% Impervious	0.5	From soil and land cover map
Max. Infiltration Rate (in/hr)	2	From soil texture
Soil Storage (in)	6	From soil texture
Tension Zone Storage (in)	4.8	80% of Soil storage
Soil Percolation Rate (in/hr)	1.5	From soil texture
GW 1 Storage (in)	5.4	Computed storage depth of a groundwater layer and put as a constant
GW 1 Percolation Rate (in/hr)	0.8	From observed hydrographs
GW 1 Coefficient hr)	14	Default
GW 2 Storage (in)	10	Computed storage depth of a groundwater layer and put as a constant
GW 2 Percolation Rate (in/hr)	0.0005	Default
GW 2 Coefficient (hr)	2500	Default
GW 1 Baseflow Coefficient (hr)	15	From observed hydrographs
GW 1 Baseflow Reservoirs	1	Guess-estimate
GW 2 Baseflow Coefficient (hr)	20	From observed hydrographs
GW 2 Baseflow Reservoirs	1	Guess-estimate

5.1.2 HL-RDHM

The HL-RDHM was developed in the early 2000s in the NWS Office of Hydrologic Development, now the Office of Water Prediction (OWP). The modeling system is grid-based, and it subsumes most modules that have been in operation at the River Forecast Centers, including the SAC-SMA model (Burnash et al. 1973), Antecedent Precipitation Index (API) model, unit hydrograph, and SNOW-17; it also incorporates new algorithms such as the kinematic wave routing, and upgrades to the SAC-SMA, including the SAC-HT (heat transfer), and SAC-HTET (heat transfer and evapotranspiration). Koren et al. (2003) offers a rather comprehensive overview of an earlier version of the model. HL-RDHM featured in both phases of the DMIP experiments (Reed et al. 2004 and Smith et al. 2012), where it was found to outperform most of contemporary distributed hydrologic models over clusters of catchments in central and western US. HL-RDHM has seen applications in the realm of flood and flash flood predictions (Reed et al. 2007; Cosgrove et al. 2012; Zhang et al. 2016).

In this project, we implemented HL-RDHM for the entire Lavaca River Basin and the bay watersheds on a full HRAP grid mesh (~ 4km in resolution). The implementation combines the gridded SAC-SMA as the water balance module with the kinematic routing scheme. The schematic of the SAC-SMA is illustrated in Fig. 5-4. Similar to the HEC-HMS SMA, the model divides the soil strata into an upper and a lower zone, with each zone further partitioned into tension and free water storages. Major differences from the HEC-HMS SMA include the following: 1) free water storage from the upper zone, rather than the groundwater zone, contributes to the interflow; and 2) the lower zone consists of both tension and free water storages. The SAC-SMA model requires seventeen parameters that are summarized in Table 5-4. Out of these seventeen parameters, eleven can be estimated from a combination of soil texture and land cover data through the so-called a priori estimation scheme.
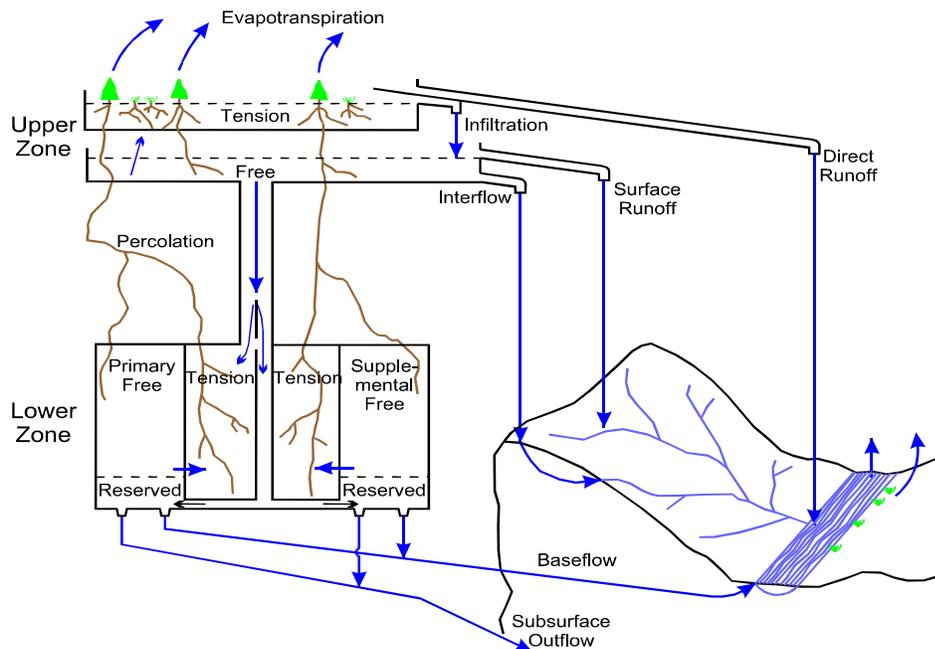
Figure 5-4   Schematic of SAC-SMA model.

31

The NWS maintains several versions of the a priori parameter grids. The one chosen for this project is the one based on the NRCS Soil Survey Geographic Database (SSURGO) and the National Land Cover Database 2006 (NLCD-2006; https://www.mrlc.gov/data/legends/national-land-cover-database-2006-nlcd2006-legend). The method of parameter estimation was originally developed by Koren et al., (2000), and was further refined by Zhang et al. (2011b). Zhang et al. (2012) compared HL-RDHM simulations using this parameter set versus those one based an earlier gridded parameter set derived from the State Soil Geographic Database, wherein the authors illustrated the superior performance of the former in soil moisture simulations.

Table 5-4   **SAC-SMA parameters and range of values**

Parameter Abbreviation	Parameter Name and unit	Range	Default
UZTWM	Upper Zone Tension Water Capacity (mm)	10-300	A priori
UZFWM	Upper Zone Free Water Capacity (mm)	5-150	A priori
UZK	Interflow depletion rate (day^{-1})	0.1-0.75	A priori
ZPERC	Ratio of maximum/minimum percolation rate	5-350	A priori
REXP	Shape parameter for percolation curve	1-5	A priori
LZTWM	Lower zone tension water capacity (mm)	10-500	A priori
LZFSM	Lower zone supplemental free water capacity (mm)	5-400	A priori
LSFPM	Lower zone primary free water capacity (mm)	10-1000	A priori
LZSK	Depletion rate of lower zone supplemental water storage (day^{-1})	0.01-0.35	A priori
LZPK	Depletion rate of lower zone primary water storage (day^{-1})	0.0001-0.05	A priori
PFREE	Percolation fraction to lower zone free water	0-0.8	A priori
PCTIM	Percentage connected impervious surface	0-100	0.001
ADIMP	Additional impervious surface	NA	0.0
RIVA	Riparian vegetated area	NA	0.04
SIDE	Deep recharge to channel baseflow	NA	0.0
RSERV	Lower zone free water not transferable to tension water	NA	0.2
EFC	Effective forest cover	NA	0.0

For each of the six parameters without a priori grids available, namely PCTIM, ADIMP, RIVA, RSERV, and EFA, a constant default value is assigned to the entire domain (see Table 5-4).

The conceptual framework of the channel routing model of HL-RDHM is illustrated in Fig. 5-4. The model assumes that each HL-RDHM pixel contains a channel segment and a collection of hillslope elements whose number depends on drainage density (see upper-right panel of Fig. 5-5). Each pixel drains to one of its eight neighboring pixels, and the direction of flow is encapsulated in the connectivity data set, which is derived from flow links generated using finer resolution digital elevation models (DEMs) using the algorithm outlined in Reed (2003). Over each pixel, the fast, or surface runoff components, are routed through conceptual hillslopes using 1-dimensional kinematic wave equation. The routed hillslope flow along with the slow components, namely the interflow and baseflow, enter the channel segment in the form of lateral inflow. The flow via the channel is routed towards the downstream pixel also using the kinematic wave equation.
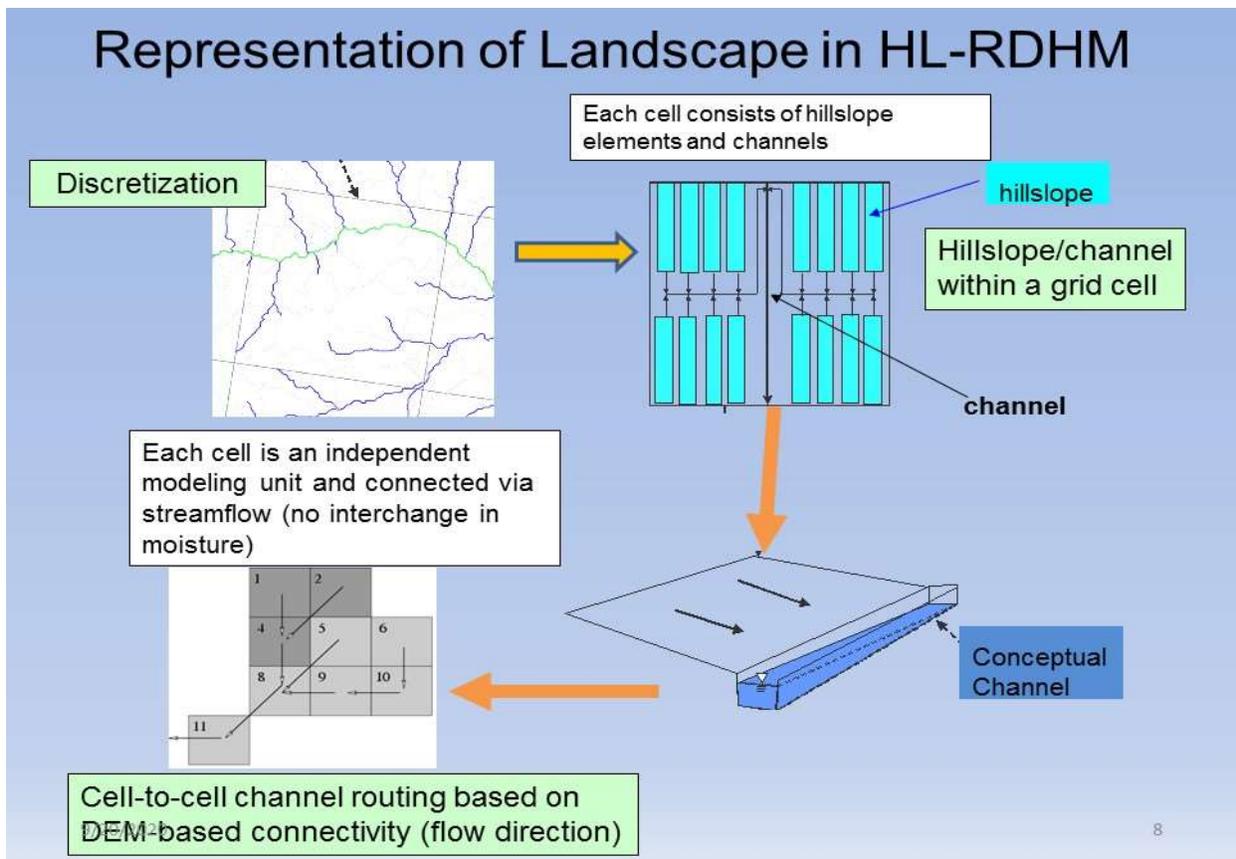
Figure 5-5   **Schematic of HL-RDHM routing model. Upper-left: an example of channel links from NHD-Plus; upper-right: a schematic of hillslope model within each model pixel; lower-left: a schematic of lateral flow from hillslope to the channel; and lower-left: routing of channel flow across model pixels**

33

With the assumption of shallow and spatially uniform overland flow depth with each hillslope unit, the continuity and momentum equations for the overland flow take the following forms:

$$\frac{\partial h}{\partial t} + L_h \frac{\partial q}{\partial x} = R_s \qquad (5\text{-}1)$$

$$q_{Lh} = \frac{2DS_h^{1/2}}{n_h} h^{5/3} \qquad (5\text{-}2)$$

where h denotes the average depth of overland flow, q the discharge per unit width; L_h the hill slope length, R_s the fast runoff; S_h the average slope; n_h hillslope roughness, D the drainage density. D is related to hillslope length: $D = \frac{1}{2L_h}$. The parameters n_h, D, S_h are typically estimated using DEM and hydrographic data.

The kinematic wave equations for the channel flow are quite similar to those of the open channel flow, except that the hydraulic geometry of the open channel A replaces the average depth h. These equations are given as follows:

$$\frac{\partial A}{\partial t} + \frac{\partial Q}{\partial x} = \left(q_{Lh} + R_g\right)\frac{f_c}{L_c} \qquad (5\text{-}3)$$

$$Q = q_0 A^{q_m} \qquad (5\text{-}4)$$

where A is the channel cross-section area; Q is the discharge, R_g the slow lateral flow; f_c the area of the pixel; and L_c the channel length within a pixel. q_0 and q_m are the coefficients that relate discharge to the cross-section area. These two coefficients can be estimated from observed discharge and cross-sectional areas for specific cross-sections where such data are available. USGS conducts such in situ measurements on a periodic basis for most of the active stations, and the data archive can be found from the online portal for each station. For example, the flow measurements for EDNT2 (Lavaca River at Edna) can be found at https://waterdata.usgs.gov/tx/nwis/measurements/?site_no=08164000&agency_cd=USGS).

A comprehensive description of the method of setting routing model and assigning a priori parameters can be found in the RDHM manual (NWS, 2008). The basic steps are summarized here, whereas additional processing steps and software packages involved are documented in **Appendix C**, and in the RDHM manual.

1. Calculating the cell-to-cell connectivity from the NHD-Plus data set (https://nhdplus.com/NHDPlus/NHDPlusV2_data.php) using the algorithm outlined in Reed (2003). Adjust the pixel area in the connectivity file based on the watershed drainage area provided by USGS.

2. Obtaining overland routing parameters, including n_h, D, S_h from a national a priori routing parameter database.

3. Collecting in situ measurements, including cross-section area, discharge, and flow velocity, from USGS, and estimating the channel routing parameters for each of the station via the rating curve method (see additional details in **Appendix C**).

4. Populating the grid with spatially varying channel routing parameters. Note that q_m estimated at a station is assigned to upstream pixels without modification, whereas q_o needs to be adjusted before being assigned to any upstream pixel to account for changes in the cross-section area along a channel. The adjustment is done using a simple geomorphological relation between cross-section area A and the size of upstream contributing area (Koren et al., 2004). For nested basins, this process starts at the station over the downstream end of the watershed, and then moves to upstream stations where q_m and q_o are re-estimated from in situ data. The latter estimates will be used to overwrite the earlier values assigned to the upstream pixels based on measurements at the downstream station. This process continues until measurement data from all stations are incorporated.

In HL-RDHM, ET consists of water evaporating from land surface and transpired by vegetation, the latter of which is extracted from upper zone tension water storage, and under stressed conditions from the lower zone storages as well. Actual ET depends on ET demand and water availability, and the former is determined using prescribed climatological monthly ET and adjustment factors that are invariant among years.

The a priori SAC-SMA and routing model parameters are refined first using HL-RDHM automatic calibration tool and then by manual adjustments. The automatic calibration tool of HL-RDHM implements the sequential line search (SLS) algorithm described in Kuzmin et al. (2008). The SLS seeks to minimize the following multi-scale objective function:

$$J = \sqrt{\sum_{k=1}^{n} \left(\frac{\sigma_1}{\sigma_k}\right)^2 \sum_{i=1}^{m_i} \left(q_{o,k,i} - q_{s,k,i}(X)\right)^2} \qquad (4\text{-}5)$$

Where $q_{o,k,i}$ and $q_{s,k,i}$ are average observed and simulated flow over time interval i and scale k, respectively; σ_1 and σ_k the standard deviation of observed flow at the base time scale (typically 1-h) and time scale k, respectively, and m_i is the number of ordinates at scale k; X is a particular combination of model parameters.

The modeling domain for HL-RDHM is shown in Fig. 5-6, where the five USGS stations of interest (Table 3-2) and the bay inlets are marked. The latter were identified by overlaying the flow connectivity grid on top of the streams and water bodies data from NHD-Plus - the inlet pixels are those situated at the terminal ends of the connectivity and roughly correspond to the streams listed in Table 3-1. The HL-RDHM model thus configured underwent both automatic and manual calibration. For simplicity and to ensure that water balance on a monthly scale is accurately captured, we only choose two scales, namely 240h and 720h, in performing the automatic calibration. The parameters that were adjusted include UZTWM, UZFWM, and UZK. These parameters are further adjusted based on visual inspection of observed and simulated hydrographs to minimize their differences. The calibrated parameter values can be found in the simulations (see Appendix C).

Figure 5-6   HL-RDHM modeling domain with USGS gauging stations and bay inlets.

5.1.3   NWM

The NWM is based on the WRF-Hydro system developed in the National Center for Atmospheric Research (Gochis et al. 2013; 2018) and has been transitioned to real-time operation at NWS since 2015 (Cosgrove et al., 2016). The NWM runs on a 1-km grid mesh and produces forecasts and analyses of streamflow, soil moisture and snowpack for the entire Conterminous US and Alaska. The NWM forecasts serves as a supplementary prediction system that complements the stage and discharge forecasts being produced at RFCs. Fig. 5-7 illustrates the various model components and a schematic of the process in producing forecast products.

Similar to RDHM, the major components include a gridded water balance module, a terrain routing module, and channel and reservoir routing modules.
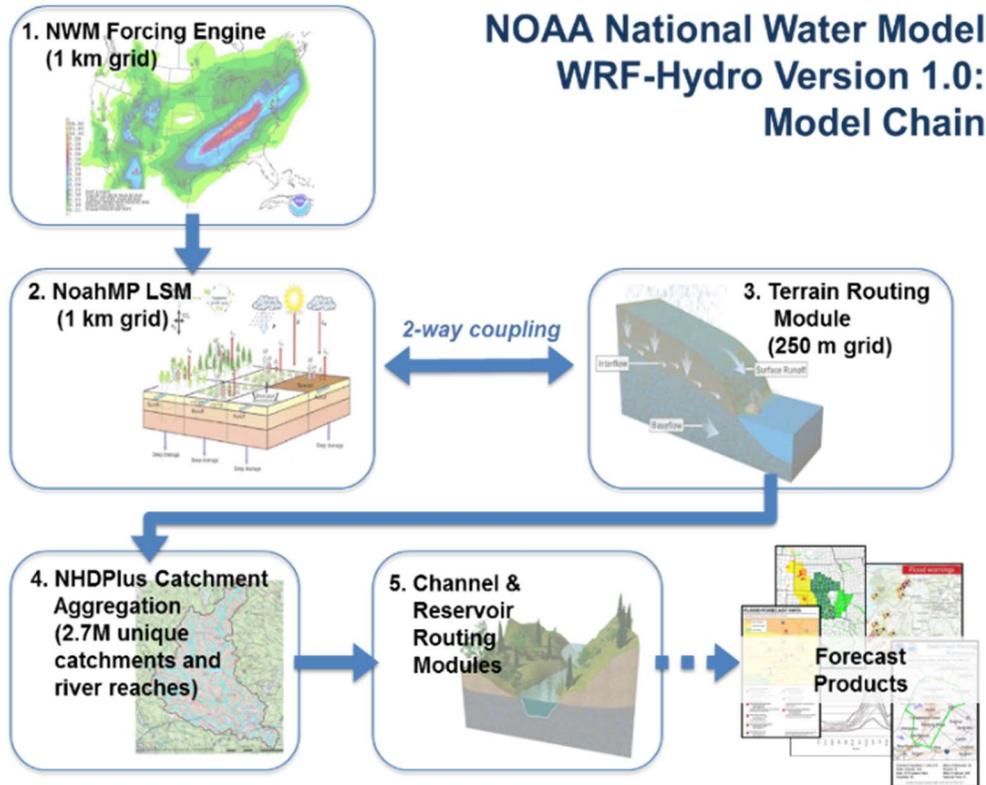
Figure 5-7   **Components of NWM and data flow diagram. Note the diagram applies to NWM 2.1 that is the current operational version. Source: NWS OWP.**

At present, the NWM uses the Noah-MP land surface model (Yang et al. 2011; Niu et al. 2011) for water balance calculations; a 2-D diffusive wave routing module for terrain routing; and the Muskingum method for channel routing (though five other options are available). The Noah-MP is an extension of the Noah model that is one of the models used in the NLDAS. Unlike SAC-SMA which simplifies soil strata into two buckets, Noah-MP offers explicit representations of soil layers down to 2-m depth and energy/water exchange among the layers. While HL-RDHM uses climatological ET demand, Noah-MP computes evaporation by performing radiative balance calculations for both canopy and soil. Additional notable features of the NWM include the follows:

- using 2-D, quasi-steady state Boussinesq model to simulate subsurface saturated flow across grid cells;

- considering runoff generated through infiltration excess, and allowing conversion from subsurface water to surface runoff through exfiltration;

- employing nested grids to model hillslope processes, i.e., computing water balance and hillslope routing on 250-m cells embedded in each 1-km pixel, and performing channel routing using connectivity built on the 1-km mesh;

- computing discharge for all stream reaches in the NHD-Plus database (see illustration in Fig. 5-8);

- using a simple nudging technique to adjust streamflow according to USGS streamflow observations (only available for real-time analysis/forecast);

- generating reservoir outflow using the level pool routing scheme;

Figure 5-8   **NWM prediction of streamflow along streams in the NHD-plus database. Source: NCAR.**

Note that NWM's use of stream reaches in the NHD-Plus database and the ability to perform reservoir routing also mark a step forward from HL-RDHM which only generates streamflow on a pixel basis and does not model flow through reservoirs. However, model calibration has been a challenge for NWM, and even at present only limited calibration was done for the operational version of NWM.

As an operational system, NWM is configured to run over different cycles, including analysis, short-range forecast, medium-range forecast, and long-range forecast (Fig. 5-9). The most relevant to the freshwater inflow estimation is the NWM real-time analysis, which is driven primarily by analysis forcings and therefore is less susceptible to errors in numerical weather forecasts. The analysis is produced on an hourly basis based on the analysis forcing data set. The

precipitation in this data set is created by blending the MRMS precipitation analysis and the analysis from the High-resolution Rapid Refresh model. Forcing variables excluding precipitation are interpolated from the HRRR analysis grids. The NWM real-time analysis and forecast products over the most recent 2-day window are available to the public through the National Center for Environmental Prediction (NCEP) ftp server.
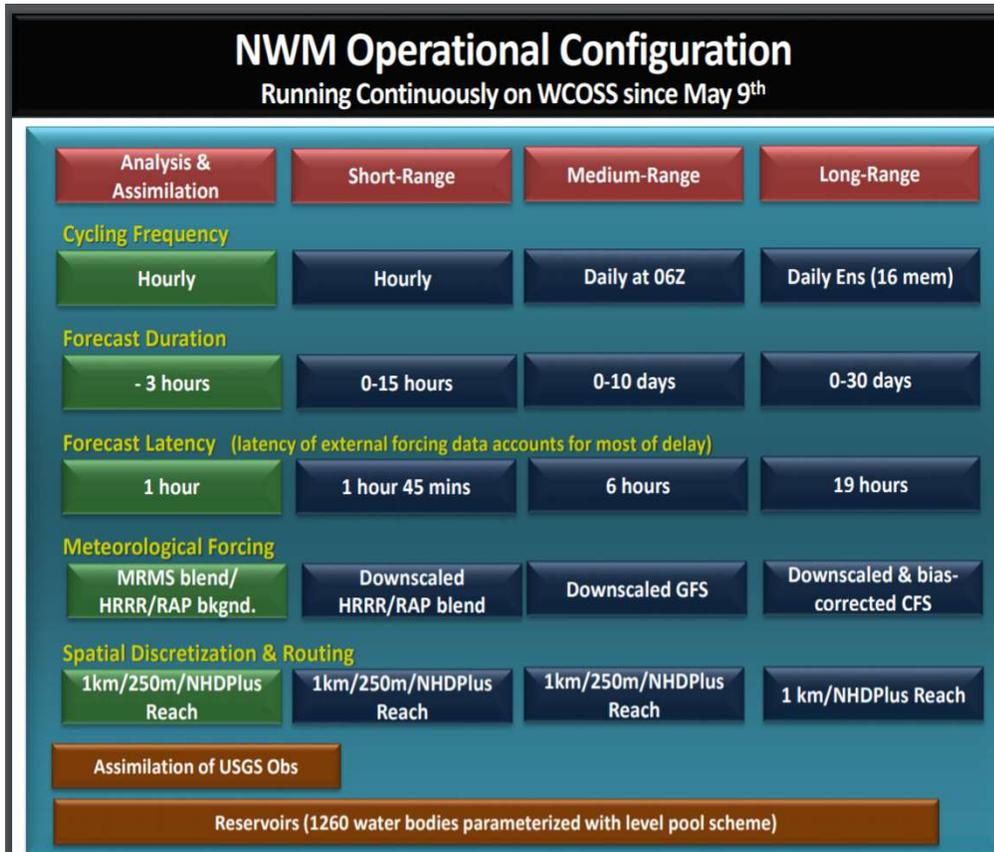
Figure 5-9   NWM prediction of streamflow along streams in the NHD-plus database. Source: NCAR

As indicated in the beginning of the section, NWM real-time analysis is only available over a short window (NWM only became operational since 2015), and is not suitable for a comprehensive assessment. Therefore, we chose to use NWM 1.2 reanalysis instead in this project. The NWM 1.2 reanalysis was created by running the version 1.2 of NWM over the 25-year window extending from 1993 to 2017, and the forcing variables were derived from the NLDAS-2. The reanalysis data is hosted on Amazon Web Service (AWS) and a description of the data set can be found at https://registry.opendata.aws/nwm-archive/.

In short, to retrieve the streamflow for a basin outlet or bay inlet, we first visually determine the feature ID of the stream segment in the closest proximity to the station in question. We then use these feature IDs as reference to extract the streamflow from the channel routing data (CHARTOUT files) to create time series of streamflow for each station. Fig. 5-10 illustrates the inlet locations superimposed on the NHD-Plus stream links which served as the basis for

extracting the streamflow from NWM. The processing steps and software packages involved can be found in **Appendix D**.
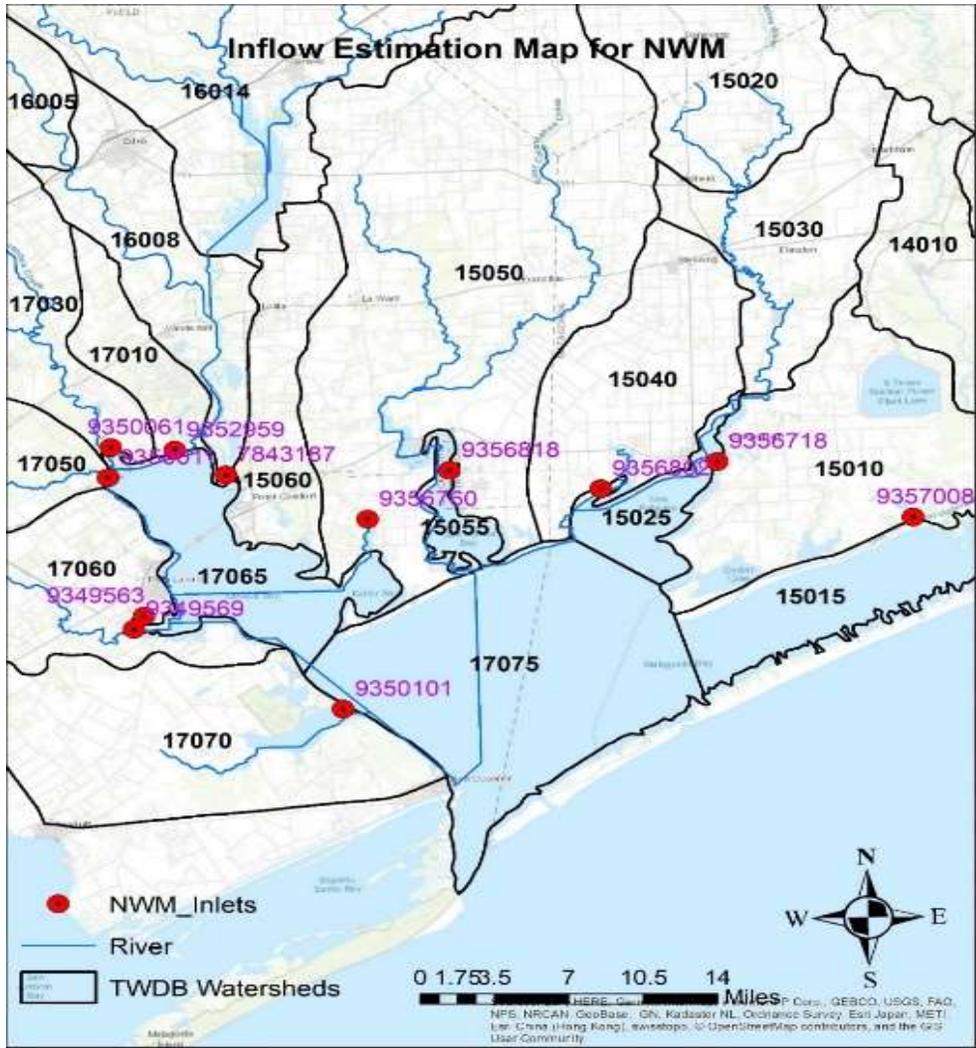
Figure 5-10   NWM inlets to Matagorda Bay. The inlets were determined from the NHD-plus database. Source: NCAR.

5.2 Model Performance Assessment

The three models, namely the TxRR, HEC-HMS and HL-RDHM were run using the NLDAS-2 forcing data to be consistent with that used in generating the NWM reanalysis. It is worth noting that the NLDAS-2 precipitation data since 2003 was created by temporally disaggregating 24-h gauge reports, mostly from NWS Cooperative Observer (COOP) network, using the NCEP Stage II hourly radar-only precipitation mosaic. As such, NLDAS-2 and MPE precipitation products examined in Section 2 share similar, though not identical ingredients. Past studies, such as Nan et al. (2010) illustrated that the two data sets are indeed closely correlated, though MPE is considered to be an overall superior product as it benefits from a number of algorithmic enhancements and manual quality controls. In this project, we picked the 2003-2017 as the period for performing our assessment to avoid potential complications associated with the change in the way the precipitation data set was created that took place around 2003. Therefore, we expect the relative performance of models driven by the NLDAS-2 forcings to mimic, in a qualitative fashion, that driven by the MPE data. As the latter will eventually serve as the source of precipitation input to the MMIPS, the results of the comparisons will help anticipate the accuracy of inflow products derived using each model.

The calibration-validation strategy consists of the following elements. The first year, i.e., 2003, is used as the warm-up window to reduce the influence of initial conditions. HEC-HMS and HL-RDHM are each calibrated using streamflow observations over 2004-2013, and the model simulations using the calibrated parameters are generated for 2014-2017. TxRR simulations are performed using the default parameter values obtained from the TWDB, which are derived from earlier calibration efforts, and no further calibration is performed. The simulations are assessed using conventional metrics including percentage bias (PB), Pearson's correlation (R), and root mean squared error (RMSE). These metrics are defined as follows:

$$PB = \frac{\sum_{i=1}^{n}(Q_{o,i}-Q_{s,i})}{\sum_{i=1}^{n}Q_{o,i}} \times 100 \tag{5-6}$$

$$R = \frac{\sum_{i=1}^{n}(Q_{o,i}-\bar{Q}_{o,i})(Q_{s,i}-\bar{Q}_{s,i})}{\sqrt{\sum_{i=1}^{n}(Q_{o,i}-\bar{Q}_{o,i})^2}\sqrt{\sum_{i=1}^{n}(Q_{s,i}-\bar{Q}_{s,i})^2}} \tag{5-7}$$

$$RMSE = \sqrt{\frac{\sum_{i=1}^{n}(Q_{s,i}-Q_{o,i})^2}{n}} \tag{5-8}$$

Where $Q_{o,i}$ and $Q_{s,i}$ are observed and simulated streamflow, respectively; and n is the number of records in the time series. In addition to these metrics, we also employ the Kendall rank correlation coefficient (Kendall, 1938) to characterize the similarity between simulated and observed flow on a seasonal basis to avoid disproportionate impacts of larger values on linear correlation coefficients. The performance of member models is first examined using the three metrics computed for each model for the calibration and validation periods individually. Note that the latter two metrics, R and RMSE, are computed for both monthly and daily scales. Then, the ability of each model in reproducing the seasonal cycle and interannual variation of streamflow is contrasted. Last, the model simulated daily series are compared for four selected

historical high flow events to gain a concrete understanding of differential model dynamics for such events.

5.2.1 Overview of model performance

Fig. 5-11 shows the comparisons of annual mean simulated and observed streamflow over the calibration (2004-2012) and validation periods (2013-2017) for the five gauged watersheds listed in Table 3-2. Among the watersheds, EDNT2 (Lavaca River) is associated with the largest overall observed volume, followed by MTPT2 (Tre Palacios River) and HTST2 (Navidad River), whereas the flow volume is much smaller for NGCT2 (Garcitas Creek) and PLPT2 (Placedo Creek). When comparing the simulated flow from the four models, it is evident that the relative magnitude is consistent between the two periods, yet varies widely among the watersheds. Taking EDNT2 for example, NWM produces the largest volume, followed by TxRR, HL-RDHM, and HEC-HMS. But for MTPT2 and HTST2, TxRR produces the largest flow volume.
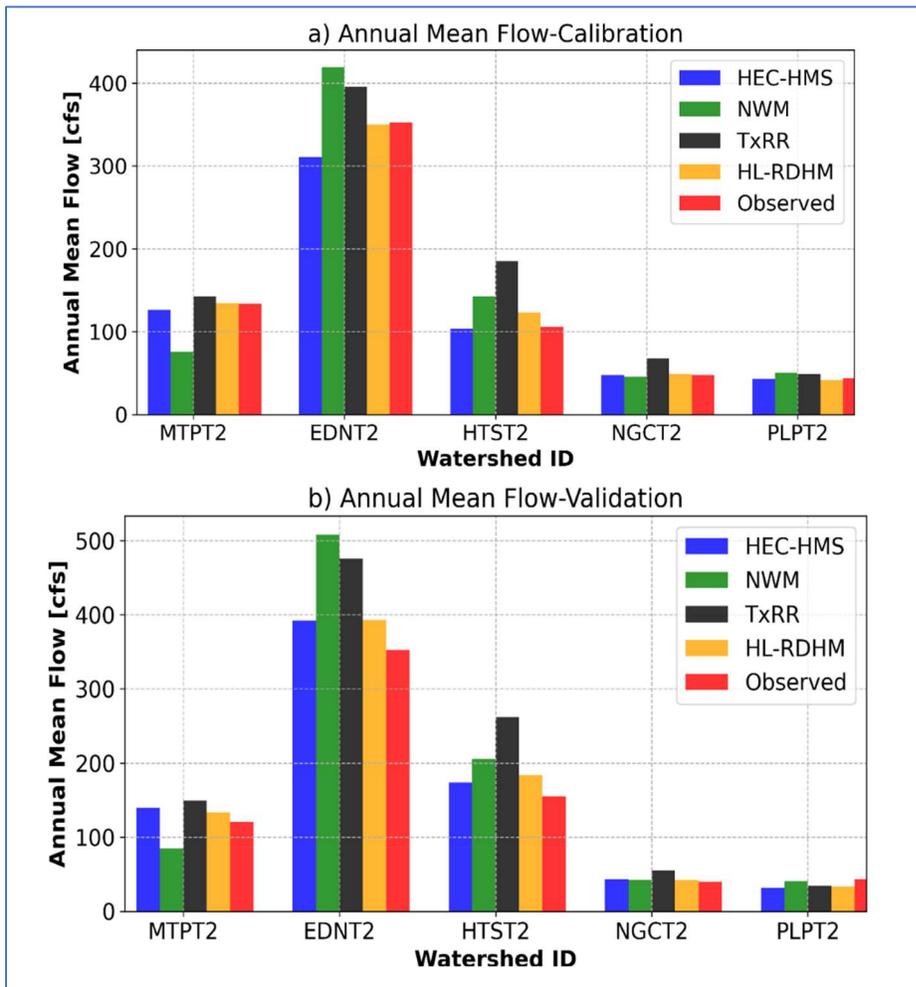
Figure 5-11   **Comparisons of annual mean flow produced by the four member models for the five USGS stations. Shaded rectangles mark observed flow.**

42
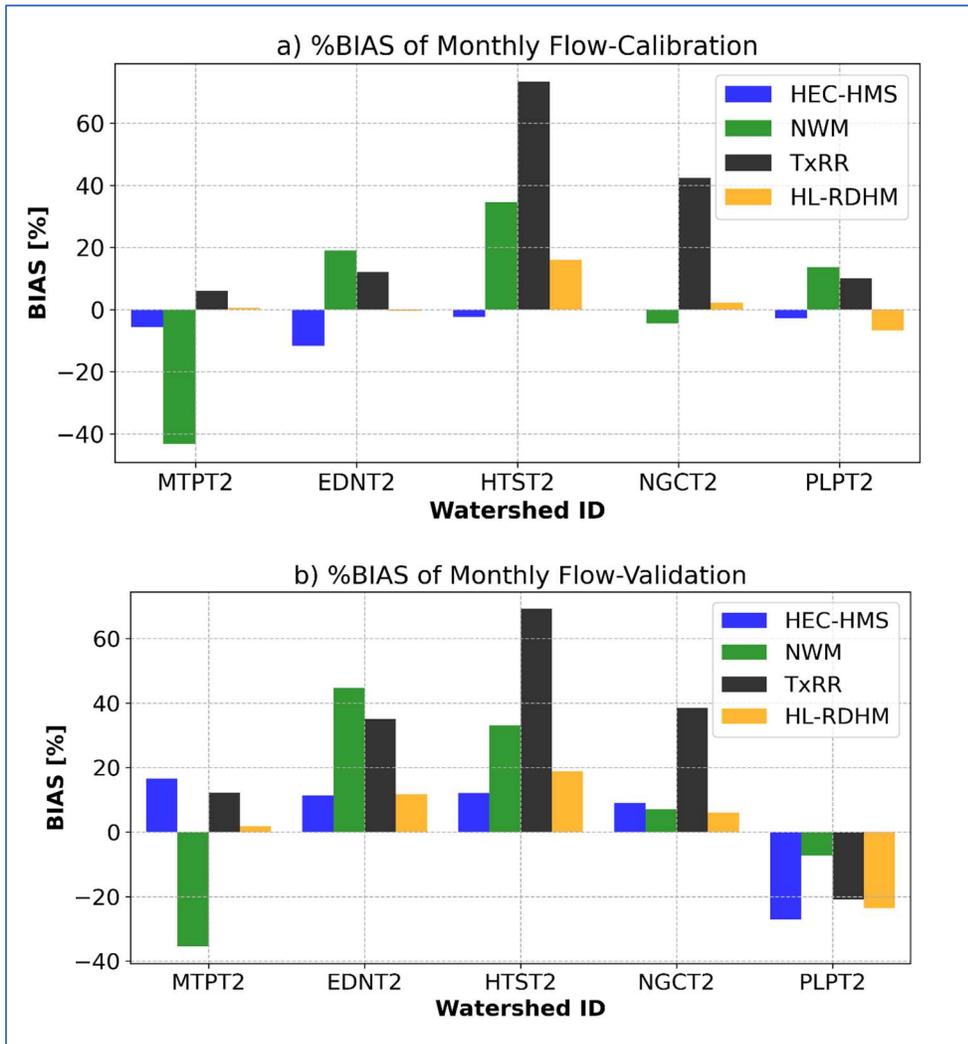
Figure 5-12   Comparisons of percentage bias between simulated flow by the four member models and observed flow at five upstream USGS stations (marked using SHEF ID). Shown are the results computed at monthly scale, and for a) calibration and validation (b) periods.

Fig. 5-12 compares the PB of simulated flow for the member models for the two periods. It appears that the relative performance of models in terms of bias varies across watersheds without a single best performer. In general, PB is more pronounced for the validation period. Additional notable observations include the following:

The PB of simulations based on the baseline model TxRR varies widely. For the calibration period, it is close to neutral for three watersheds, namely MTPT2, EDNT2, and PLPT2, and in the meantime it is quite large for the other two watersheds (HTST2 and NGCT2), exceeding 60% for HTST2. The PB of TxRR simulations is more pronounced for the validation period, though the distribution of bias across watersheds is broadly similar to that for the calibration period.

HEC-HMS and HL-RDHM outperform TxRR and NWM in terms of overall consistency in bias for the calibration period. For EDNT2, the largest watershed, HL-RDHM simulations exhibit the best (nearly neutral) PB for the calibration period, and second-best PB for the validation period (with HEC-HMS simulations being the best). The PB of NWM reanalysis is mixed for both periods. For MTPT2, the PB is negative for both periods, whereas it is conspicuously positive for EDNT2 and HTST2, and particularly so for the validation period.

The comparisons of correlation and RMSE are shown in Figs. 5-13, and 5-14, respectively. For the calibration period, both monthly and daily flow based on TxRR exhibit the highest correlation for three out of five watersheds, including EDNT2. The performance of the other models is mixed over this period. Daily flow from HL-RDHM appears to underperform other models. For the validation period, HEC-HMS slightly outperforms other models for three out of five watersheds at the monthly scale, whereas it outperforms all other models. TxRR performs reasonably well for most of the watersheds. NWM underperforms over EDNT2, with its both monthly and daily flow exhibiting much lower correlation than the corresponding results from the other three models. HL-RDHM tends to perform relatively poorly for some of the basins at a daily scale, though it produces reasonable correlation at the monthly scale.
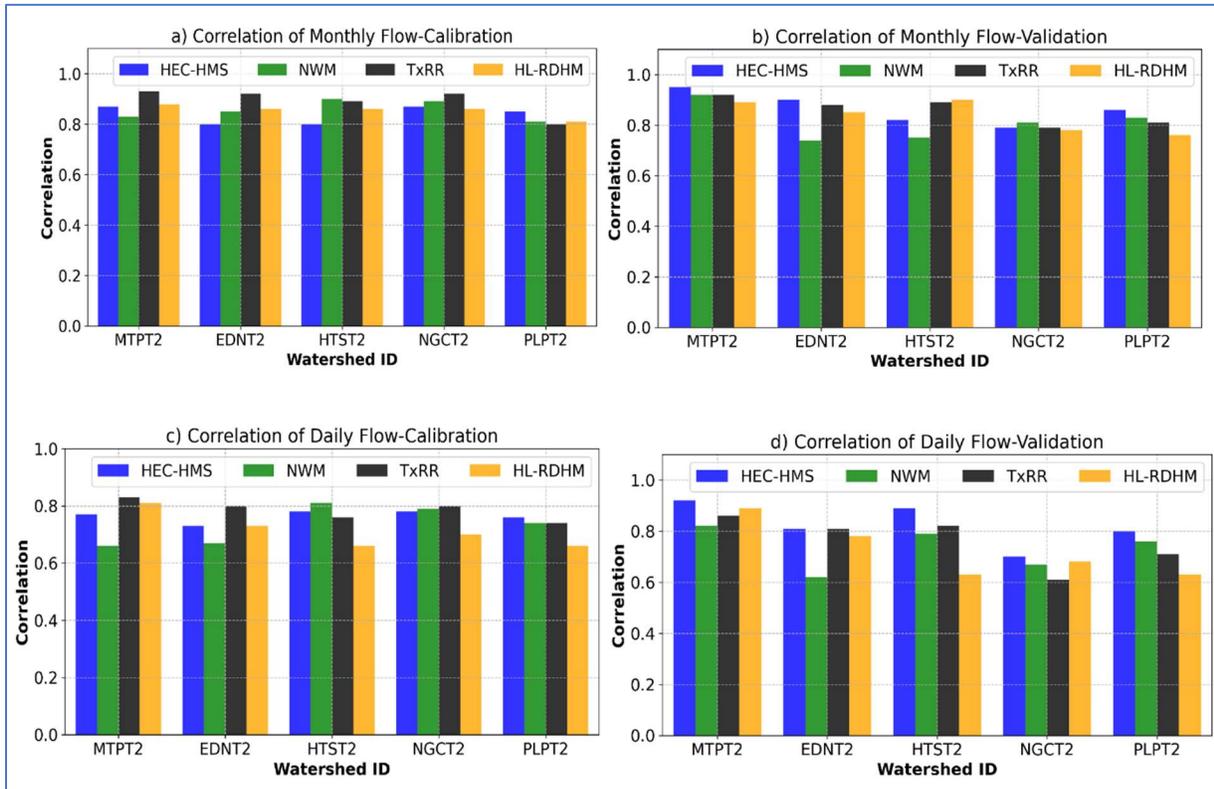
Figure 5-13   Comparisons of correlation between simulated flow by the four member models and observed flow at five upstream USGS stations (marked using SHEF ID). Shown are the results computed at monthly and daily scales, and for the calibration and validation periods.
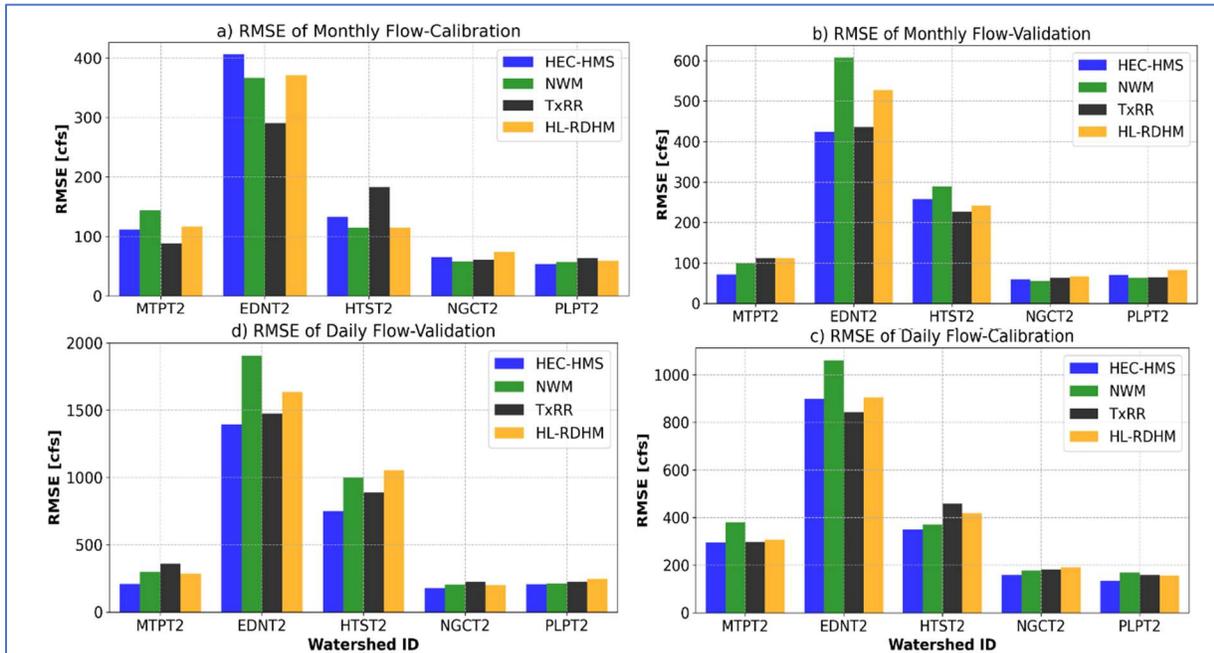
Figure 5-14 **Comparisons of RMSE between simulated flow by the four member models and observed flow at five upstream USGS stations (marked using SHEF ID). Shown are the results computed at monthly and daily scales, and for the calibration and validation periods.**

When comparing Figs 5-13 and 5-14, it is evident that the relative magnitude of RMSE broadly echoes that of correlation in the following sense: a) TxRR slightly outperforming other models for the calibration period, and b) HEC-HMS is an overall the best performer for the validation period, and its outperformance is uniform across watersheds for the validation period. Note that over the validation period, NWM performs rather poorly for the three most important watersheds (MTPT2, EDNT2 and HTST2) due to a combination of relatively large bias and low correlation of the simulated flow (Figs. 5-13 and 5-14). Tables 5-5 and 5-6 summarize the RMSEs for monthly and daily simulated flow for calibration n and validation periods, respectively, where the best performer for each watershed is highlighted in green.

Table 5-5 **RMSE of monthly and daily simulations – Calibration Period, with best performers highlighted in green**

Station	Monthly RMSE (cfs)				Daily RMSE (cfs)			
	TxRR	HEC-HMS	NWM	HL-RDHM	TxRR	HEC-HMS	NWM	HL-RDHM
MTPT2	88	111	144	116	296	295	379	307
EDNT2	291	406	367	371	842	898	1060	903
HTST2	183	133	114	115	458	350	370	418
NGCT2	60	65	58	74	182	158	177	190
PLPT2	63	54	57	59	159	135	169	156

Table 5-6 **RMSE of monthly and daily Simulations – Validation Period; best performers highlighted in green**

Station	Monthly RMSE (cfs)				Daily RMSE (cfs)			
	TxRR	HEC-HMS	NWM	HL-RDHM	TxRR	HEC-HMS	NWM	HL-RDHM
MTPT2	112	71	100	112	358	209	298	286
EDNT2	435	424	607	527	1473	1393	1905	1634
HTST2	226	258	289	242	888	750	1001	1053
NGCT2	63	60	56	67	225	178	205	200
PLPT2	64	71	62	82	225	206	211	247

At the monthly scale, the performance of member models is mixed as judged by RMSE, whereas at the daily scale, HEC-HMS emerges as perhaps the best performer among the models. TxRR performs well for the three larger watersheds, and particularly so for EDNT2, the largest watershed. NWM and HL-RDHM perform comparably for the validation period, with HL-RDHM outperforming NWM for the EDNT2 but underperforming NWM for the two smaller watersheds (NGCT2 and PLPT2). Note that the relative performance of member models is determined as much by the effort of calibration as by the realism of model physics or appropriateness of initial parameterization. Among these models, TxRR was calibrated in the 1990s, and this may explain its reasonably good performance for the earlier period and large bias for the later one. NWM was not calibrated specifically for the region, but it nevertheless performs relatively well for some of the smaller basins. By contrast, HEC-HMS underwent quite extensive automatic and manual calibration focusing on optimizing daily flow, and therefore it is unsurprising that it performs well at a daily scale. The calibration for HL-RDHM entailed searching in a limited parameter space and this may have constrained the accuracy of the simulation for both periods.

5.2.2 Season Cycle and Interannual Variation

A key potential advantage of models such as HEC-HMS and NWM lies in their use of energy-based ET schemes, which account for the impacts of temporal variation in forcings on ET demand. In order to determine whether the incorporation of such schemes indeed yields improvement to the water balance calculation, we compare the seasonal as well as interannual streamflow volumes produced by the member models. Fig. 5-15 shows the comparison of mean monthly flow for each watershed, and Table 5-7 summarizes the proximity of simulated monthly to observed values via Kendall rank correlation coefficient tau.

Among these watersheds, the seasonal distribution of streamflow varies (Fig. 5-15). When focusing on the calibration period, the observed streamflow exhibits summertime peak over three watersheds near the bay, i.e., MTPT2, NGCT2, and PLPT2, whereas the peak is attained in the winter over the upstream watershed HSHT2. For the largest watershed EDNT2, the streamflow apparently exhibits multiple peaks, including a primary one in the early summer and a lesser one in the winter, most likely a result of combining flows from upstream and downstream basins with differing seasonal patterns. The seasonal distribution for the validation period differs considerably from that for the earlier period. Interestingly, the monthly flows for all five watersheds exhibit a conspicuous peak in August, which reflects the disproportionate influence of Hurricane Harvey that took place in August 2017.

Among the models, there does not appear to be a clear split between TxRR and the rest three models with more sophisticated water balance and ET schemes (Table 5-7). In fact, TxRR performs reasonably well for two of the three larger watersheds (MTPT2 and EDNT2) over both the calibration and validation periods. For MTPT2, it nearly perfectly reproduces the observed monthly flow for the calibration, and it also performs remarkably well for the validation period with Kendall's tau=0.91. However, for HSHT2, the northmost watershed, TxRR grossly overestimates the flow during spring and early summer (Fig. 5-15). This overestimation is also seen for EDNT2, albeit with lesser severity. Note that all the other three models produce reasonable monthly flow for HSHT2 over the calibration period. It is also worth noting that the alternative models all perform quite well for the three watersheds over the south (MTPT2, NGCT2 and PLPT2) for the calibration period (Fig. 5-15; Table 5-7). Again, the best performing model is highlighted in green. NWM produces the highest rank correlation for the latter two watersheds. Broadly speaking, the performance of models does not translate to the validation period (Fig. 5-16; Table 5-7), and the relative performance among models is not sufficiently consistent to draw any meaningful conclusions about the role of water balance schemes. For example, NWM features arguably the most complex water balance scheme and it does appear to outperform TxRR in terms of reproducing the seasonality of flow for some of the watersheds for the calibration period. NWM, moreover, has the clear downside of exaggerating the springtime flow for EDNT2, which raises questions about the physicality of its water balance and ET calculation in the Lavaca River drainage.

Table 5-7   **Kendall Rank Correlation for simulated mean monthly flow; best performers highlighted in green**

Station	Calibration				Validation			
	TxRR	HEC-HMS	NWM	HL-RDHM	TxRR	HEC-HMS	NWM	HL-RDHM
MTPT2	0.70	0.64	0.61	0.67	0.91	0.70	0.73	0.45
EDNT2	0.61	0.61	0.52	0.52	0.64	0.67	0.64	0.52
HTST2	0.52	0.52	0.61	0.55	0.79	0.58	0.76	0.76
NGCT2	0.61	0.52	0.85	0.73	0.64	0.67	0.73	0.73
PLPT2	0.76	0.48	0.82	0.48	0.67	0.70	0.61	0.45
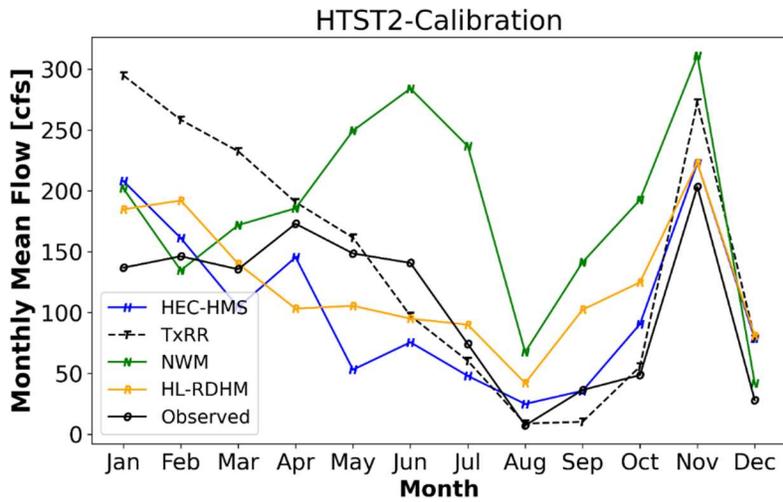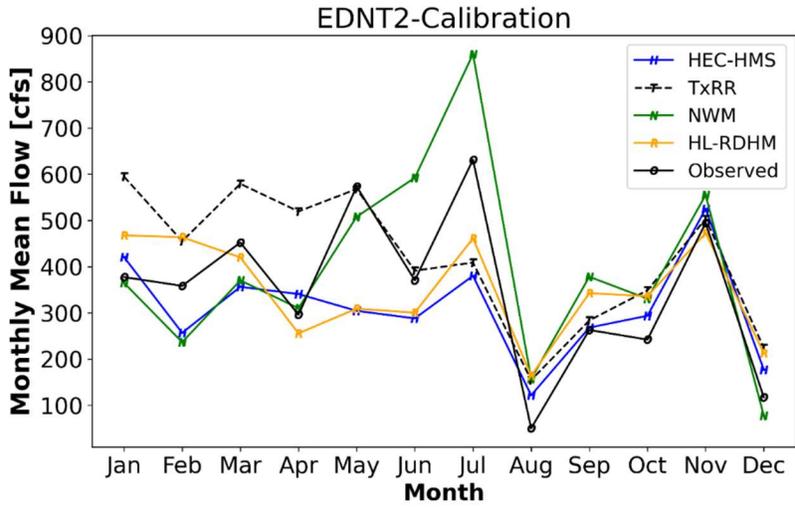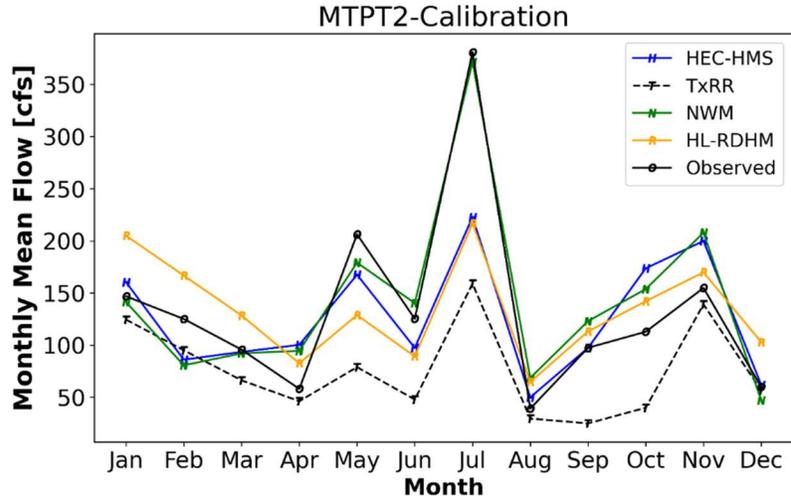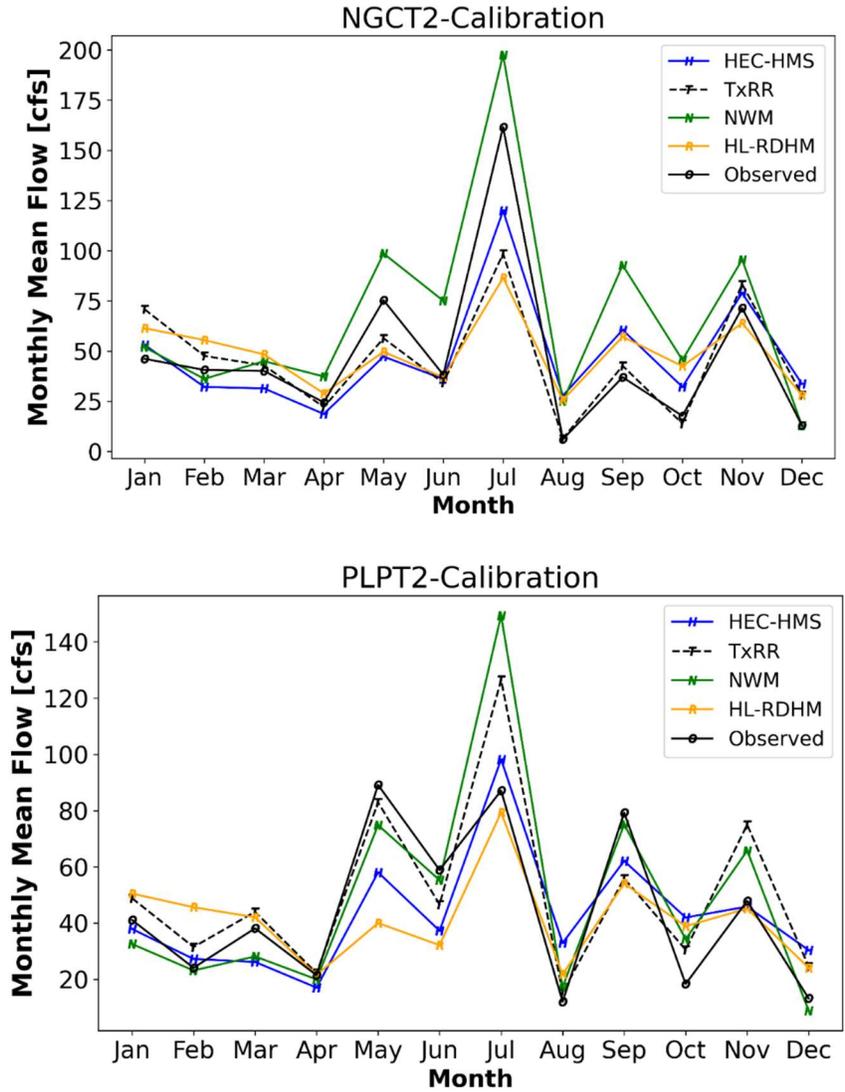
Figure 5-15   **Mean monthly observed flow and simulated flow from four member models for each gauged watershed over the calibration period.**
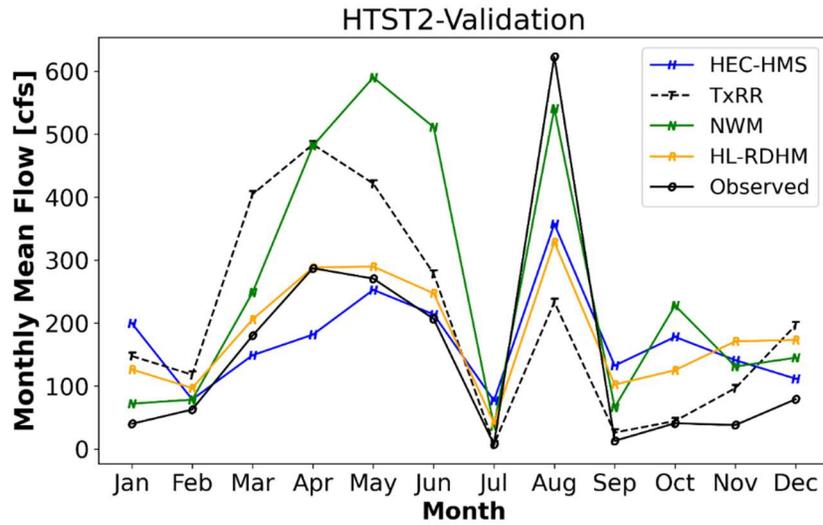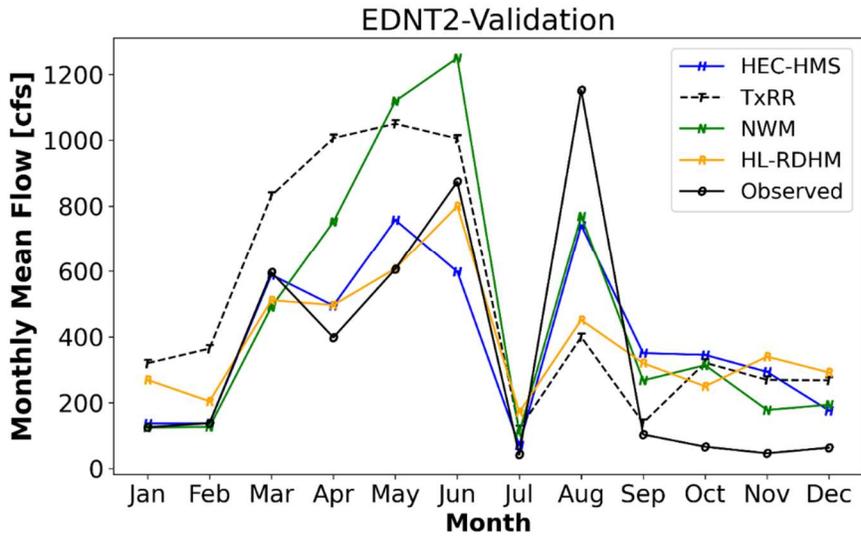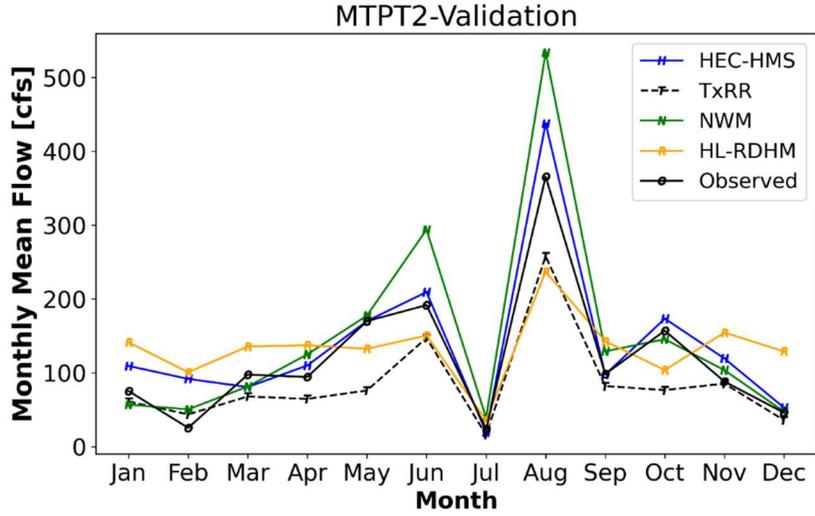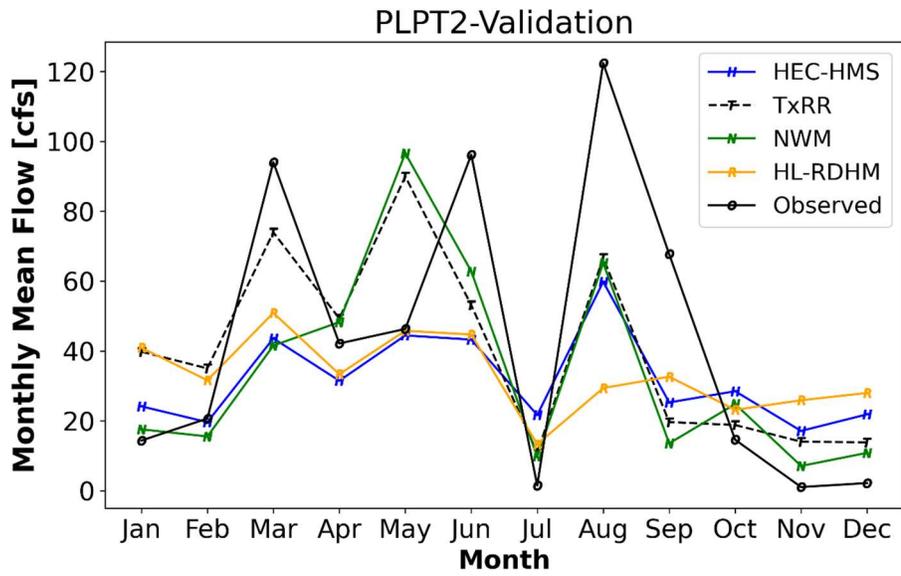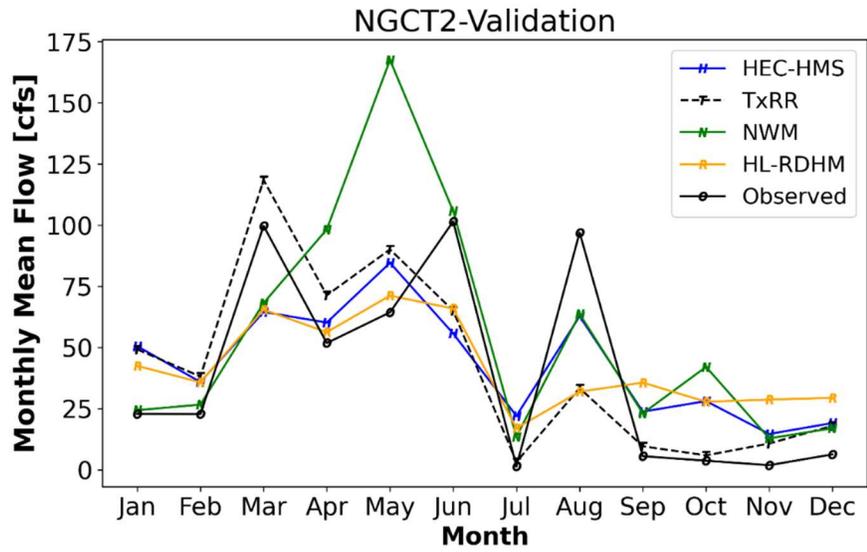
Figure 5-16   **Mean monthly observed flow and simulated flow from four member models for each gauged watershed over the validation period.**

The Pearson's correlation for simulated annual mean flow from each model is shown in Table 5-8. It appears that all models are able to accurately depict the interannual variation for both periods, and the differences among models are quite minor. For the calibration period, NWM performs consistently well across the basins, though the correlation is only marginally higher than TxRR. For the validation period, however, NWM's performance trails behind TxRR and the other two models. HEC-HMS, the other model that features a physically-based ET scheme, in fact underperforms TxRR for a majority of basins for the calibration and its performance is mixed for the validation period. For both periods, HL-RDHM, despite its reliance on climatological ET demands, performs reasonably well for all watersheds except PLPT2: its correlation values are only slightly below those for NWM for the calibration period, and are comparable to NWM and TxRR for the validation period. It is worth pointing out that the ET process as represented by HEC-HMS, NWM and HL-RDHM depends not only on ET demand but also on its interaction with soil water storage. It is possible that the underperformance of HEC-HMS has to do with its relatively simplistic uptake scheme which only withdraws water from the upper zone to the canopy. By contrast, the SAC-SMA in HL-RDHM allows water to be withdrawn from both upper and lower zone storages. These explanations, however, are difficult to corroborate at present without detailed data on soil moisture and percolation.

Table 5-8   **Pearson's Correlation for simulated annual flow; best performers highlighted in green**

Station	Calibration				Validation			
	TxRR	HEC-HMS	NWM	HL-RDHM	TxRR	HEC-HMS	NWM	HL-RDHM
MTPT2	0.98	0.98	0.98	0.96	0.98	0.96	0.99	0.98
EDNT2	0.98	0.92	0.99	0.97	0.96	0.96	0.90	0.93
HTST2	0.95	0.91	0.96	0.96	0.91	0.85	0.87	0.91
NGCT2	0.99	0.94	0.99	0.97	0.93	0.93	0.96	0.98
PLPT2	0.92	0.91	0.94	0.87	0.91	0.97	0.95	0.89

As the validation period encompasses only 5 years, the validation statistics may be distorted by a few large events. The outperformance of NWM over the earlier period may in fact be a result of enhanced representation of runoff processes and water balance, given that the model did not undergo systematic calibration as did HEC-HMS and HL-RDHM.

5.2.3 Model Behaviors during historical high-flow and low-flow events

To further illuminate differences among the models in reproducing streamflow, we closely examine the flow series from the four models over six episodes. These include four historical storm events which produced high flows over either the upstream and downstream parts of the Lavaca River Basin, and two neighboring episodes during the 2011 drought. Note that four of the episodes occurred prior to 2013 fall within the calibration period, whereas two episodes were in the validation period. These events are summarized in Table 5-9:

Table 5-9   Events for model comparisons

Type	Event	Storm Type	Reference
High Flow	Nov 2004	Frontal System	https://www.weather.gov/crp/20041121_Flood
	Apr 2009	Thunderstorm	https://www.weather.gov/hgx/severe_events_april
	Apr 2014	Thunderstorm	N/A
	Aug 2017	Hurricane Harvey	https://www.weather.gov/hgx/hurricaneharvey
Low Flow	Aug-Sep 2011	N/A	https://senate.texas.gov/cmtes/82/c510/0110BI-JohnNielsen-Gammon.pdf
	Sep-Oct 2011	NA	

Note that the Nov 2004 and Aug 2017 storms were both large enough to produce flooding across the Lavaca River Basin, whereas the Apr 2009 and Apr 2014 storms were severe thunderstorms with limited spatial coverage. Both latter events produced flooding over the upstream portion of the watershed and the impacts over the lower reaches were limited. Our comparison will focus on model response at the northmost subbasin HTHS2 (Navidad River above Hallettsville), and the southmost subbasin PLPT2 (Placedo Creek near Placedo) that is situated close to the bay.

The results for the Nov. 2004 event are shown in Fig. 5-17. For this event, all models are able to reasonably resolve the magnitude of flood peaks for the HTST2. Among these models, the simulation from HEC-HMS presents the closest match to the observation. TxRR, HL-RDHM and NWM all over-simulate the event peak, and the over-simulation is the most severe for NWM. By contrast, for PLPT2, all models perform relatively poorly: TxRR and NWM produce peaks much higher than the observed, whereas HEC-HMS and HL-RDHM both under-simulate. Among the models, NWM produces a peak that is nearly four times that observed. This over-simulation by NWM is consistent with the positive bias it exhibits on an overall basis and for the spring (Figs. 5-11 and 5-15, respectively). It is also interesting to note that NWM and TxRR both under-simulate the initial small peak on Nov 18 while exaggerate the major peak.
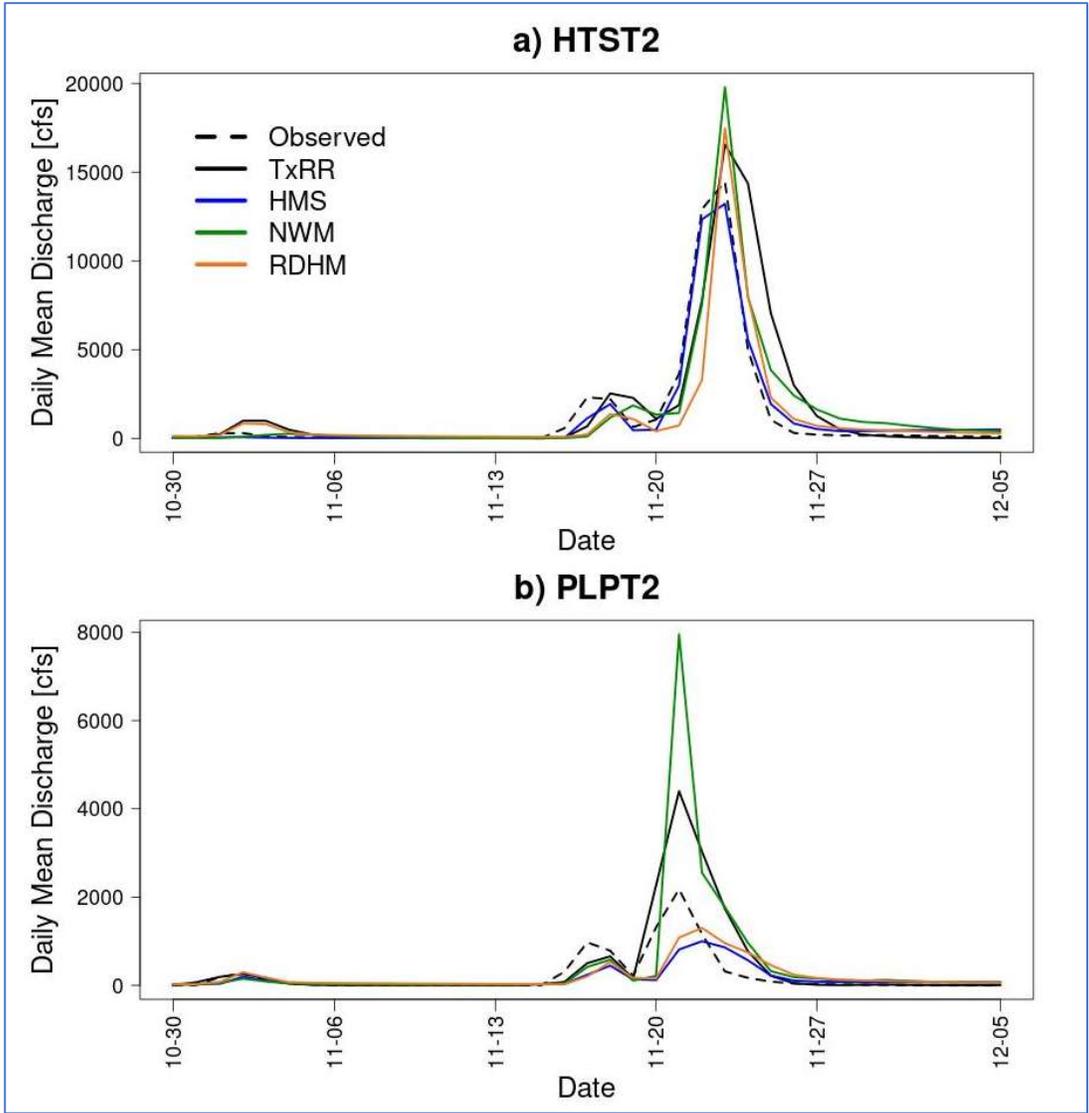
Figure 5-17   **Comparisons of simulated flow from member models and observed for the Nov. 2004 storm event.**

The hydrographs for the Apr 2009 event are shown in Fig. 5-18. For HTST2, all models except for HL-RDHM perform rather well, and HEC-HMS and NWM almost perfectly reproduced the flood peaks. TxRR and HL-RDHM both under-simulate the peak, with the peak by the latter model only about 1/3 of the observed. For PLPT2, the storm failed to produce any significant streamflow, mostly because the area is outside of the storm coverage. All models tend to over-simulate the streamflow, with the severe bias exhibited by the results of NWM and TxRR. Relatively speaking, the flow simulations from HEC-HMS and HL-RDHM are closer to observations than those from the other two models.
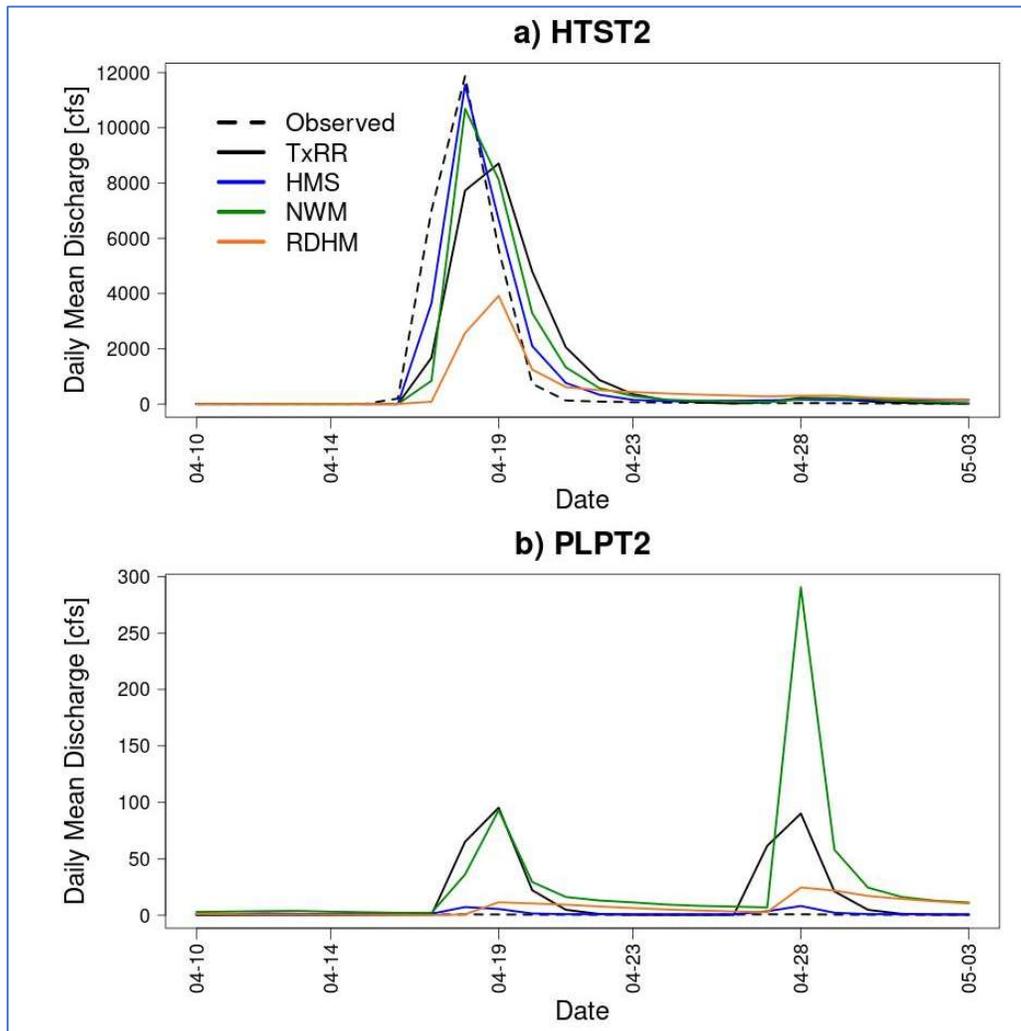
Figure 5-18   **Comparisons of simulated flow from member models and observed for the Apr. 2009 storm event.**

Fig. 5-19 shows the hydrograph comparisons for the Apr. 2014 event. Similar to the Apr. 2009 event, this event also featured heavy rainfall over the north. For HTST2, the models were all able to reproduce the peak with reasonable accuracy. Among the models, HEC-HMS produces the lowest peak that is nearly 3000cfs below the observation, whereas HL-RDHM conspicuously over-simulates. The peaks based on TxRR and NWM simulations are comparable and quite close to the observed. For PLPT2, the peak discharge occurred at a later date (around April 24) with much subdued magnitude (~700cfs). Interestingly, all models severely under-simulate this peak. HEC-HMS, for example, almost entirely misses the event, while hydrographs from other models show small bumps that are poorly correlated with the observations.
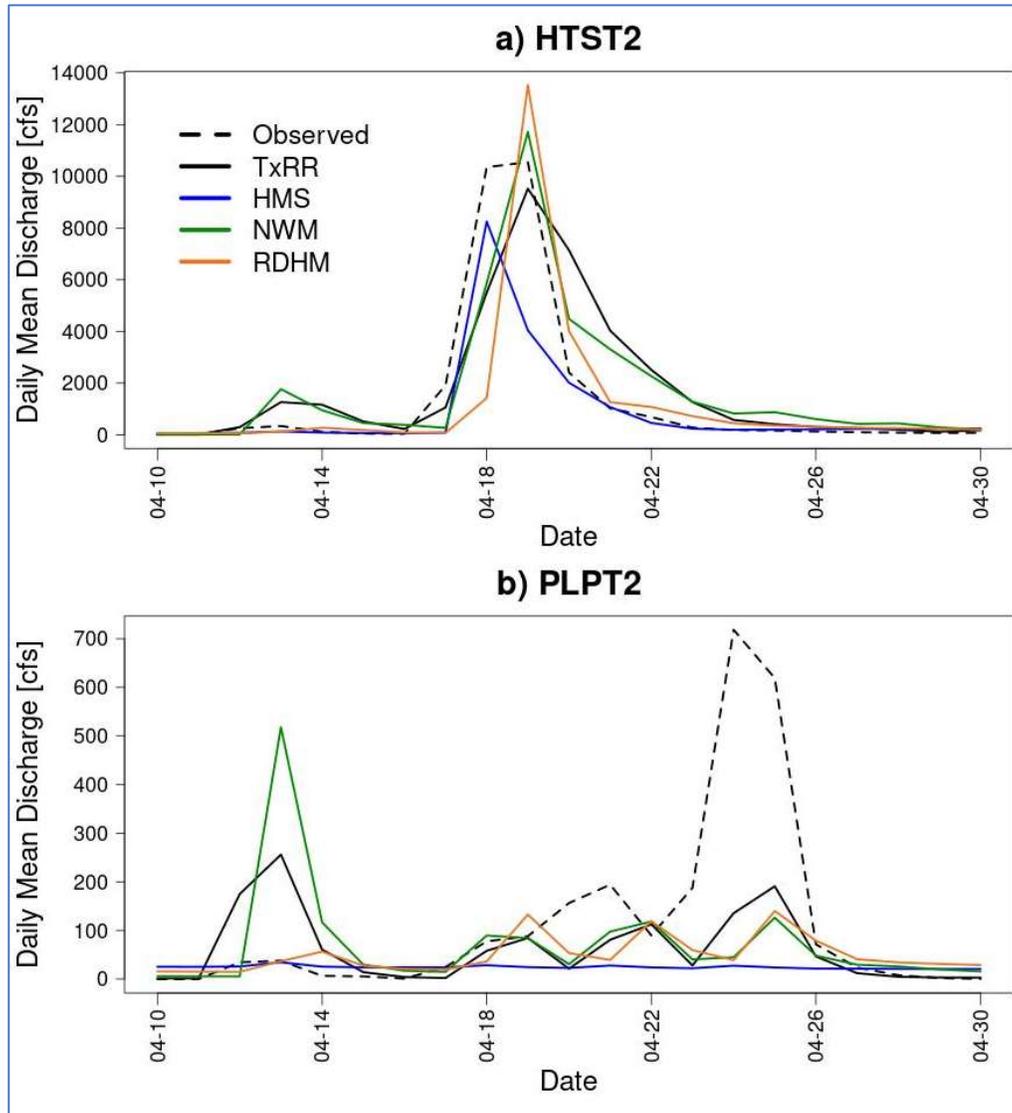
Figure 5-19   **Comparisons of simulated flow from member models and observed for the Apr. 2014 storm event.**

The last high flow event of interest is Hurricane Harvey that took place between Aug 25-28 and produced flooding in the coastal bend and along southeastern Texas. Fig. 5-20 shows the hydrographs at the two outlets. Perhaps the most striking feature is the under-simulation of the flood peak by all models at both locations. This under-simulation is overall more severe for HTST2, where all simulated peaks are about 1/3 below the observed one. Among the models, TxRR and HEC-HMS fare slightly better, whereas hydrographs from NWM and HL-RDHM appear to be two days behind the observed. For HTST2, the under-simulation is not as severe for all models except for HL-RDHM, which produces a peak less than 1/8 of the observed. The delay in response is again evident for TxRR and HL-RDHM, and to a lesser extent for HEC-HMS.
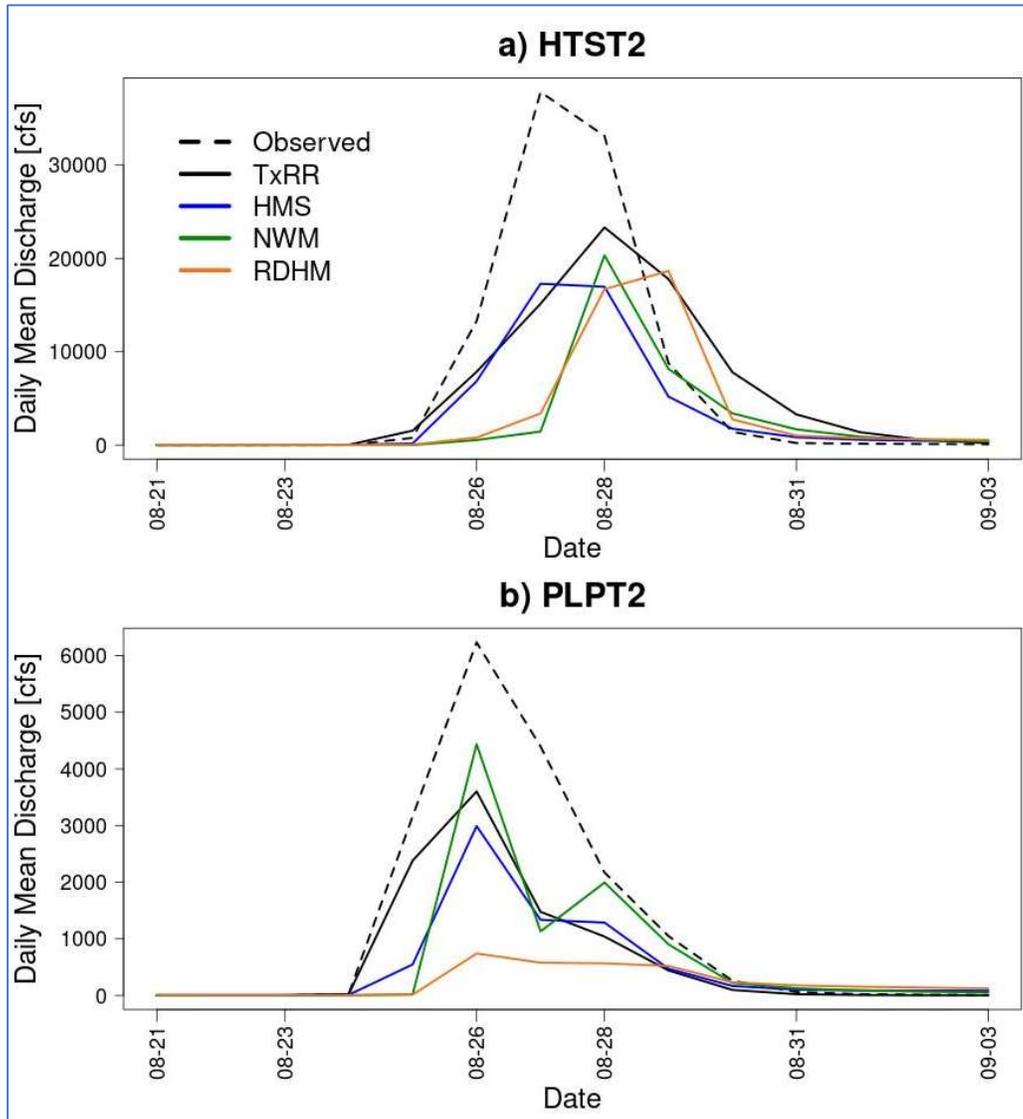
Figure 5-20   **Comparisons of simulated flow from member models and observed for Hurricane Harvey in Aug-Sep 2017.**

58

The under-simulation can be attributed to a variety of factors, such as inaccuracy of NLDAS-2 precipitation data and inadequate representation of land surface processes. As noted earlier, NLDAS-2 precipitation data set relies on the radar and gauge reports, and for extreme events such as Harvey, there were concerns that in situ reports were compromised by the errors induced by wind (Nespor and Sevruk 1999) and by the mechanic limitations, or even failures of tipping bucket gauges (Habib et al. 2008; Duchon et al. 2010). At present, only the gauges in the Advanced Surface Observation System (ASOS) USGS networks are shielded, and the vast majority of USGS records that enter the data stream for NLDAS-2 and MPE are not. The current version of NLDAS does not incorporate any mechanism for bias-correcting reports of precipitation gauges arising from the wind effects (Xia, 2007), though the developer has studied the wind-related bias and acknowledged its importance (Xia, 2006). Other issues complicating rainfall observations include transmission failures, and the lack of COOP manual observations during the event because of flooding. The lags exhibited by NWM and HL-RDHM flow simulations for HTST2 may be reflective of underestimation of rainfall by the gauge network over parts of the watershed. The reason that no such conspicuous lag is seen in HEC-HMS and TxRR simulations is likely a result of the lumped nature of the latter two models that to an extent masks the observational issue. To elaborate, the lumped models consider precipitation to be uniformly distributed over each watershed. When spatial averaging of precipitation is performed as required by these models, it is possible that such an operation spreads rainfall to parts of a watershed that are in fact in dry conditions and would not produce any runoff if precise, albeit biased, rainfall information is used. And this allows runoff to be artificially generated over the earlier periods. Another potentially complicating factor concerns the fidelity of the flow data over the event – the stage was most likely beyond the range where empirically estimated stage-discharge relationship can be reliably applied, and this could have induced large errors in the flow rate estimates.

The hydrographs for the two neighboring time windows during the drought of 2011 are shown in Figs. 5-21 and 5-22. For the first time window (mid-August through late September; Fig. 5-21), streamflow at both HTST2 and PLPT2 stays close to zero, underscoring the prevailing dry conditions across the region. All models over-simulate the streamflow at both stations, though the severity of over-simulation varies. At HTST2, HL-RDHM and HEC-HMS each produce a minor peak (< 20 cfs) at around August 24, whereas no corresponding response is observed. NWM and TxRR simulations stay flat, yet their magnitude is persistently higher than the observation. Between the two models, NWM's over-simulation of the low flow is particularly noticeable. At PLPT2, NWM, HEC-HMS both produce spurious responses that are visually conspicuous, whereas TxRR and HL-RDHM simulations are close to the reality (near zero).

For the later time window (Fig. 5-22), streamflow at both stations remains consistently close to zero. All models produce considerable runoff over October 8-15, clearly in response to rainfall pulses around the time. Among the models, TxRR simulation exhibits the most severe biases at the two stations. At HTST2, the peak from TxRR simulation is close to 700cfs. This behavior of TxRR contrasts sharply with its rather reliable performance over the earlier period. The other three models do not perform as consistently between the sites. NWM simulation, for example, reasonably tracks the observed series for HTST2, but its bias is quite pronounced for PLPT2. To summarize, it appears that the member models, including TxRR, have considerable difficulties in capturing the water balance during the severe drought. For NWM, the small yet persistent inflation of inflow is concerning, as it possibly underscores issues in the representation of

groundwater table. TxRR correctly suppresses runoff response for minor rainfall input over the summer, but it produces grossly exaggerated response in the fall. Table 5-10 summarizes the cumulative flow for the entire 2011 over the two sites. For HTST2, TxRR exhibits the most severe positive volumetric bias, whereas HEC-HMS performs the best. By contrast, for PLPT2, TxRR performs the best whereas HEC-HMS and HL-RDHM perform the worst.

Table 5-10: Cumulative flow (in af) for the year of 2011 at HTST2 and PLPT2

Watershed	Observed	TxRR	HEC-HMS	NWM	HL-RDHM
HTST2	4748	30523	3405	24517	24624
PLPT2	2827	5246	9276	8135	9388

Evidently, the spurious response of TxRR in the fall is a major factor underlying its large, positive overall bias for the year. But it is rather interesting to note that its performance, and the performance of HEC-HMS among the models contrasts sharply for the two watersheds. Again, the streamflow simulations alone are not adequate for offering definitive diagnosis about mechanistic deficiencies of each model during droughts as severe as the 2011 episode. It is hoped that, in future studies, root zone soil moisture and groundwater table data be incorporated to help reconstruct the dynamics in the vadose and groundwater zones, which will perhaps offer clues to the lack of response of the watersheds during the summer-fall, and help identify model representation issues that give rise to the large, divergent biases exhibited by different models.
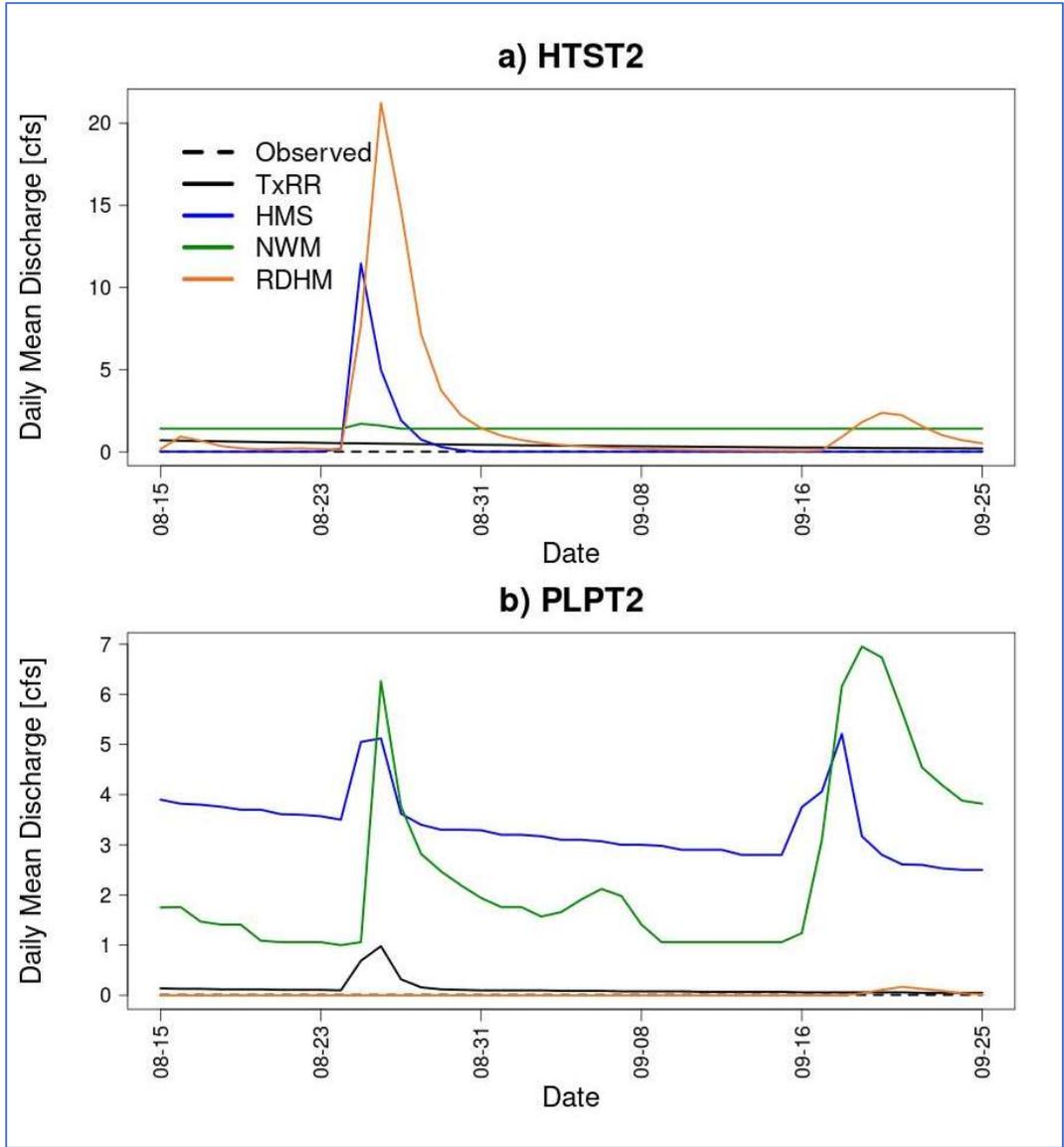
Figure 5-21   Comparisons of simulated flow from member models and observation for during the drought of 2011 (Part I).
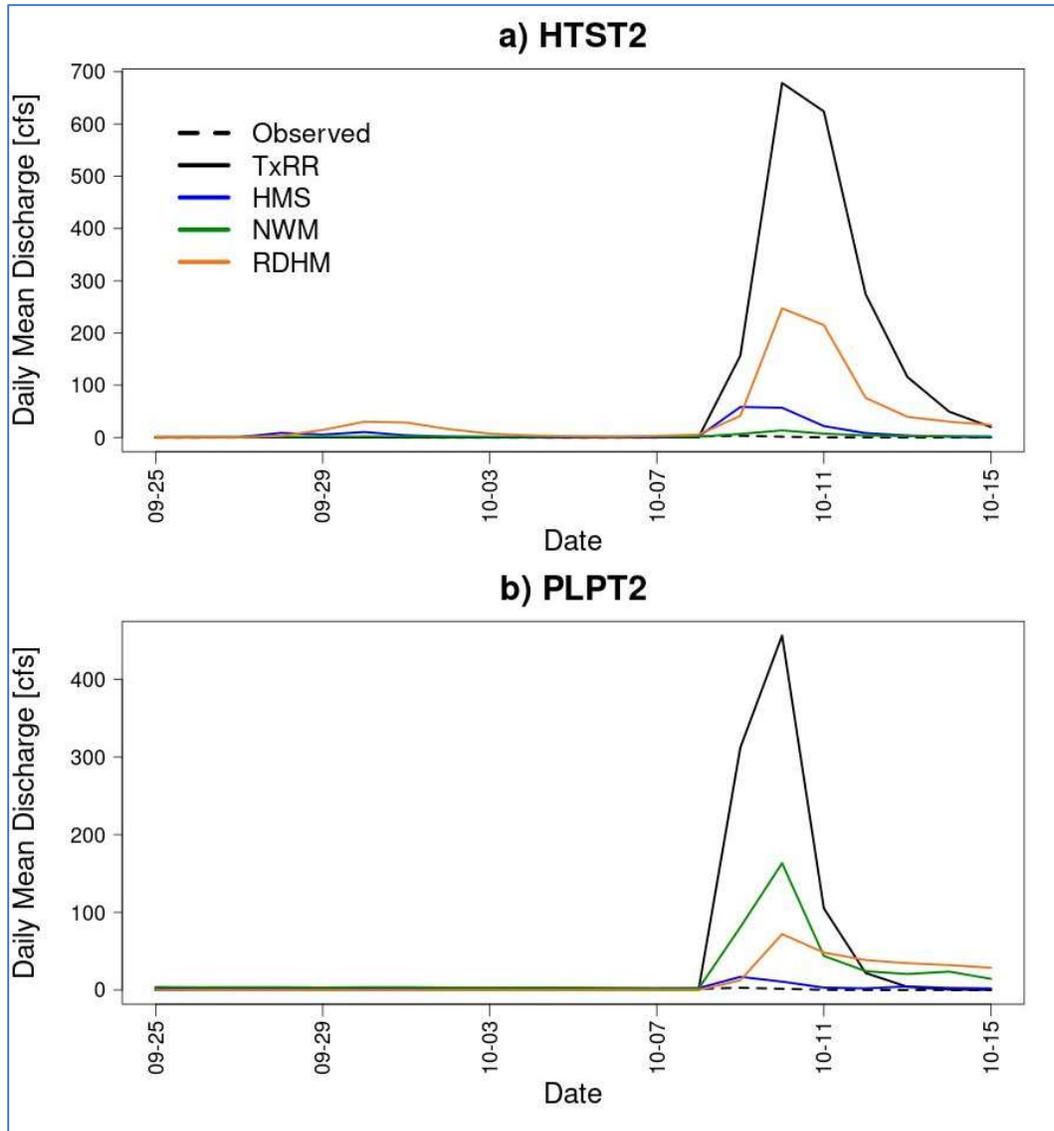
Figure 5-22   **Comparisons of simulated flow from member models and observation for during the drought of 2011 (Part II).**

To summarize, the case studies illustrate that the behaviors of models across the four events vary widely among events, and there is not a single model that consistently outperform the rest. Some of the model bias and error characteristics as illustrated earlier are reflected to an extent in the event-wise comparisons. Among the models, the baseline model TxRR performs rather well for HTST2, the northern watershed, but it has a tendency to over-simulate for the smaller basin PLPT2, and this can be possibly explained by both a lack of calibration, and possible bias in the NLDAS-2 rainfall series that stems from inadequacy in the rain gauge network. NWM, which did not undergo extensive calibration, exhibits similar issues in resolving the response over the two watersheds, though its performance is reasonable for HTST2 for all events examined. The models that were calibrated, i.e., HEC-HMS and HL-RDHM, do manage to avoid the egregious over-simulation as seen in the results of TxRR and NWM for three of the events. Yet, the effects

of calibration are uneven – for Hurricane Harvey, the simulations from the two models depart substantially from the observation and they are not in any material fashion superior to those of NWM and TxRR. On the other hand, all models exhibit issues in reproducing low flow during the 2011 drought, including the two models that were calibrated for this period (i.e., HEC-HMS and HL-RDHM). Mechanisms behind the spurious runoff produced by each model are not yet clear; a close examination of model states is needed to diagnose the behaviors and identify remedies.

5.3   MMIPS and experimental ensemble inflow simulations

In this section we describe the preliminary configurations of member models of MMPIS for the ungauged, bay watersheds, and present examples of ensemble inflow simulations using MMIPS for 2003-2017. Among the models, the default, operational version of TxRR is set up for HEC-HMS and HL-RDHM are implemented for each ungauged bay watershed with parameter values borrowed from an upstream basin. To maintain consistency with the current practice of the TWDB, all models except NWM ingest observed inflow at upstream USGS stations to replace the model simulated flow. The USGS stations that are connected to each of the bay watershed can be found in Table 3-1.

As NWM is run at NWS and is not amenable to calibration, we develop a simple postprocessing scheme per Task 3 to mitigate the biases in the NWM flow analysis. In this scheme, both simulated and observed mean monthly flows are calculated for each of the five upstream outlets using NWM reanalysis data over the entire period (2003-2017). Then a bias factor is calculated for each month over each watershed by taking the ratio of the observed to the simulated monthly flow volume. The monthly bias factors are then averaged across the watersheds, and the resulting mean bias factors are summarized in Table 5-11.

Table 5-11   Monthly mean bias factors applied to NWM simulations for the bay watersheds

Month	1	2	3	4	5	6	7	8	9	10	11	12
Bias	0.70	0.79	0.92	1.00	1.19	1.33	1.50	1.90	1.53	1.12	0.81	0.57

These mean monthly bias factors are then applied to the flow simulation of NWM for each bay watershed with the assumption that the bias characteristics of NWM over these locations broadly resemble those over the upstream watershed. In the remainder of this section, only the bias-corrected NWM inflow estimates will be shown and compared against other inflow products. For HEC-HMS and HL-RDHM, the parameter values estimated over upstream watersheds through calibration are transferred downstream. Table 5-12 describes the pairs of donor and recipient watersheds, i.e., the catchments from which the parameter values were derived and those receiving the parameter values, respectively.

As HL-RDHM and NWM are grid-based models, the specific locations of inlets need to be identified for each model in order to retrieve the inflow estimates. To this end, we manually locate the stream segments in the NHD-Plus database that intersect with the bay. Fig. 5-23 shows such bay inlet locations across the eleven bay watersheds. The NWM streamflow analysis for each segment can be looked up from the reanalysis database using the identifier of each segment as the key.
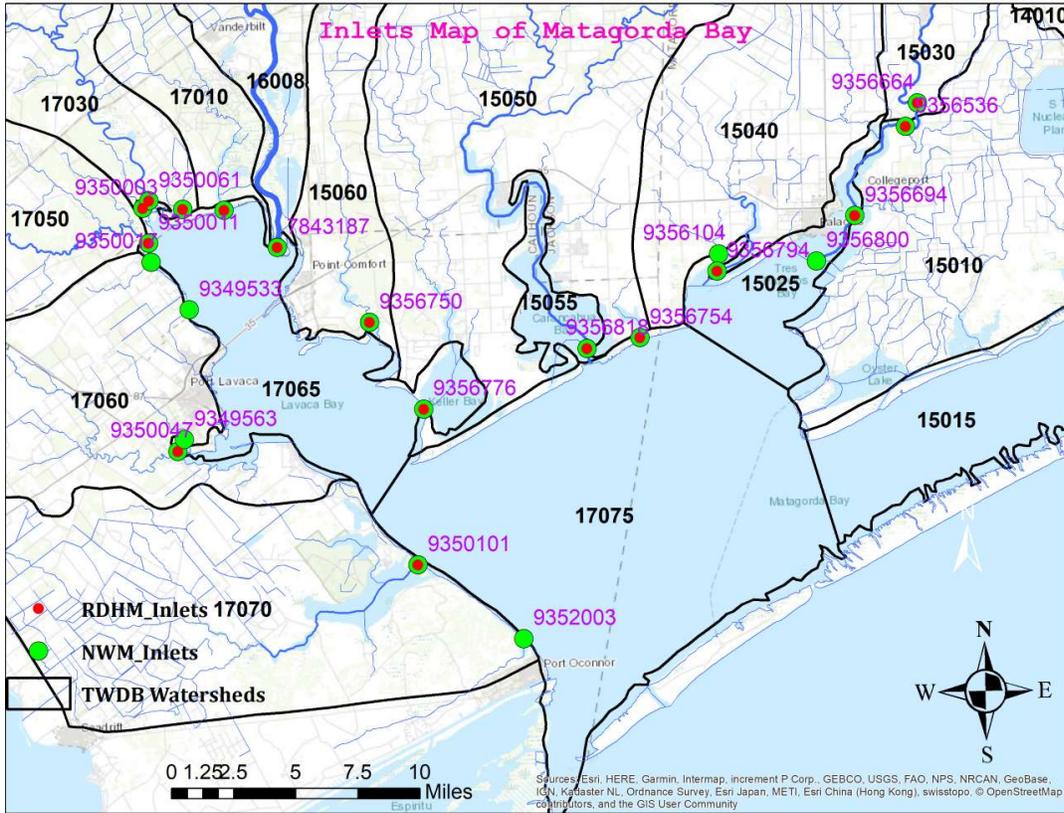
Figure 5-23   **Map of bay inlets identified from NHD-Plus used in NWM (yellow) and HL-RDHM (red). Superimposed in purple are segment identifier from NHD-Plus.**

Table 5-12   **Bay watersheds and upstream donor watersheds from which parameters are derived**

Recipient Bay Watershed	Upstream Donor Watershed	
TWDB ID	Outlet SHEF ID	TWDB ID
15010	MTPT2	15020
15030	MTPT2	15020
15040	MTPT2	15020
15050	EDNT2	16005
15060	EDNT2	16005
16008	EDNT2	16005
17010	EDNT2	16005
17030	NGCT2	17020
17050	PLPT2	17040
17060	PLPT2	17040
17070	PLPT2	17040

For HL-RDHM, we create outlet points for a subset of the inlets that are situated in independent (non-overlapping and unconnected) model pixels and have realistic upstream contributing areas. As the HL-RDHM implementation uses a relatively coarse grid mesh (~4-km), there are cases where more than one inlet is present in a pixel. In such cases, only the one with the largest contributing area is retained. In addition, the inlets associated with invalid upstream contributing areas are eliminated to avoid the incorporation of erroneous runoff quantities. This identification process results in 13 inlet locations for the HL-RDHM and 22 for NWM (Table 5-13).

Table 5-13   Bay inlets identified from NHD-Plus Database and availability of flow data in NWM and HL-RDHM

Bay Watershed ID	Inlet Segment (NHD-Plus)	NWM data availability	HL-RDHM Designator	Lon (degree)	Lat (degree)
15010	9356536	X	MTGA4	-96.1548	28.75596
15010	9356694	X	MTGA12	-96.1824	28.71432
15010	9356800	X	-	-96.2059	28.68041
15010	9356904	-	-	-96.2291	28.64531
15010	9356944	-	-	-96.2294	28.60338
15010	9356966	-	MTGA9	-96.2271	28.59445
15030	9356664	X	MTGA4	-96.1491	28.76946
15040	9356794	X	MTGA11	-96.2621	28.70107
15040	9356104	X		-96.285	28.6937
15050	9356818	X	MTGA5	-96.3746	28.64222
15050	9356776	X	MTGA8	-96.4728	28.60582
15050	9356754	X	MTGA13	-96.3425	28.65221
15060	9356750	X	MTGA7	-96.5218	28.66397
16008	7843187	X	MTGA1	-96.5757	28.70121
17010	9352959	X	MTGA14	-96.6132	28.72655
17030	9350061	X	MTGA3	-96.663	28.73266
17030	9349999	X	MTGA14	-96.6377	28.72076
17030	9350003	X	MTGA3	-96.6737	28.72969
17050	9350011	X	MTGA2	-96.6674	28.70649
17060	9350047	X	MTGA6	-96.6602	28.56984
17060	9349563	X	-	-96.6521	28.59982
17060	9349533	X	-	-96.644	28.65692
17060	9350017	X	-	-96.6711	28.68262
17060	9350169	-	-	-96.5787	28.58371
17070	9350101	X	MTGA10	-96.4943	28.50519
17070	9352003	X	-	-96.4187	28.46444

For each bay watershed, we compute both a *local runoff series*, which is the inflow generated by runoff solely over the watershed domain, and an *aggregate inflow series*, which is the sum of local runoff and contribution from upstream drainage if the latter exists (as the case for 17030, 17060, 16008, and 15030; see Table 3-1). For each model, the aggregate inflow series for all bay inlets are further summed up to yield the total inflow series. Table 5-14 summarizes the multi-year mean inflow volumes produced by each model over 2003-2017.

Table 5-14   Mean annual total inflow to Matagorda Bay computed by each model

Model	TxRR	HEC–HMS	NWM	HL–RDHM
Inflow (af/yr)	1,802,902	1,846,745	1,528,159	1,443,280

Among the models, HEC-HMS produces the largest inflow volume, followed by TxRR, whereas the volumes from NWM and HL-RDHM are much lower (15% and 20% relative to that by TxRR, respectively). Fig. 5-24 shows the time series of simulated total annual inflow to the bay by the four models over the period of 2003-2017.   For most of the years, the two distributed models, namely NWM and HL-RDHM, produce appreciably less inflow than the lumped models (TxRR and HEC-HMS). Between NWM and HL-RDHM, NWM produces larger inflow volumes for a majority of years (ten out of fifteen). Curiously, for a few recent years (2011-2016), NWM-based inflow volumes are comparable and slightly larger than those from TxRR and HEC-HMS, whereas the results of HL-RDHM are much lower for the same period. Only over some of the earlier years (e.g., 2003-2005) does HL-RDHM produce larger volumes than NWM. This is possibly linked to the positive bias that NWM simulations exhibit at Lavaca River near Edna – as NWM does not ingest USGS flow observations, this bias is retained in the inflow series.
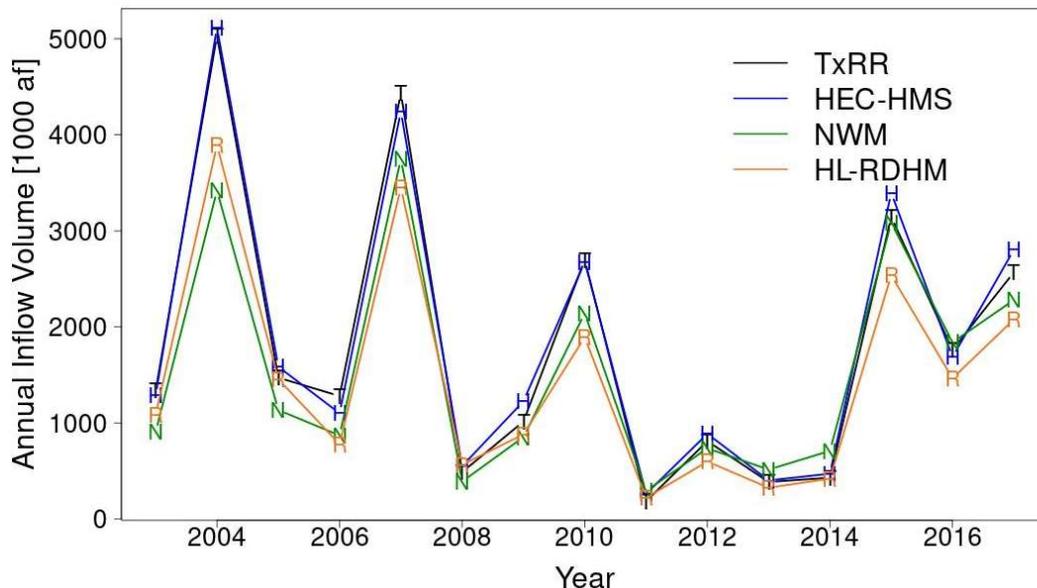
Figure 5-24   Time series of annual freshwater inflow calculated from the four models that comprise the MMIPS, namely i)TxRR, ii) HEC-HMS; iii) NWM and iv) HL-RDHM.

The simulated inflows by member model are further compared for each watershed. Fig. 5-25 shows the comparisons of mean annual aggregate inflow and local runoff across watersheds. It is clear in Fig. 5-25a that the contrasts between the results of lumped (TxRR and HEC-HMS) and distributed models (NWM and HL-RDHM) as shown in Table 5-14 are not uniformly seen across watersheds (Fig. 5-25b). For 16008 (Lavaca River), the drainage with the largest aggregate inflow volume, NWM in fact produces the largest inflow volumes. This is consistent with the earlier observation of over-simulation by NWM at Lavaca River at Edna. A closer look at the local runoff reveals that NWM and HL-RDHM both produce larger volumes of runoff than the lumped models do (Fig. 5-25b). However, the opposite is true for a majority of smaller watersheds (eight out of ten), where the two distributed models produce overall smaller volumes. The under-production of inflow is particularly evident for two watersheds over the east, namely 15010 (Oyster Bayou) and 15040 (Turtle Creek), for which inflow volumes from NWM and HL-RDHM are miniscule in comparison to those by TxRR and HL-RDHM. Apparently, on a cumulative basis, the differences over these smaller watersheds more than offset those for 16008 (the Lavaca River).
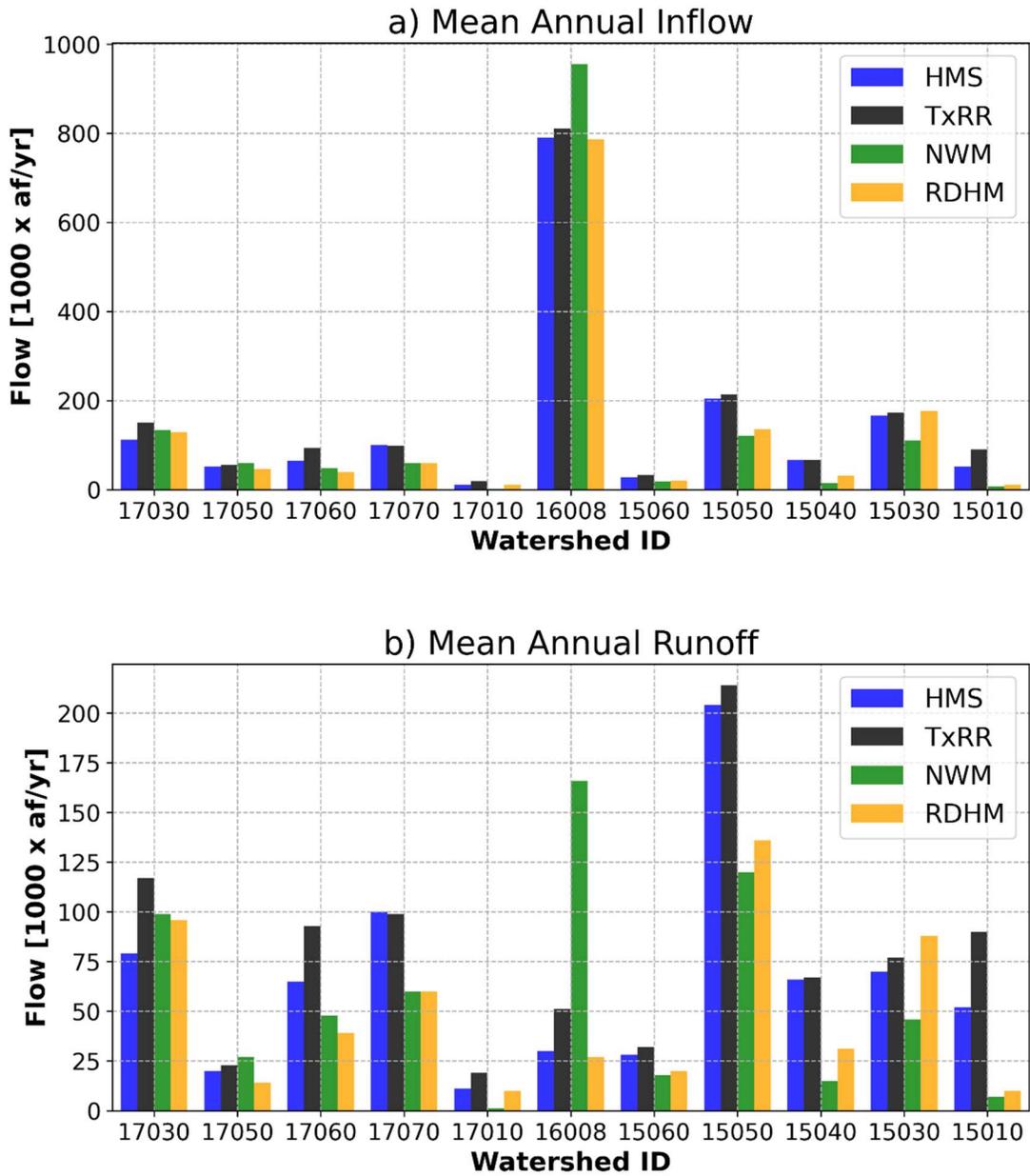
Figure 5-25 **Mean annual inflow into the bay (a) and local runoff (b) for each watershed as estimated from four member models. Watershed IDs highlighted by red rectangles are those incorporating inflow from upstream USGS stations.**
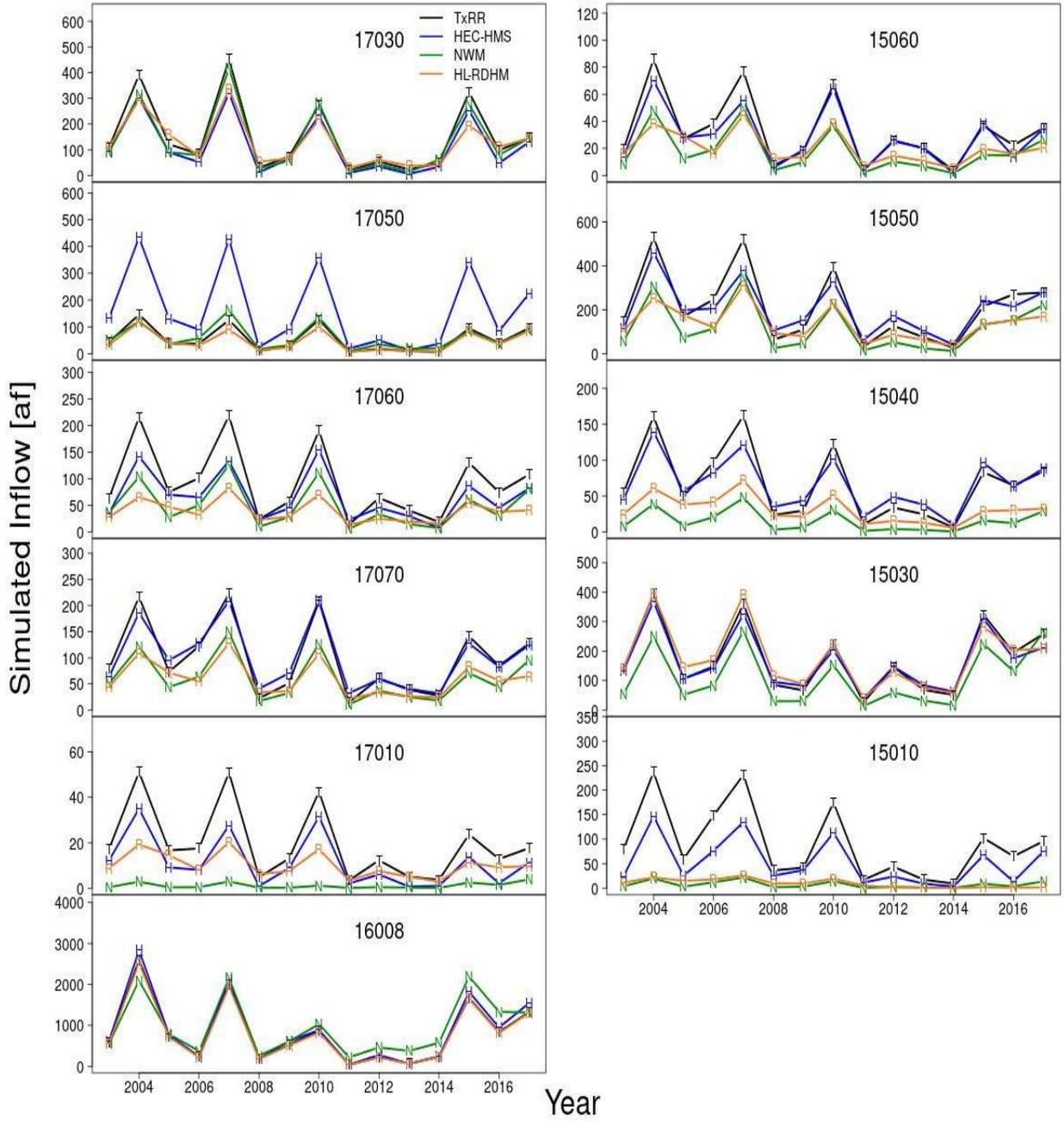
Figure 5-26 **Annual aggregate inflow into Matagorda Bay for each watershed as estimated from four member models.**

The year-to-year variation of the aggregate inflow volumes for each watershed is characterized in Fig. 5-26. A noticeable feature is that broad similarity is observed among the series produced by TxRR, HEC-HMS and HL-RDHM for three out of the four watersheds with upstream inflow, namely 17030 (Garcitas Creek), 16008 (Lavaca River), and 15030 (Tres Palacios Creek). This similarity can be attributed to a combination of the similarity in local runoff volume and the dilution of the differences by ingesting upstream inflow. The exception is 17060 (Chocolate Bayou), where the local runoff produced by member models diverges and the upstream inflow is quite small in magnitude. Another interesting feature is that for watershed 16008 (Lavaca River), NWM-based annual inflow series is comparable to, or lower than those from other three models until 2010, and starts to clearly surpass the latter from 2011 until 2016. Therefore, the larger overall inflow volume from NWM as seen in Fig. 5-25a mostly reflects the difference in model results over the later period.

To summarize, there are two prominent features that emerge from the comparisons, namely 1) both distributed models produce smaller total inflow volumes than the lumped models do on a multi-watershed mean basis, and 2) between the two distributed models, NWM tends to produce larger volumes than HL-RDHM. These features are rather unsurprising. The split between distributed and lumped models has much to do with the differing spatial extents of drainage as represented by the two groups of models: the lumped models consider the entirety of each bay watershed as the contributing area to the bay, whereas the distributed models only incorporate runoff generated over parts of each bay watershed that are hydrologically connected to the bay according to digital terrain data. Neither of the two approaches, however, is perfect. Due to the flatness of coastal terrain, the boundaries of bay watersheds as defined by the TWDB are subject to errors, and there is a distinct possibility that the inflow is inflated by the lumped models because of the overrepresentation of drainage areas. The distributed models, on the other hand, are potentially advantageous for their explicit reliance on the hydrologic connectivity which allows for a more precise definition of upstream contributing areas. This potential advantage, however, may be offset by errors in the connectivity which can be considerable in low gradient coastal zones. Between NWM and HL-RDHM, the larger flow volumes produced by NWM are mostly likely related to the fact that it uses a finer grid mesh and features more bay inlets than HL-RDHM does. At present, it is difficult to appraise the relative accuracy of inflow series supplied by each model directly without in situ streamflow records.

We close this section by examining the empirical distribution of total inflow into the bay derived from the simulation of each member model. Fig. 5-27 shows the flow duration curves, i.e., the empirical distribution of total daily aggregate inflow. As in Fig. 2-5a, the ith point in the figure represents the percentage of time the daily volume falls between q_{i-1} and q_i. Among the models, TxRR stands out by featuring conspicuously larger percentage of days with low daily volumes (i.e., between 1 and 10^2 af), whereas all three alternative models produce larger percentage of days with volumes over the middle-low ranges (10^2 to 10^3 af). The percentage of days with volumes in the range of 10^3 to 10^4 af is comparable among models, with the value for HL-RDHM slightly lower those from other models. Interestingly, despite the fact that NWM and HL-RDHM both produce relatively small volumes of total inflow on average, the "baseflow" in the simulated inflow by these models is slightly higher than that produced by TxRR. A possible explanation is that TxRR simulation tends to recede deeper after most runoff events. Fig. 5-28 demonstrates this for an event that occurred in late October and November of 2004, where deeper recession curves are evident in TxRR's simulation.
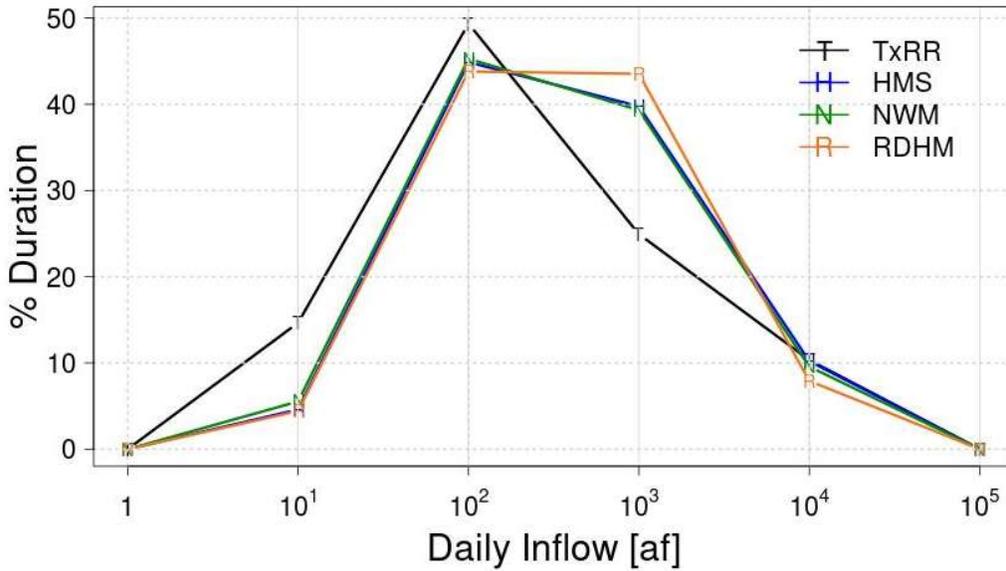
Figure 5-27 Flow duration curves based on simulated daily inflow by each model. Each point represents the percentage of time that total daily aggregate inflow volume by a given model is within a category marked by the corresponding abscissa and its preceding one.
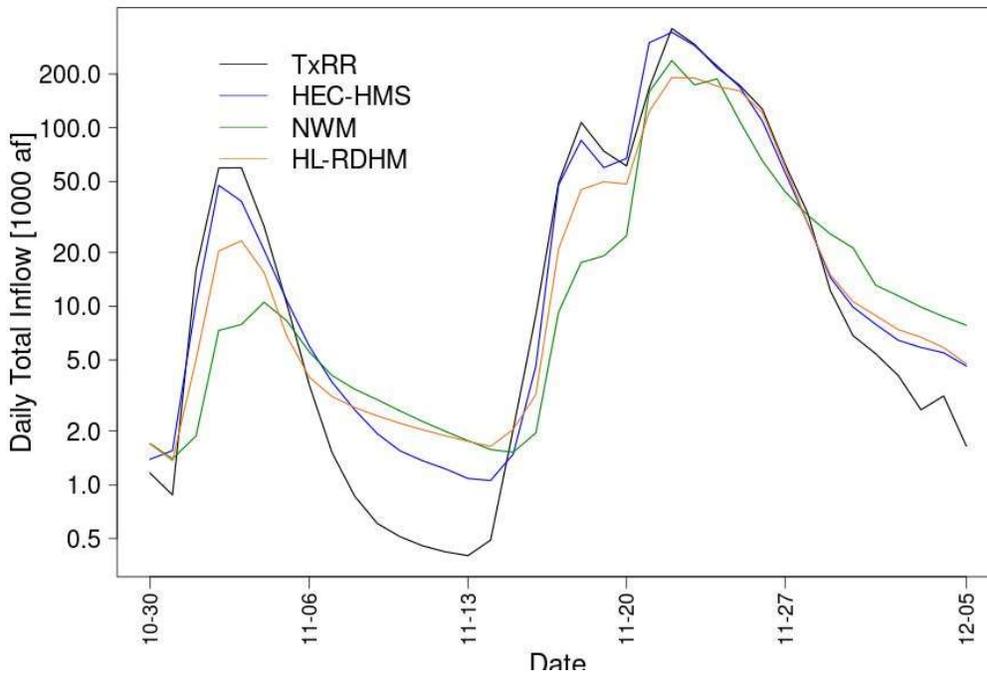
Figure 5-28 Inflow time series for the event of Oct-Nov 2004. Note that TxRR flow recedes to a lower level after each peak.

It is unclear as to which distribution is a close approximation of the reality. Yet, comparisons of flow duration curves over an upstream gauging station (Lavaca River at Edna) reveal a similar feature - the three alternative models tend to produce inflated baseflow, whereas TxRR-based results are in closer agreement with observations (Fig. 5-29). This suggests that the simulations from the alternative models over low-to-medium flow categories may not be as reliable. Note that all four member models represent baseflow using exponential functions with an empirically determined decay parameter. Therefore, the differences in the baseflow volume most likely reflect differences in calibration approach rather than those in model physics, though there remains a possibility that the storage or capacity of the lower zone or groundwater reservoirs are exaggerated in the three alternative models. As baseflow levels have clear implications for the health of coastal ecosystem, additional calibration efforts are warranted to minimize possible distortions of inflow under average conditions as well as during drier times.
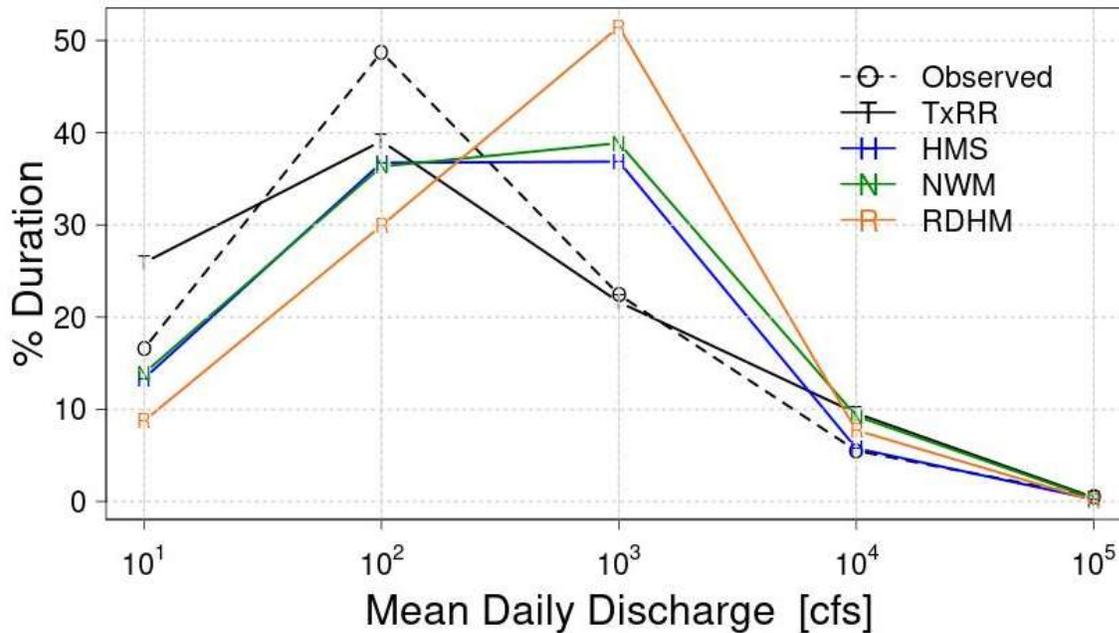
Figure 5-29   **Flow duration curves for observed and simulated discharge series at EDNT2 (Lavaca River at Edna).**

6 Summary, Conclusions and Recommendations

This report describes the project by the UTA team to improve and augment the TWDB's capabilities of estimating and predicting the freshwater inflow to Matagorda Bay. The project consists of two primary components. The first one entails developing and implementing tools necessary to ingest the MPE products from NWS, and evaluating its potential impacts on the inflow estimates produced by the TxRR model. The second one focuses on establishing a multi-model inflow prediction system, referred to as MMIPS, that incorporates models extensively tested and deployed by partnering agencies, namely the HEC-HMS (USACE), NWM (NWS), and HL-RDHM (NWS). The latter component further comprises elements including model implementation and validation, limited postprocessing (for NWM), and demonstration and comparison over inlets to Matagorda Bay. The anticipated benefits of these tasks are multifold. First, the project is expected to help the TWDB improve inflow estimates through the infusion of up-to-date, widely used precipitation products, and by exploiting the complementary strengths of various modeling paradigms. It further lays the ground for the state to migrate from the current, single-trace inflow estimates towards future, ensemble-based inflow estimates that would provide information on the uncertainties in such estimates. Second, all three alternative models can produce hourly flow and do serve the purpose of flood prediction in various capacities. And the adoption of these models will enable the system to be used for predicting and assessing fluvial flooding over coastal basins, many of which are currently not covered by NWS river forecast operations. In a long run, building this prediction capability will help the TWDB to fulfill its new role in overseeing flood preparedness across the state. Third, deployment of these products and systems will improve agency's interoperability with federal partners including NWS and USACE. On only hand, the TWDB's modeling effort will benefit from infusing knowledge and expertise with respect to hydrologic modeling available at these agencies. On the other hand, the TWDB could use MMIPS products to help the federal agencies in achieving their missions and goals. For example, USACE's HEC-HMS system is commonly configured to run in an event-wise mode which requires the specifications of loss factors. The soil moisture conditions produced by the HEC-HMS component of the MMIPS can be used to estimate and supply the loss factors in real time. As another example, MMIPS flow estimates, in particular the hourly estimates from the distributed models, can serve as upstream boundary conditions for hydraulic models set up for creating inundation maps for designated past events, and perhaps even in near real-time during major storm events.

The first project component yielded tools for processing the gridded MPE and creating MAP series that can be directly ingested into TxRR. The MPE product is widely used by federal agencies including USACE and NWS, and by river authorities. The product is known for its resolution and quality, as it is created by integrating radar, gauge and limited satellite products, and therefore benefits from the combination of complementary strengths of these products (Seo et al. 2010; Zhang et al. 2011a). This has been confirmed in past studies such as that by Villarini et al. (2011). The comparison of the MAP series derived based on the MPE and the default gauge data set, as well between the TxRR simulations driven by the two data sets, reveals substantial, consistent differences. The MPE-based precipitation on a multi-year average basis is uniformly higher across the eleven watersheds that drain to Matagorda Bay. Interestingly, the differences between the two sets of precipitation data are more pronounced over the east half of the watersheds, reaching 15% in one of the watersheds. A proximate reason for this east-west

contrast is the difference in bias behaviors of two radar units that cover the eastern and western portions of the bay. The differences in TxRR-based inflow volumes mirror the differences in the precipitation data sets used in driving the TxRR simulations, but their magnitude is broadly higher, with MPE-driven runoff volumes exceeding that by gauge product by more than 20% for a majority of bay watersheds. Further analysis indicates that the gauge-MPE contrast is the most acute at the tail end of the rainfall spectrum, with MPE showing a frequent occurrence of large daily accumulation. The possible sharp increases in larger precipitation amounts in the MPE data set help explain the magnification of the difference in TxRR simulated flow driven by gauge and MPE, as efficiency of runoff production per models has a tendency to increase with rainfall intensity. Taken together, these observations suggest that the transition from gauge-based to MPE-based inflow simulation will have rather major impacts on the estimated inflow volumes to Matagorda Bay.

An important, and heretofore unanswered question is whether replacing the gauge product with MPE will lead to distortion of inflow by TxRR if the model does not undergo another round of calibration. Since the model was calibrated using the gauge-based product, the calibrated parameter values mostly likely have absorbed some of the biases in the precipitation data set. As pointed out earlier, examining the biases in TxRR streamflow simulations over upstream, gauged watersheds will help infer the biases over ungauged locations. Should large biases appear over the upstream basins, there will be a need to remedy the bias through either model calibration or postprocessing.

Note that the scope of the project is limited to the development of tools and comparison of products, whereas the actual quality of the MPE product, and its variation geographically within the region and over time, warrant future investigations. Validation of MPE, as well as interpolated gauge products, against independent gauge data will also be needed to appraise the relative strengths of the products over different portions of the bay and for different time windows, and it will further inform about the necessity of implementing and applying postprocessing schemes to correct biases in earlier MPE products as recommended by Zhang et al. (2011a). In addition, we also suggest that the inflow series produced with MPE data as the forcing be tested through TxBLEND model simulations to examine the impacts on salinity. This would help determine whether the rainfall errors indeed contributed to the striking discrepancies between observed and model-simulated salinity noted by Schoenbaechler et al. (2011). It is also worth pointing out that the MPE data set only became available since the late 1990s. The NWS OWP has attempted to address the earlier data gaps through infusion of radar archive from a commercial source (e.g., NowRAD; Zhang et al., 2017), satellite, and Manualized Digitized Radar data (Baeck and Smith, 1995). The office recently released a new archival forcing dataset, namely the Analysis of Record for Calibration (AORC; Kitzmiller et al. 2018) for the purpose of hydrologic calibration in NWS line offices, and this data set extends the record back through 1979 (note for the last two decades it is based primarily on MPE). The earlier AORC data, through its use of radar reflectivity index, has shown superior skill in resolving light rainfall relative to the NLDAS product. It will be useful to integrate the AORC data to re-compute the historical inflow for the bays and estuaries for the pre-NEXRAD era.

The MMIPS as established in this project currently relies on four member models, out of which three will be implemented and run internally (namely TxRR, HL-RDHM, and HEC-HMS), whereas one (NWM) will be run externally at NWS and its data will be ingested. The project has

produced implementations of HL-RDHM and HEC-HMS for the region along with model parameters that were calibrated to match observed flow records over five upstream USGS stations for 2003-2017. In order to anticipate the accuracy of the inflow estimates, the team conducted a set of validation experiments wherein results of the four models were compared against observations over the five stations. In these experiments, all four models were driven by an identical set of forcing input (i.e., NLDAS-2). Among the models, HL-RDHM and HEC-HMS underwent calibration as indicated earlier, and their results were contrasted with the series generated by running the operational version of TxRR without calibration for the entire period, and the NWM v1.2 reanalysis data acquired from an archive. The comparisons point to mixed results across watersheds, time scales (monthly and daily), and between the calibration and validation periods (2004-2012, and 2013-2017, respectively). For the calibration period, as judged by RMSE, TxRR and NWM are the best performers on the monthly scale, whereas on the daily scale HEC-HMS outperforms others for four out of five watersheds. For EDNT2 (Lavaca River at Edna), the station with the largest upstream drainage area and highest flow rates, TxRR remains the best performer at both time scales. By contrast, for the validation period, TxRR's performance trails behind HEC-HMS and NWM on the monthly scale, and HEC-HMS emerges as the best performer for all stations on the daily scale. Additional findings of note include: i) TxRR simulations in general are positively biased, and this bias is quite appreciable at EDNT2 and HTST2 (Navidad River) over both periods; ii) NWM appears to perform well for some of the smaller watersheds, but its bias is quite large and highly variable across watersheds; and iii) HL-RDHM simulations exhibit lower correlation than the results from other models, and this translates into higher RMSE values.

It was postulated that the sophisticated land surface and ET schemes implemented in alternative models would allow them to outperform TxRR in representing seasonal cycle and interannual variations. The results, however, are not sufficiently clear to confirm or reject this hypothesis. For HTST2 (Navidad River), TxRR simulations exaggerate the minor springtime peak that is most likely related to heavy rainfall brought by frontal and convective systems over this time window. Three alternative models produce more realistic seasonal cycle for this watershed over the calibration period, but for validation period they tend to underrepresent the peak in August that is a result of the Hurricane Harvey. For other watersheds, the performance is mixed, and TxRR in some cases outperforms other models (e.g., over MTPT2). Among the models, it appears that NWM, which features the most complex land surface scheme, performs the best in capturing interannual variation of runoff. Yet, it is premature to establish a causative link between the model complexity and accuracy in the portrayal of interannual variation based on this performance alone: HEC-HMS also implements a dynamic ET module and yet its annual simulations are less correlated to observations than TxRR's. A comparison over an extended period of time is needed among the models to verify the persistence of the differences and their statistical significance.

The team also performed a set of comparison over four historical high flow events and the drought episode of 2011. The high flow events include the episode during Hurricane Harvey where flow over several stations was the highest in recent history. The relative performance of models again varies widely across the events. The most notable features include the follows: 1) there appears to be a tendency for TxRR to underestimate the flow peak over these events, while the bias behaviors of other models are less consistent; 2) for Hurricane Harvey, all models underrepresent the peak and flow volumes; 3) simulated flows tend exhibit large departures from

75

observations during events where the spatial extents of heavy rainfall are limited; and this likely reflects issues in the NLDAS-2 precipitation product; and 4) all models overrepresent flows during the 2011 drought with varying degrees. Interestingly, small, but persistent baseflow is observed in NWM simulations during prolonged dry periods in 2011, possibly underscoring issues with mass conservation. TxRR produces relatively realistic baseflow among the models over this period, though it grossly overrepresent flow in response to a rainfall episode in the fall.

To establish MMIPS and prepare for its operational use over Matagorda Bay, the team set up two member models (HL-RDHM and HEC-HMS) for each of the eleven bay watersheds, and developed tools for extracting and process inflow from NWM v1.2 reanalysis. The subtasks involved include setting up the flow connectivity over the watersheds, configuring the models to ingest observed streamflow (or reservoir release), transferring model parameters derived through calibration at upstream watersheds for HL-RDHM and HEC-HMS, and implementing a simple bias correction scheme for NWM outputs developed using simulation/observation pairs over the five gauged upstream watersheds.

As the bay watersheds are ungauged, it was not possible to validate the inflow simulations, and instead a cross-model comparison was performed. The results of the comparison point to a dichotomy between the lumped (TxRR and HEC-HMS) and distributed models (NWM and HL-RDHM), with the former producing overall larger inflow volumes into the bay. A closer scrutiny of model results over each watershed reveals that the under-production of inflow by the latter models occurs in a majority of smaller watersheds and are attributable to the differences in the representation of areas that drain to the bay. The distributed models were implemented using hydrologic connectivity based on topography data, and inlets were visually identified from the NHD-Plus data set and whose contributing areas often constitute only a part of each watershed as defined in the TWDB database. Unsurprisingly, this relatively small drainage areas translate into smaller runoff volumes. It is not yet clear which sets of estimates are closer to reality: visual inspection suggests that there is a distinct possibility the contributing areas are inflated in the TWDB watershed definitions. On the other hand, it is also possible that the distributed models' use of more precise, topography-based definitions of hydrologic connectivity leads to overlooking of areas that do contribute inflow to the bay, as flow directions may not be accurately defined due to the low topographic gradients over the region. In addition, some of the ephemeral, less well-defined drainage pathways are left out in the current NWM and HL-RDHM implementations (Table 5-13). Furthermore, there are also possible temporary reductions in the inflow volumes during high-flow events due to storages by coastal wetlands (Langevin et al. 2005; Rasmussen 2008), which are widely present along Matagorda Bay (http://www.beg.utexas.edu/research/programs/coastal/wetlands/matagorda-bay). The cumulative effects of overlooking small reaches, flow pathways and wetland storages on the inflow volumes need to be further scrutinized. Another notable finding from the comparison of the inflow series by member models is that the three alternative models produce higher median flow than that based on TxRR. Further analysis at a USGS station along the upstream portion of Lavaca River suggests that the three alternative models may have inflated the baseflow across a substantial portion of the region, and additional calibration effort is warranted to fine tune the baseflow release component of these models.

The establishment of the MMIPS will mark a major shift from the current single-model, single-trace inflow product generation towards a multi-model ensemble-based paradigm akin to that

being practiced by the NLDAS of NWS. NLDAS relies on four land surface models to generate land surface conditions and disseminate these to the public, and users may choose a subset or the entirety of the products for decision support purposes. A key advantage of this multi-model paradigm is that the ensemble helps inform the users about the possible range of outcomes, and the users will have the ability to factor in the risk associated with certain decisions. As the inflow estimates from MMIPS have not been validated, we suggest that, for simplicity, the traces produced by all member models be considered as equally probable representations of the actual inflow for the time being.

While the analyses carried in the project underscore a number of promising aspects of alternative models, these at the same time point to limitations of the model implementations and system configurations that require further enhancements. Some of the next steps that we recommend of undertaking in future efforts are summarized below:

1) further improving the historical precipitation data sets; for example, the AORC dataset from NWS (1979-2018) can be incorporated and evaluated along with gauge data predating the NEXRAD era; it can then be used to retrospectively generate inflow to the bay through TxRR simulations;

2) assessing the biases in TxRR flow simulations based on gauge and MPE products over upstream gauged catchments, and devise strategies for mitigating the biases in MPE-driven inflow simulations should the magnitude of biases be deemed sufficiently severe. Possible mitigation strategies include a postprocessing scheme akin to that developed for NWM, and re-calibration of model specifically using the MPE, or the AORC product;

3) refining the configuration and parameterization of member models including HL-RDHM and HEC-HMS. HL-RDHM in many respects is comparable to NWM and it offers the flexibility of setting up and calibration. A few immediate augmentations will include replacing the full HRAP mesh with ¼ HRAP grid mesh to resolve smaller streams currently not represented by the former, and identify additional bay inlets to be included in the inflow calculation;

4) introducing flow duration curves as a target for calibration of HEC-HMS and HL-RDHM, or introducing a statistical bias correction scheme to improve the representation of baseflow. This will help address the artificial inflation of inflow by these models during average conditions;

5) evaluating a newer NWM reanalysis based on NWM v2.0 that recently became available; the accuracy of this newer data set likely more closely reflects that of the real-time analysis generated using NWM v2.1. As NWM real-time flow analysis features corrections at gauged locations through a nudging approach, its accuracy could be somewhat higher than the corresponding retrospective analysis. Therefore, it will also be helpful archiving and evaluating NWM real-time flow analysis on an on-going basis; the

outcomes of the evaluation will serve as the basis for an enhanced bias correction scheme;

6) performing TxBLEND simulations based on each inflow trace of MMIPS, and using the salinity profile thus created to corroborate, and appraise the inflow series. Ideally, the most accurate inflow series is the one that leads to the most realistic salinity series. The results will help determine additional measures needed to improve each member model;

7) developing a postprocessor of the MMIPS that would translate the ensemble traces into probabilistic inflow estimates in a way that resembles the postprocessing of ensemble weather and streamflow forecast (Demargne et al. 2014); NWS now routines produce flow forecast with exceedance probability (Fig. 6-1), and methods such as Bayesian model averaging (Raftery et al. 1997) could be readily used for this purpose. The probabilistic inflow would help users appraise the uncertainties in the inflow estimates and plan for actions accordingly;

8) re-evaluating the spatial extents of bay watersheds by combining NHD-Plus dataset, aerial photos and high-resolution digital elevation model; and introducing remotely sensed surface water, from, say Landsat imageries for events such as Harvey to assess and corroborate the flow paths used in HL-RDHM, HEC-HMS, and NWM. If warranted, the connectivity grids for the models can be adjusted prior to the operational use of these models.

9) incorporating ancillary data, such as soil moisture and groundwater table observations, to closely examine the model states across wet and dry conditions, and appraise their physical realism. In particular, the tendency of all member models to produce spurious runoff response during extreme drought of 2011 needs to analyzed to help determine calibration or postprocessing strategies that would prevent similar artifacts from appearing in future drought events;
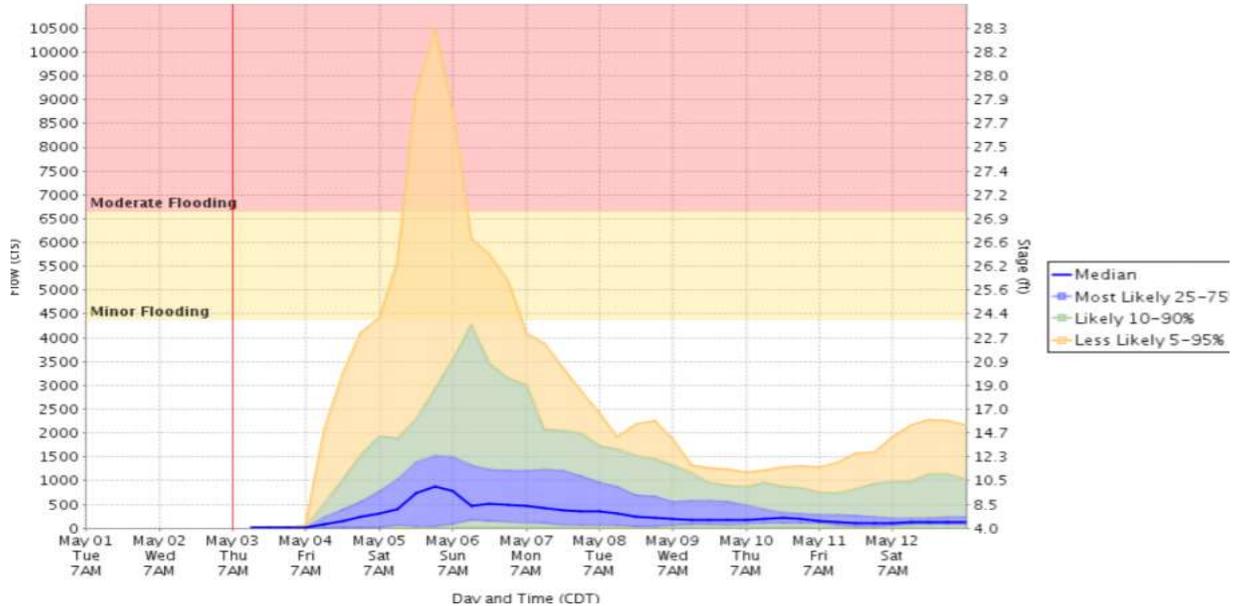
Figure 6-1   Example of ensemble stage prediction generated by WGRFC. Source: NWS

In addition to these enhancements, we also recommend that concerted monitoring efforts be undertaken across the Texas coast to gather inflow data for corroborating model outputs. Collecting streamflow over small, tidally influenced coastal streams is challenging, but even limited, ad hoc data will go a long way in identifying model deficiencies and determining the directions of improvement. We also suggest that, once the MMIPS is set up and passes initial internal evaluations at the TWDB, follow-on efforts to be undertaken to extend the coverage of MMIPS to other bays and estuaries along the Texas coast. As a starter, the East Matagorda Bay receives freshwater inflow only from neighboring small streams after the diversion of Lower Colorado River, and present estimates from TxRR have been deemed uncertain. It will be beneficial to implement MMIPS for all bay watersheds that drain to the Lavaca-Colorado Estuary System.

The UTA project team estimates that adopting the MMIPS for Matagorda Bay will require the TWDB half a year assuming one full time employee being committed to this task. The specific steps associated with adoption include

1. setting up models, parameter data sets, and forcings on TWDB computing platforms;

2. setting up real-time ingest of MPE precipitation data, and NWM real-time forcings (https://www.nco.ncep.noaa.gov/pmb/products/nwm/);

3. configuring TxRR, HL-RDHM and HEC-HMS for continuous simulation and to ingest MPE precipitation data on an hourly increment;

4. configuring HEC-HMS to ingest the NWM forcing data sets needed for ET calculations, which include temperature, relatively humidity, wind speed, and net radiation;

5. setting up automatic ingest of NWM streamflow analysis and programs for performing postprocessing

Extending the coverage of MMIPS to the entirety of Lavaca-Colorado estuary system will require approximate 1.0 years to complete. Implementing a full version of MMIPS for the rest of Texas bays and estuaries will require up to five years. A potential way of expediting the process is to implement a simplified version of MMIPS that only relies on TxRR simulations and NWM real-time analysis, while gradually introducing other models over time.

7 Acknowledgement

8   References

Agrawal, A., 2005. PrePro2004: a data model with pre and post-processor for HEC-HMS (Doctoral dissertation, Texas A&M University). 199 p.

Baeck, M.L. and Smith, J.A., 1995. Climatological analysis of manually digitized radar data for the United States east of the Rocky Mountains. Water Resources Research, 31(12), pp.3033-3049.

Bennett, T.H. 1998. Development and Application of a Continuous Soil Moisture Accounting Algorithm for the Hydrologic Engineering Center Hydrologic Modeling System (HEC-HMS). Davis, CA: University of California, Davis. 358 p.

Bennett, T.H. and Peters, J.C., 2000. Continuous soil moisture accounting in the hydrologic Engineering Center Hydrologic Modeling System (HEC-HMS). In Building partnerships (pp. 1-10).

Burnash, R.J.C., Ferral, R.L. and McGuire, R.A., 1973. A generalised streamflow simulation system–conceptual modelling for digital computers. Joint Federal and State River Forecast Center. Sacramento, Technical Report. 204 p.

Chu, X. and Steinman, A., 2009. Event and continuous hydrologic modeling with HEC-HMS. Journal of Irrigation and Drainage Engineering, 135(1), pp.119-124.

Cosgrove, B.A., Lohmann, D., Mitchell, K.E., Houser, P.R., Wood, E.F., Schaake, J.C., Robock, A., Marshall, C., Sheffield, J., Duan, Q. and Luo, L., 2003. Real-time and retrospective forcing in the North American Land Data Assimilation System (NLDAS) project. Journal of Geophysical Research: Atmospheres, 108(D22).

Cosgrove, B.A., Clark, E., Reed, S.M., Koren, V.I., Zhang, Z., Cui, Z. and Smith, M.B., 2012. Overview and initial evaluation of the Distributed Hydrologic Model Threshold Frequency (DHM-TF) flash flood forecasting system. NOAA technical report NWS. 54 p.

Cosgrove, B., Gochis, D., Clark, E.P., Cui, Z., Dugger, A.L., Feng, X., Karsten, L.R., Khan, S., Kitzmiller, D., Lee, H.S. and Liu, Y., 2016. An Overview of the National Weather Service National Water Model. AGUFM, 2016, pp.H42B-05.

De Silva, M.M.G.T., Weerakoon, S.B. and Herath, S., 2014. Modeling of event and continuous flow hydrographs with HEC–HMS: case study in the Kelani River Basin, Sri Lanka. Journal of Hydrologic Engineering, 19(4), pp.800-806.

Demargne, J., Wu, L., Regonda, S.K., Brown, J.D., Lee, H., He, M., Seo, D.J., Hartman, R., Herr, H.D., Fresch, M. and Schaake, J., 2014. The science of NOAA's operational hydrologic ensemble forecast service. Bulletin of the American Meteorological Society, 95(1), pp.79-98.

Duchon, C.E. and Biddle, C.J., 2010. Undercatch of tipping-bucket gauges in high rain rate events. Advances in Geosciences, 25, p.11.

Fleming, M., 2002. Continuous hydrologic modeling with HMS: parameter estimation and model calibration and validation (Doctoral dissertation, MSc Thesis, Tennessee Technological University). 186 p.

Fulton, R.A., Breidenbach, J.P., Seo, D.J., Miller, D.A. and O'Bannon, T., 1998. The WSR-88D rainfall algorithm. Weather and forecasting, 13(2), pp.377-395.

Georgakakos, K.P., Seo, D.J., Gupta, H., Schaake, J. and Butts, M.B., 2004. Towards the characterization of streamflow simulation uncertainty through multimodel ensembles. Journal of Hydrology, 298(1-4), pp.222-241.

Gochis, D.J., Yu, W. and Yates, D.N., 2013. The WRF-Hydro model technical description and user's guide, version 1.0. NCAR Tech. Doc. 120 p.

Gochis, D.J., Barlage, M., Dugger, A., FitzGerald, K., Karsten, L., McAllister, M., McCreight, J., Mills, J., RafieeiNasab, A., Read, L. and Sampson, K., 2018. The WRF-Hydro modeling system technical description,(Version 5.0). NCAR Technical Note, 107 p.

Greene, D.R. and Hudlow, M.D., 1982, June. Hydrometeorologic grid mapping procedures. In AWRA Int. Symp. on Hydrometeorology, Denver, CO. 20 p.

Habib, E.H., Meselhe, E.A. and Aduvala, A.V., 2008. Effect of local errors of tipping-bucket rain gauges on rainfall-runoff simulations. Journal of hydrologic engineering, 13(6), pp.488-496.

He, Y., Zhang, Y., Kuligowski, R., Cifelli, R. and Kitzmiller, D., 2018. Incorporating satellite precipitation estimates into a radar-gauge multi-sensor precipitation estimation algorithm. Remote Sensing, 10(1), p.106.

Kendall, M.G., 1938. A new measure of rank correlation. Biometrika, 30(1/2), pp.81-93.

Kim, H.C. and Montagna, P.A., 2009. Implications of Colorado river (Texas, USA) freshwater inflow to benthic ecosystem dynamics: A modeling study. Estuarine, Coastal and Shelf Science, 83(4), pp.491-504.

Kitzmiller, D., Van Cooten, S., Ding, F., Howard, K., Langston, C., Zhang, J., Moser, H., Zhang, Y., Gourley, J.J., Kim, D. and Riley, D., 2011. Evolving multisensor precipitation estimation methods: Their impacts on flow prediction using a distributed hydrologic model. Journal of Hydrometeorology, 12(6), pp.1414-1431.

Kitzmiller, D., Miller, D., Fulton, R. and Ding, F., 2013. Radar and multisensor precipitation estimation techniques in National Weather Service hydrologic operations. Journal of Hydrologic Engineering, 18(2), pp.133-142.

Kitzmiller, D.H., Wu, W., Zhang, Z., Patrick, N. and Tan, X., 2018. The Analysis of Record for Calibration: A High-Resolution Precipitation and Surface Weather Dataset for the United States. AGUFM, 2018, pp.H41H-06.

Koren, V.I., Smith, M., Wang, D., Zhang, Z., 2000. Use of soil property data in the derivation of conceptual rainfall-runoff model parameters. In: Proceedings of the 15th Conference on Hydrology. AMS, Long Beach, CA, pp. 103–106.

Koren, V., Reed, S., Smith, M., Zhang, Z. and Seo, D.J., 2004. Hydrology laboratory research modeling system (HL-RMS) of the US National Weather Service. Journal of Hydrology, 291(3-4), pp.297-318.

Kuzmin, V., Seo, D.J. and Koren, V., 2008. Fast and efficient optimization of hydrologic model parameters using a priori estimates and stepwise line search. Journal of Hydrology, 353(1-2), pp.109-128.

Langevin, C., Swain, E. and Wolfert, M., 2005. Simulation of integrated surface-water/ground-water flow and salinity for a coastal wetland and adjacent estuary. Journal of Hydrology, 314(1-4), pp.212-234.

Mesinger, F., DiMego, G., Kalnay, E., Mitchell, K., Shafran, P.C., Ebisuzaki, W., Jović, D., Woollen, J., Rogers, E., Berbery, E.H. and Ek, M.B., 2006. North American regional reanalysis. Bulletin of the American Meteorological Society, 87(3), pp.343-360.

Nan, Z., Wang, S., Liang, X., Adams, T.E., Teng, W. and Liang, Y., 2010. Analysis of spatial similarities between NEXRAD and NLDAS precipitation data products. IEEE Journal of Selected Topics in Applied Earth Observations and Remote Sensing, 3(3), pp.371-385.

National Weather Service, 2008. HYDROLOGY LABORATORY-RESEARCH DISTRIBUTED HYDROLOGIC MODEL (HL-RDHM) USER MANUAL V. 2.4.2. 108 p.

Nešpor, V. and Sevruk, B., 1999. Estimation of wind-induced error of rainfall gauge measurements using a numerical simulation. Journal of atmospheric and oceanic technology, 16(4), pp.450-464.

Niu, Guo-Yue, Zong-Liang Yang, Kenneth E. Mitchell, Fei Chen, Michael B. Ek, Michael Barlage, Anil Kumar et al. "The community Noah land surface model with multiparameterization options (Noah-MP): 1. Model description and evaluation with local-scale measurements." Journal of Geophysical Research: Atmospheres 116, no. D12 (2011).

Rabalais, N.N., Turner, R.E., Wiseman, Jr, W.J. and Dortch, Q., 1998. Consequences of the 1993 Mississippi River flood in the Gulf of Mexico. Regulated Rivers: Research & Management: An International Journal Devoted to River Research and Management, 14(2), pp.161-177.

Raftery, A.E., Madigan, D. and Hoeting, J.A., 1997. Bayesian model averaging for linear regression models. Journal of the American Statistical Association, 92(437), pp.179-191.

Rasmussen, T., 2008. Methods for evaluating wetland condition: wetland hydrology. Office of Water, US Environmental Protection Agency, Washington, DC. EPA-822-R-08-024. US EPA.

Reed, S. M., 2003. Deriving flow directions for coarse-resolution (1-4 km) gridded hydrologic modeling. Water Resources Research, 39(9). 11 p.

Reed, S., Koren, V., Smith, M., Zhang, Z., Moreda, F., Seo, D.J. and Participants, D.M.I.P., 2004. Overall distributed model intercomparison project results. Journal of Hydrology, 298(1-4), pp.27-60.

Reed, S., Schaake, J. and Zhang, Z., 2007. A distributed hydrologic model and threshold frequency-based method for flash flood forecasting at ungauged locations. Journal of Hydrology, 337(3-4), pp.402-420.

Russell, M.J., Montagna, P.A. and Kalke, R.D., 2006. The effect of freshwater inflow on net ecosystem metabolism in Lavaca Bay, Texas. Estuarine, Coastal and Shelf Science, 68(1-2), pp.231-244.

Scharffenberg, W., Bartles, M.J., Brauer, T., Fleming, M, and Karlovits, G. 2018. Hydrologic modeling system HEC-HMS 4.3 User's Manual. 624 p. Available at https://www.hec.usace.army.mil/software/hec-hms/documentation/HEC-HMS_Users_Manual_4.3.pdf

Schoenbaechler, C., Guthrie, C.G., Matsumoto, J., Lu, Q. and Negusse, S., 2011. TxBLEND Model Calibration and Validation for the Lavaca-Colorado Estuary and East Matagorda Bay. Texas Water Development Board, Austin. TX. 72 p.

Seo, D.J., 1998a. Real-time estimation of rainfall fields using radar rainfall and rain gage data. Journal of Hydrology, 208(1-2), pp.37-52.

Seo, D.J., 1998b. Real-time estimation of rainfall fields using rain gage data under fractional coverage conditions. Journal of Hydrology, 208(1-2), pp.25-36.

Seo, D.J., Breidenbach, J.P. and Johnson, E.R., 1999. Real-time estimation of mean field bias in radar rainfall data. Journal of Hydrology, 223(3-4), pp.131-147.

Seo, D.J. and Breidenbach, J.P., 2002. Real-time correction of spatially nonuniform bias in radar rainfall data using rain gauge measurements. Journal of Hydrometeorology, 3(2), pp.93-111.

Seo, D.J., 2013. Conditional bias-penalized kriging (CBPK). Stochastic environmental research and risk assessment, 27(1), pp.43-58.

Singh, W.R. and Jain, M.K., 2015. Continuous hydrological modeling using soil moisture accounting algorithm in Vamsadhara River basin, India. Journal of Water Resource and Hydraulic Engineering, 4(4), pp.398-408.

Smith, M.B., Koren, V., Reed, S., Zhang, Z., Zhang, Y., Moreda, F., Cui, Z., Mizukami, N., Anderson, E.A. and Cosgrove, B.A., 2012. The distributed model intercomparison project–Phase 2: Motivation and design of the Oklahoma experiments. Journal of Hydrology, 418, pp.3-16.

Villarini, G., Smith, J.A., Baeck, M.L., Marchok, T. and Vecchi, G.A., 2011. Characterization of rainfall distribution and flooding associated with US landfalling tropical cyclones: Analyses of Hurricanes Frances, Ivan, and Jeanne (2004). Journal of Geophysical Research: Atmospheres, 116(D23).

Xia, Y., 2006. Optimization and uncertainty estimates of WMO regression models for the systematic bias adjustment of NLDAS precipitation in the United States. Journal of Geophysical Research: Atmospheres, 111(D8).

Xia, Y., 2007. Calibration of LaD model in the northeast United States using observed annual streamflow. Journal of Hydrometeorology, 8(5), pp.1098-1110.

Xia, Y., Mitchell, K., Ek, M., Sheffield, J., Cosgrove, B., Wood, E., Luo, L., Alonge, C., Wei, H., Meng, J. and Livneh, B., 2012. Continental-scale water and energy flux analysis and validation for the North American Land Data Assimilation System project phase 2 (NLDAS-2): 1. Intercomparison and application of model products. Journal of Geophysical Research: Atmospheres, 117(D3).

Yang, Z.L., Niu, G.Y., Mitchell, K.E., Chen, F., Ek, M.B., Barlage, M., Longuevergne, L., Manning, K., Niyogi, D., Tewari, M. and Xia, Y., 2011. The community Noah land surface model with multiparameterization options (Noah-MP): 2. Evaluation over global river basins. Journal of Geophysical Research: Atmospheres, 116(D12).

Zaslavsky, D. and Rogowski, A.S., 1969. Hydrologic and morphologic implications of anisotropy and infiltration in soil profile development. Soil Science Society of America Journal, 33(4), pp.594-599.

Zhang, J., Howard, K., Langston, C., Kaney, B., Qi, Y., Tang, L., Grams, H., Wang, Y., Cocks, S., Martinaitis, S. and Arthur, A., 2016. Multi-Radar Multi-Sensor (MRMS) quantitative precipitation estimation: Initial operating capabilities. Bulletin of the American Meteorological Society, 97(4), pp.621-638.

Zhang, Y., Reed, S. and Kitzmiller, D., 2011a. Effects of retrospective gauge-based readjustment of multisensor precipitation estimates on hydrologic simulations. Journal of Hydrometeorology, 12(3), pp.429-443.

Zhang, Y., Zhang, Z., Reed, S. and Koren, V., 2011b. An enhanced and automated approach for deriving a priori SAC-SMA parameters from the soil survey geographic database. Computers & geosciences, 37(2), pp.219-231.

Zhang, Y., Seo, D.J., Kitzmiller, D., Lee, H., Kuligowski, R.J., Kim, D. and Kondragunta, C.R., 2013. Comparative strengths of SCaMPR satellite QPEs with and without TRMM ingest versus gridded gauge-only analyses. Journal of Hydrometeorology, 14(1), pp.153-170.

Zhang, Y., Reed, S., Gourley, J.J., Cosgrove, B., Kitzmiller, D., Seo, D.J. and Cifelli, R., 2016. The impacts of climatological adjustment of quantitative precipitation estimates on the accuracy of flash flood detection. Journal of Hydrology, 541, pp.387-400.

Zhang, Z., Koren, V., Reed, S., Smith, M., Zhang, Y., Moreda, F. and Cosgrove, B., 2012. SAC-SMA a priori parameter differences and their impact on distributed hydrologic model simulations. Journal of Hydrology, 420, pp.216-227.

Zhang, Y., Kitzmiller, D., Seo, D.J., Kim, D. and Cifelli, R., 2017. Creation of multisensor precipitation products from WSI NOWrad reflectivity data. Journal of Hydrologic Engineering, 22(5), p.E4015001.

9   Appendices

A. Processing MPE data and creating mean areal precipitation time series

The MPE data being created at WGRFC are on the HRAP grid mesh. The hourly precipitation total data for each hour is stored in the so-called "xmrg" file format. The naming convention for the xmrg file is as follows:

xmrgMMDDYYYYHHz

Where MM: 2-digit month, DD: 2-digit day, YYYY: 4-digit year, and HH: 2-digit hour. The last character 'z' indicates that the date-time is in Zulu time (UTC). For example, xmrg0313200008z stores the rainfall accumulation ending on March 13, 2000 08z. The project team has delivered two archives to the TWDB.

The archive MPE data for 1998-2017 are included in the archive **xmrg-wgrfc.tgz**, whereas the scripts for processing the MPE data can be found in **MPE-MAP.tgz**

Archive name	Content
xmrg-wgrfc.tgz	MPE data from WGRFC for 1998-2017
MPE-MAP.tgz	Scripts for computing mean areal precipitation from raw xmrg files; list of xmrg files and basin boundaries for Matagorda Bay watersheds
	Examples of MAP series used in the project
xmrg-util.tgz	Utilities for decoding and manipulating xmrg files

These tools are best used in a unix/linux environment. The UTA project team performs most of the analysis on a Dell Workstation with 32GB memory and 15TB storage space. It is recommended that a Linux workstation with at least 16GB memory and 8TB storage be set up.

Below is a table summarizing the hardware, operating systems and software settings recommended for using the tools. Note all the compilers and utilities listed here can be obtained for free.

Hardware requirement	Workstation with >16GB memory and >8TB storage
Operating systems	Linux with Kernel 4.x and above
Compilers	Gnu C, C++ and gfortran; or Intel C, C++ and Fortran compilers
Utilities	Gnu tar; shell; Gnu Make
	Python3, R
Libraries	C++ Boost, libz, libm

To use the tools, the following steps will be involved.

1. Preparations

Save the three archives in a directory on the workstation, say /data/xmrg-works

Uncompress the xmrg-util.tgz by issuing the following command:
[#####@#### TWDB-deliverables]$ tar zxvf xmrg-util.tgz

The files are now dumped to the directory "xmrg-util". Use 'ls' to list the files under the directory:

[#####@#### TWDB-deliverables]$ ls xmrg-util
compMAP_64x/ XMRG_LIB_64x/ xmrgtoasc/

The first directory "compMAP_64x" contains the codes for computing MAP-X from the xmrg files. The directory "xmrgtoasc" contains the codes for dumping the content of a xmrg file into ArcGIS ascii grid format. In order to compile these, one needs to step the XMRG libraries under "XMRG_LIB_64x". The commands are shown below.

[#####@#### TWDB-deliverables]$ cd xmrg-util/XMRG_LIB_64x/
[#####@#### XMRG_LIB_64x]$ls
com_header.h*   fill_miss2d.o* HRAP.o*   write_grid2.f* XMRG.o*
endian.c*   GNUmakefile*   linux.h*   write_grid2.o* xmrgutil.a*
endian.o*   GNUmakefile,v* make.log*   XMRG.cc*
filesystem.hpp* HRAP.cc*   models.h*   XMRG.cc.bak*
fill_miss2d.c*   HRAP.h*   projection.h* XMRG.h*

Among these files, GNUmakefile is the makefile for compiling the codes. Before compiling, making sure: 1) gnu make is installed; and b) boost libraries are installed. Now issue the following command:

[#####@#### TWDB-deliverables]$ make clean
[#####@#### XMRG_LIB_64x]$ make

This will create "xmrgutil.a". Once this is done, one may proceed to compile the executables. Let's first set up the xmrgtoasc utility:

[#####@#### TWDB-deliverables]$ cd ../xmrgtoasc
[#####@#### TWDB-deliverables]$ rm xmrgtoasc.x
[#####@#### TWDB-deliverables]$ make clean; make

If successful, this will create an executable "xmrgtoasc.x" in the current directory. Add the current path to your default path so that it can be invoked regardless of directory you are in.

87

Now, switch to directory compMAP_64x, and compile the executable for computing the basin average precipitation.

[#####@#### TWDB-deliverables]$ cd ../compMAP_64x
[#####@#### TWDB-deliverables]$ make clean; make

If successful, this will create an executable "compMAP_64x.x". Also add the current directory to your default path.

2.   Now, proceed to use xmrgtoasc.x to view the xmrg files.

The xmrg files are in the archive xmrg-WGRFC.tgz. To untar, use the following command:

[#####@#### MPE]$ tar zxf xmrg-WGRFC.tgz

This will extract all the xmrg files under media/home2/WGRFC/data/

[#####@#### MPE]$ cd media/home2/WGRFC/data/2000

Type the following command after the prompt to create the ascii formatted grid:

[#####@#### MPE]$ xmrgtoasc.x xmrg0313200008z.gz -o xmrg0313200008z.asc

Then one can use any editor to view the asc file:

ncols 425
nrows 390
xllcorner 290.000000
yllcorner 10.000000
cellsize 1.000000
NODATA_value -1.000000
0.000000 0.000000 0.000000 0.000000 0.000000 0.000000 0.000000 0.000000 0.000000 0.000000 0.000000
0.000000 0.00
0000 0.000000 0.000000 0.000000 0.000000 0.000000 0.000000 0.000000 0.000000 0.000000 0.000000 0.000000
0.000000
 0.000000 0.000000 0.000000 0.000000 0.000000 0.000000 0.000000 0.000000 0.000000 0.000000 0.000000
0.000000 0.0
00000 0.000000 0.000000 0.000000 0.000000 0.000000 0.000000 0.000000 0.000000 0.000000 0.000000 0.000000
0.00000
0 0.000000 0.000000 0.000000 0.000000 0.000000 0.000000 0.000000 0.00

The header contains the dimension and the location of the grid in the HRAP coordinate system.

3.   Compute MAP series from a list of xmrg files.

[#####@#### TWDB]$ tar zxf MPE-MAPX.tgz
[#####@#### TWDB]$ cd MAPX/delivery/Scripts
[#####@#### Scripts]$ ls
compMAP_64x.x* convert.coord.hh.R* Matagorda_Grid.zip* xmrg.wg.lst*

88

comp.mapx.log* Matagorda.asc*   ws-coords/   xmrg.wg.sub.lst*
comp.mapx.sh* Matagorda_Grid/   ws.matagorda.lst*

The script "comp.mapx.sh" is for producing the MAP series for Matagorda Bay watersheds. To run it requires, one needs to create a list of xmrg file, and a list of files with basin masks. An example of xmrg list is given in "xmrg.wg.lst". This is what is in the file:
[#####@#### Scripts]$ more xmrg.wg.lst

/media/home2/WGRFC/data/1998/xmrg0101199800z.gz
/media/home2/WGRFC/data/1998/xmrg0101199801z.gz
/media/home2/WGRFC/data/1998/xmrg0101199802z.gz
/media/home2/WGRFC/data/1998/xmrg0101199803z.gz
/media/home2/WGRFC/data/1998/xmrg0101199804z.gz
/media/home2/WGRFC/data/1998/xmrg0101199805z.gz
/media/home2/WGRFC/data/1998/xmrg0101199806z.gz
/media/home2/WGRFC/data/1998/xmrg0101199807z.gz
/media/home2/WGRFC/data/1998/xmrg0101199808z.gz
/media/home2/WGRFC/data/1998/xmrg0101199809z.gz
/media/home2/WGRFC/data/1998/xmrg0101199810z.gz
/media/home2/WGRFC/data/1998/xmrg0101199811z.gz

For real-time operation, this list needs to be constantly updated. If the model is configured to run daily, the list may contain the names for the most recent 24 xmrg files.

The file "ws.matagorda.lst" contains the files that store the basin masks.

ws-coords/14010
ws-coords/15010
ws-coords/15015
ws-coords/15020
ws-coords/15025
ws-coords/15030
ws-coords/15040
ws-coords/15050
ws-coords/15055
ws-coords/15060
ws-coords/16001
ws-coords/16005
ws-coords/16007
ws-coords/16008
ws-coords/16014
ws-coords/17010
ws-coords/17020
ws-coords/17030
ws-coords/17040
ws-coords/17050
ws-coords/17060
ws-coords/17065
ws-coords/17070
ws-coords/17075

Each line represents one file. For convenience, all the files are stored under ws-coords. Here is an example of the basin mask:

```
> more ws-coords/15015
631 138
632 138
629 137
630 137
631 137
632 137
628 136
629 136
630 136
631 136
627 135
628 135
629 135
630 135
627 134
628 134
```

There are two columns, for x and y-coordinates for each pixel in the basin (in HRAP coordinate system). Masks for all the basins that drain to Matagorda-Lavaca system are included here. Before running the script, one needs to make sure compMAP_64x.x is in the current directory (the one sitting in the same directory needs to be removed).

[#####@#### Scripts]$ rm compMAP_64x.x

Then run the script, simply type

>comp.mapx.sh

The output time series for each of the watersheds can be found under MAPX/delivery/TS. Here is one example:

```
> head  ../TS/15040.mapx01
$MAPX FROM FILES:../TS
NEXRAD      MAP L  MM  1   15040
 1  2001 12  2007  1  F8.3
15040   19980101 00  0.000
15040   19980101 01  0.000
15040   19980101 02  0.000
15040   19980101 03  0.000
15040   19980101 04  0.000
15040   19980101 05  0.000
15040   19980101 06  0.000
```

The time series in the data card format, with a 3-line header and a table consisting of "WS-ID YYYYMMDD HH Precip", which represent watershed ID, date, time (in Zulu time), and precipitation amount is in mm.

Note that the mask for each basin was derived from the polygon basin boundary stored in the shapefile supplied by the TWDB using the R script named "convert.coord.hh.R" (also under MAPX/delivery/Scripts). In case the basin boundaries are updated, one may convert the polygon to update the "Matagorda.asc" that serves as the basis for the R script. Running the R script will create a new set of masks.

4. Conversion of the hourly MAPX time series into daily accumulations needed for TxRR input. This is accomplished in a python script "PCP_Input_TxRR_From_MAPX.py" under MAPX/delivery/Scripts. The script performs the following tasks:

   1) translating the time labels of the hourly series from zulu time to local (Central time). We used central daylight saving time as the target time zone for convenience but this could be changed in the future;
   2) aggregating the resulting time series onto daily scale, and merging the results into one comma delimited file;

The script can be run by typing the following commands:

[#####@#### Scripts]$ python3 PCP_Input_TxRR_From_MAPX.py

An example output is included in the deliverable named "date_ws_avg_precip.csv" (under MAPX/delivery/Scripts). This file contains daily precipitation time series for all basins.

```
>more date_ws_avg_precip.csv
,date,16007,16014,16001,16005,15020,15050,17030,15030,17020,16008,14010,15060,15040,17010,15
010,17040,17050,15025,15055,17060,17065,15015,17075,17070
1/1/1998,1/1/1998,0.003897638,0.001181102,0.001141732,0.001614173,0,0,0,0.000984252,0,0,0.001614
173,0,0,0,0,0,0.004527559,0,0,0.001062992,0.002322835,0,0,0,0.002952756,0,0,0,0,0.000314961
1/2/1998,1/2/1998,0.026574803,0.026181102,0.000551181,0.008307087,0,0,0.000748031,0.019606299,
0.001456693,0.013031496,0.040629921,0.026653543,0.001889764,0.001968504,0.011653543,0.009763
78,0.048503937,0.024291339,0.010551181,0,0.027244094,0.013503937,0.027322835,0.012480315,0.0
17165354
```

B. HEC-HMS model configuration and parameter estimation

The files needed for setting up and running HEC-HMS can be found in HEC-HMS.zip

Archive name	Content
HEC-HMS.zip	HEC-HMS configuration files, maps, forcings, and example results

The HEC-HMS set up was developed for version 4.3 on Microsoft Windows 7 platform. In order to run HEC-HMS in real time. It is recommended that a Linux workstation with at least 32GB memory and 10TB storage be set up.

Below is a table summarizing the hardware, operating systems and software settings recommended for using the tools.

Hardware Requirements	Workstation with >32GB memory and >10TB storage
Operating systems	Windows 7, 8, 10
Compilers	N/A
Utilities	xmrgtodss, HEC-DSS (optional)
	ArcGIS, Python3
Libraries	N/A

This appendix details the model configuration, preparation of forcing inputs, and parameter estimation.

Model Configuration:

The main component is basin model that was set up based on the shapefile provided by the TWDB, at this stage we excluded the watershed delineation procedure in GIS because we already have the sub-watersheds. We get the area, latitude, and longitude from the given shapefile using the GIS tool. We used simple canopy as Canopy method, simple surface as Surface Method, SMA as loss method, Clark Unit Hydrograph as Transformed Method and Linear Reservoir as Base Flow Method. All the parameters of the methods are estimated using soil, land use information and USGS observed flow.

Moreover, the control specifications include a starting date and time, ending date and time, and a time interval. All the input and output time-series and other paired-value data are stored in HEC's Data Storage System (DSS). The default outputs include peak flow and total volume for each hydrologic element in the basin model. Table 9-1 shows that selected methods for this study.

Basin Average Precipitation: We downloaded the hourly CONUS NLDAS_FORA0125_H: NLDAS Primary Forcing Data L4 Hourly 0.125 x 0.125-degree V002 data from Earth data system of NASA (https://disc.gsfc.nasa.gov/datasets/NLDAS_FORA0125_H_002/summary). As

our model is a lumped model, we converted the gridded precipitation to basin average precipitation using zonal statistic tool available in ArcGIS. After making the basin average rainfall, we wrote a python script to make time series rainfall from each of the hourly csv file for 15 years, the total number of files processed was more than 131K, so processing this large number of files altogether needs big memory of the computer system and takes long time. A schematic of the module is shown in the following Fig 9-1 where we loop through each NetCDF files and passing the basin boundary to compute the basin average values and saves as csv files in the designated directory.
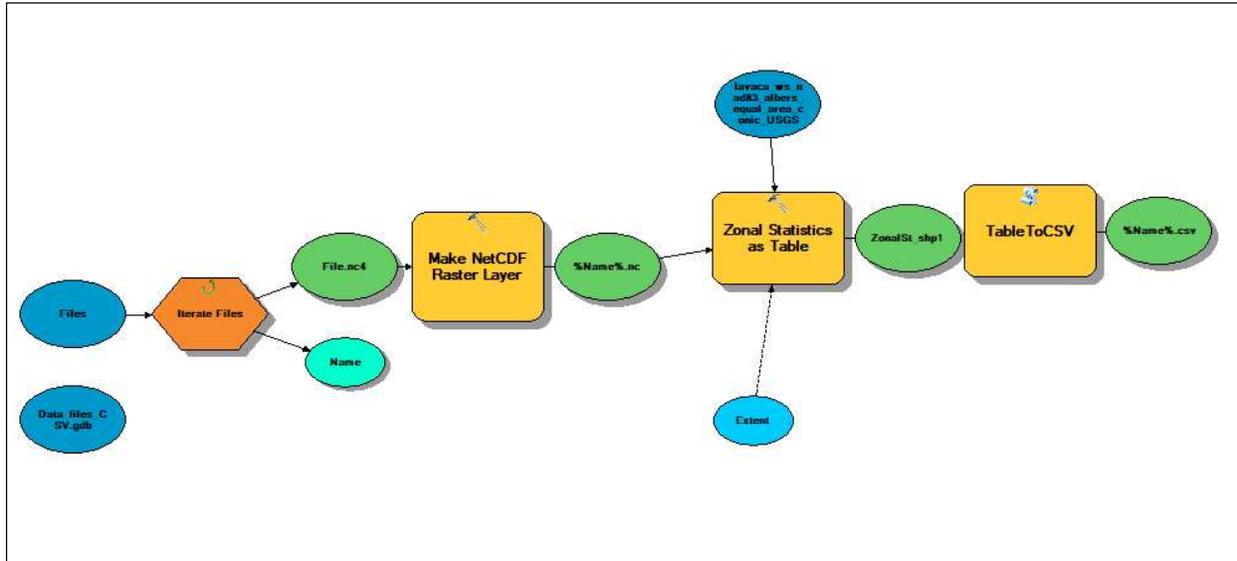
Figure 9-1   Schematic of the process of creating mean areal precipitation for HEC-HMS.

Table 9-1 HEC-HMS components and models of choice.

Component	Model
Surface	Simple Surface
Canopy	Simple Canopy
Loss	SMA
Transform	SCS Unit Hydrograph
Baseflow	Linear Reservoir
Routing	Muskingum

The surface, canopy, loss, and baseflow methods for the SMA-based model utilize a total of 17 parameters; eight parameters namely canopy storage, surface storage, infiltration rate, percent impervious, soil percolation rate, soil storage, tension zone storage, groundwater layer 1 percolation rate have been estimated from soil (Fig. 9-2) and land use (Fig. 9-3) data, four parameters have been estimated from streamflow recession analysis (groundwater layers 1 and 2

93

storage depth and coefficient), and five parameters have been calibrated (groundwater layer 2 percolation rate, groundwater layers 1 and 2 baseflow coefficient and baseflow reservoir count). It is necessary to mention that the groundwater layer 1 represents interflow, and groundwater layer 2 represents groundwater flow.
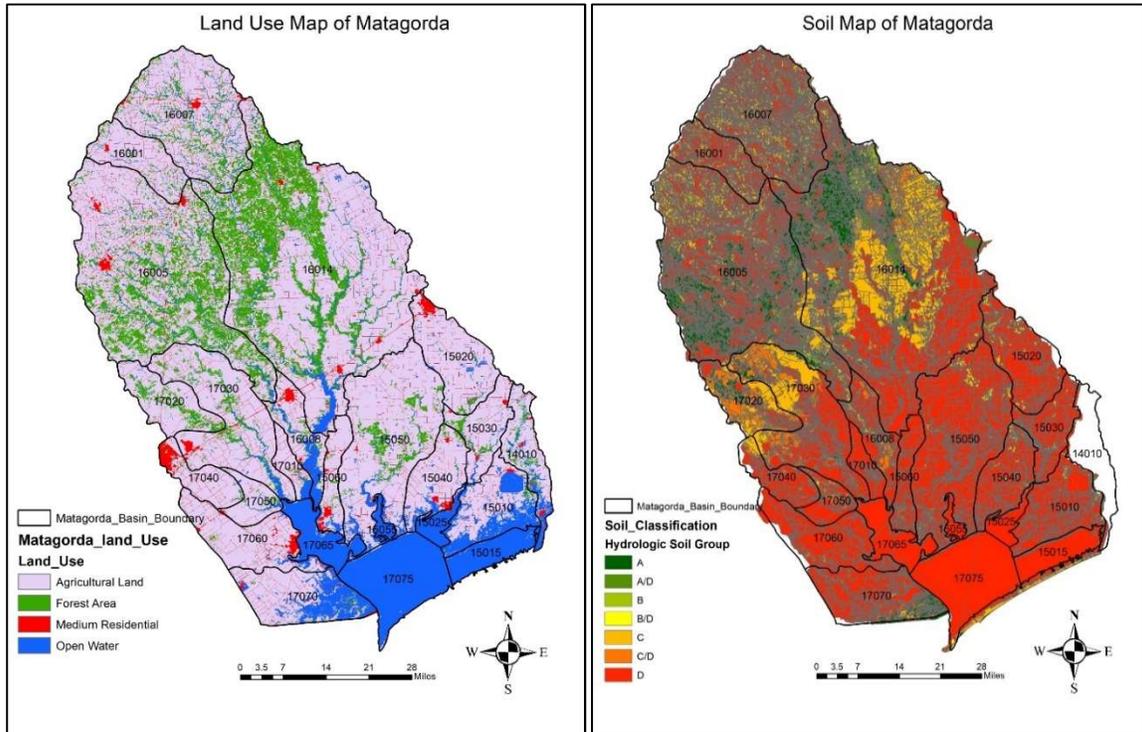
Figure 9-2   Soil(left) and land cover (right) of watersheds draining to Matagorda Bay.

The soil map has been downloaded from soil SSURGO website using ArcGIS SSURGO downloader. (https://www.arcgis.com/apps/View/index.html?appid=cdc49bd63ea54dd2977f3f2853e07fff). Then classified the soil data using ArcGIS tool, based on the soil group as shown in the Fig. 9-1. In this study, the USGS (https://www.usgs.gov/core-science-systems/science-analytics-and-synthesis/gap/science/land-cover-data-download?qt-science_center_objects=0#qt-science_center_objects) land use information of Texas for the year 2011 has been used because of study period which is from 2003 to 2017, that's why we omitted the land use data for 2006 and 2016. The steps followed for estimating the model parameters are adopted from tutorial provided on Dr. Venkatesh Merwade's research page and available at the following address: https://web.ics.purdue.edu/~vmerwade/education/geohms.pdf and the model set-up was adopted from 'Advanced Hydrology' course material at UTA.

1) Parameters estimated from Land Cover: The maximum canopy storage and percent impervious grids are both estimated from land use data (Fig. 9-3). The values provided in Table 9-3 (Bennett 1998), canopy interception values are estimated. Since Matagorda watershed is basically a rural watershed and it is considered covered by general vegetation, we estimated the canopy interception as 0.05 inch or 1.27 for our initial model setup. It is observed from the Fig.

B-3 that the watershed is mostly covered by 'Agricultural Land' and some part is covered by 'Forest'.

Table 9-2   Canopy interception values in the HEC-HMS surface model.

Type of Vegetation	Canopy Interception	
	In.	mm
General Vegetation	0.05	1.270
Grasses and Deciduous Trees	0.08	2.032
Trees and Coniferous Trees	0.1	2.540

2) Parameters estimated from SSURGO Data: Six SMA parameters are estimated from the SSURGO database, maximum surface storage, maximum infiltration rate, maximum soil percolation rate, soil storage, tension zone storage, and groundwater layer 1 maximum percolation rate. Surface storage values are estimated for each sub-basin from Table 9-3, that shows the default values of surface depression storage. It is also discernible from Fig-1 that the watershed is dominated by soil group D which are clay loam, silty clay loam, sandy clay, silty clay, or clay. This Hydrologic Soil Group (HSG) has the highest runoff potential. They have very low infiltration rates when thoroughly wetted and consist chiefly of clay soils with a high swelling potential, soils with a permanent high water table, soils with a claypan or clay layer at or near the surface and shallow soils over nearly impervious material. In this study, we considered 'Flat, Furrow Land, with moderate to gentle slope, however we assumed that the surface is dry initially and maximum storage is 0.2 in.

Table 9-3 Values of surface depression storage from Fleming (2002).

Description	Slope (%)	Surface Storage	
		In.	mm
Paved Impervious Areas	NA	0.125-0.25	3.18-6.35
Flat, Furrowed Land	0-5	2.00	50.8
Moderate to Gentle Slopes	5-30	0.25-0.50	6.35-12.70
Steep, Smooth Slopes	>30	0.04	1.02

3) Parameters estimated from USGS Streamflow Data: First we plotted the daily streamflow data for 3 to 4 storms occurring during different months of the year considering the storms are fairly isolated; we chose the storms such that streamflow hydrograph returns to normal for a couple days before runoff from the next storm is visible. we know that streams convey stored water from

95

three different sources such as stream channels, surface soil known as interflow, and groundwater as baseflow. We break up a streamflow hydrograph into its various components and calculate the variables necessary for soil moisture accounting in HEC-HMS. We downloaded the available streamflow data from USGS website and create a hydrograph of the streamflow data on a semi-logarithmic plot as shown in the following Fig. 9-3 for USGS station 08164000.
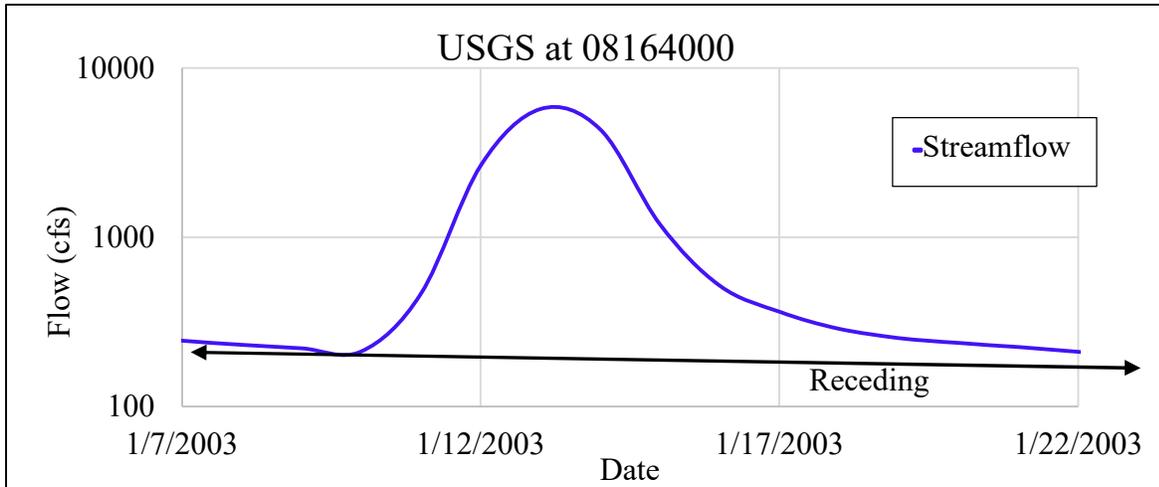
Figure 9-3   Example hydrograph for recession analysis.

The tail-end of the receding limb represents the time when groundwater is the only source contributing to streamflow, when both surface runoff and interflow stop. There should be an inflection point visible in this area of the graph to help you identify the correct portion of the hydrograph. The Fig-B5 shows the procedure of groundwater separation from hydrograph, projecting a line backwards from the tail-end of the receding limb to the time of peak flow, maintaining the slope of that tail-end portion and connecting the line to the point at which the hydrograph begins to rise as a result of runoff .This line represents the groundwater contribution to streamflow, or GW2.
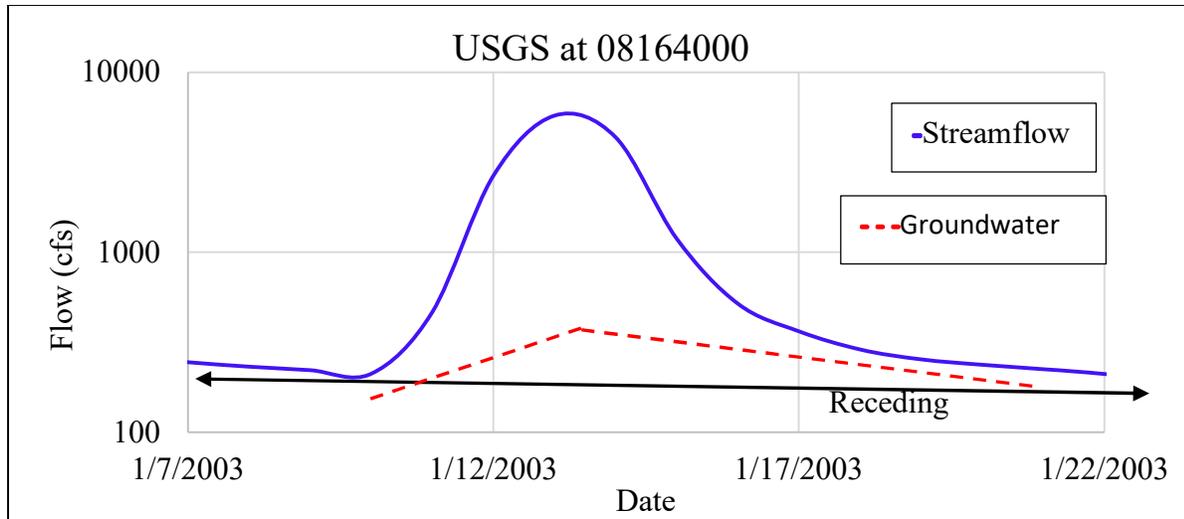
Figure 9-4   **Schematic for separating groundwater contribution to streamflow.**

After that subtracted the groundwater from the streamflow, we get the interflow and this interflow represents GW1. We know that the equation of a recession curve of a hydrograph is expressed by the following equation 1:

$q_1 = q_0 K_r = q_0 * \exp(-\alpha t)$

Where q_0 is the initial streamflow, q_1 is the streamflow at a later time t, K_r is a recession constant less than 1, and $\alpha = -\ln K_r$. The time stop for streamflow regression analysis is assumed to be 1 day. Using the area of shallowest slope of the streamflow hydrograph and Equation B1, we calculated the Groundwater 2 α-value for each step. we get the final α-values after averaging all and calculated the Groundwater 2 Recession Coefficient using Equation B2, as shown below:

$Recession\ Coefficient = 1/\alpha$

Using the same section of the streamflow hydrograph and Equation B3, calculated the Groundwater 2 Storage depth for each step and get the final Groundwater B2 after averaging them.

Storage Depth. $S_t = q_t / A\alpha$

Where S_t is the storage in the basin at time, t and A is the area of the watershed. we repeated the same calculations using the Runoff and Interflow graph to determine the Groundwater 1 Recession Coefficient and Groundwater 1 Storage Depth.

Table 9-4 shows a brief description of how we estimated the model parameters for this study.

4) Maximum Infiltration Rate. The maximum infiltration rate or infiltration capacity is the fastest rate at which precipitation can seep from the ground surface into the soil profile and it is

97

greatest when the soil is saturated, however, it decreases significantly as the water content of the soil decreases. Since the maximum hydraulic conductivity is the saturated hydraulic conductivity, the maximum infiltration rate of each map unit is taken as the weighted average of the saturated hydraulic conductivity for the topmost horizon of each component this is shown in the following Table 9-4. This is achieved using the component percent and the saturated hydraulic conductivity of the first horizon (Fleming 2002)

Table 9-4 Example I of a multi-component soil unit and saturate hydraulic conductivity values.

Cokey: 4560	Cokey: 5428	Cokey: 2856
Component %: 40	Component %: 26	Component %: 41
Layer 1 saturated hydraulic conductivity (μm/s): 6.25	Layer 1 saturated hydraulic conductivity (μm/s): 22.20	Layer 1 saturated hydraulic conductivity (μm/s): 85.38

Sample Calculation:

Max. Infiltration Rate = (40*6.25/100)+(26*22.20/100)+(41*85.38/100) = 43.28 μm/s

5) Maximum Percolation Rate. Percolation is the process by which water is transferred through the soil profile and groundwater layers and limited by the lowest hydraulic conductivity (Zaslavsky and Rogowski 1969). As described in Bennett (1998) and Fleming (2002), the average saturated hydraulic conductivity of all horizons in a component is used to calculate the maximum percolation rate. The maximum percolation rate is taken as the weighted average of the horizon-average saturated hydraulic conductivity for all components in a map unit and is used for both the soil profile and groundwater layer 1 percolation rates, a sample calculation is shown as per the information provided in Table 9-5.

Table 9-5 Example II of a multi-component soil unit and saturated hydraulic conductivity values.

Cokey: 4560	Cokey: 5428	Cokey: 2856
Component %: 40	Component %: 26	Component %: 41
Average saturated hydraulic conductivity (μm/s): 5.78	Average saturated hydraulic conductivity (μm/s): 10.15	Average saturated hydraulic conductivity (μm/s): 32.92

Sample Calculation:

Max. Percolation Rate = (40*5.78/100)+(26*10.15/100)+(41*32.92/100) = 18.45 μm/s

6) Maximum Soil Profile Storage. The maximum soil storage is the storage depth available in voids and soil pores when the soil is dry that can be drained by gravity or evaporation (HEC 2000). The soil profile storage is calculated by multiplying the component percent, average porosity, and the depth from the soil surface to the deepest horizon together for each component and then summing these values to reach a total for each map unit as provided in Table 9-6.

Table 9-6   **Example of a multi-component soil unit with properties for computing maximum storage**

Cokey: 4560	Cokey: 5428	Cokey: 2856
Component %: 40	Component %: 26	Component %: 41
Porosity (%): 30	Porosity (%): 32	Porosity (%): 47
Depth from soil surface (cm): 195	Depth from soil surface (cm): 130	Depth from soil surface (cm): 200

Sample Calculation:

$$\text{Max. Storage} = (\frac{40}{100} * \frac{30}{100} * 195) + (\frac{26}{100} * \frac{32}{100} * 130) + (\frac{41}{100} * \frac{47}{100} * 200) = 72.756 \text{ cm}$$

7) Maximum Tension Zone Storage. The soil moisture tension is defined as the tension with which the water is held in the soil matrix, usually the soil moisture tension refers to 15 atmospheric pressure and the maximum tension zone storage is the storage depth available in the form of water attached to soil particles and this water can only be removed via evaporation, suction, or contact with a dry, porous material (HEC 2000). However, Field capacity is the amount of water left in the soil after the gravitational water has been removed. The tension zone storage is calculated by multiplying the component percent, average field capacity, and the depth from the soil surface to the deepest horizon together for each component and then summing these values to reach a total for each map unit as provided in Table 9-7. We know that in the SMA model, the soil profile is divided by the tension zone and the upper zone. However, SMA does not require a value for the upper zone directly; rather it calculates the storage depth of the upper zone as the maximum soil profile storage minus the maximum tension zone storage (HEC 2000).

Table 9-7 Example of a multi-component soil unit with properties for computing maximum tension storage.

Cokey: 4560	Cokey: 5428	Cokey: 2856
Component %: 40	Component %: 26	Component %: 41
Field capacity (%): 26	Field capacity (%): 12	Field capacity (%): 40
Depth from soil surface (cm): 195	Depth from soil surface (cm): 130	Depth from soil surface (cm): 200

Sample Calculation:

$$\text{Max. Tension Storage} = (\frac{40}{100} * \frac{26}{100} * 195) + (\frac{26}{100} * \frac{12}{100} * 130) + (\frac{41}{100} * \frac{40}{100} * 200)$$

$$= 57.00 \text{ cm}$$

All the calculation above is done for gridded model and later converted to basin average values in order use it in our lump model.

8) Parameters of SCS Unit Hydrograph:

99

Time of Concentration (Tc): We adopted the SCS method for watershed lag that was developed by Mockus in 1961 for estimating the time of concentration and storage coefficient. The following equation B-4 and B-5 represent the lag time,

$$L = \frac{l^{0.8}(S+1)^{0.7}}{1900Y^{0.5}}$$

Applying $L = 0.6T_c$, that yields

$$Tc = \frac{l^{0.8}(S+1)^{0.7}}{1140Y^{0.5}}$$

Where:

L = lag time, h

Tc = Time of concentration, h

l = flow length, ft

Y = Average watershed land slope, %

S = maximum potential retention, in

$$S = \frac{1000}{CN} - 10$$

CN = Curve Number

Flow length: In the watershed lag method of computing time of concentration, flow length is defined as the longest path along which water flows from the watershed divide to the outlet. We measured the Flow length using GIS techniques. Mockus (USDA 1973) developed an empirical relationship between flow length and drainage area using data from Agricultural Research Service (ARS) watersheds.

$$l = 209A^{0.6}$$

where,

l = flow length,ft

A = Drainage area in acres

Sample Calculation: We calculated the land slope using DEM data in GIS and calculated Tc and S as follows:

For TWDB ID 15010:

$A = 148.91 \text{ mile}^2 = 95301.83 \text{ acres}$

$l = 209A^{0.6} = 209*95301.83^{0.6} = 203052 \text{ feet}$

$S = \frac{1000}{93} - 10 = 0.7526 \text{ in}$

$Tc = \frac{l^{0.8}(S+1)^{0.7}}{1140Y^{0.5}} = \frac{203052^{0.8}(0.7526+1)^{0.7}}{1140(1.5)^{0.5}} = 18.69 \text{ hrs}$

Storage Coefficient: We calculated the storage coefficient according to Sabol (1988) because we already have all the values for this equation it is presented in equation B-6.

$$R = \frac{T_c}{1.46 - 0.0867\left(\frac{L^2}{A}\right)}$$

100

$$R = \frac{18.69}{1.46 - 0.0867\left(\frac{203052^2}{95301.83*43560}\right)} = 31.203 \text{ hrs}$$

The following Table 9-8 presents the time of concentration and storage coefficient of all the sub-watersheds within Matagorda Bay watershed

Table 9-8 Features of each bay watershed and SMA parameter values

TWDB ID	Area (mile²)	Area (Ac)	Flow Path ,l (ft)	Aver_slope, Y(%)	CN	Storage, S(In)	Tc(hr)	Storage Coefficent, R(hr)
15010	148.91	95301.83	203052	1.5	93	0.752	18.69	31.206
15020	156.06	99879.78	208849	2	87	1.542	21.48	36.36
15030	93.94	60122.05	154016	1.5	87	1.546	19.46	28.85
15040	107.34	68695.87	166842	1	88	1.405	24.42	37.36
15050	384.40	246016.20	358694	1	87	1.481	46.04	109.86
15060	63.38	40564.57	121628	0.5	88	1.413	26.88	36.62
16001	107.15	68572.91	166662	4	85	1.726	13.32	20.37
16005	709.31	453960.44	518033	4.6	77	3.064	40.69	143.57
16007	331.14	211932.09	327993	4	84	1.968	24.29	54.03
16008	88.49	56633.37	148590	0.5	89	1.218	29.74	43.48
16014	1070.50	685121.91	663143	3.5	78	2.896	55.18	302.45
17010	36.60	23423.45	87486	0.5	89	1.289	19.90	24.58
17020	107.29	68664.76	166796	2	80	2.492	22.41	34.29
17030	273.37	174956.67	292351	2	84	1.836	30.35	62.23
17040	71.14	45531.96	130358	0.5	86	1.593	29.88	41.66
17050	49.73	31828.48	105156	0.5	87	1.516	24.64	32.06
17060	151.49	96955.96	205159	1	87	1.434	29.06	48.76
17070	162.32	103883.04	213832	0.5	90	1.073	37.95	64.99

9. Routing Parameters: In this study we adopted the Muskingum as hydrologic routing method which is a flood routing method that uses a simple conservation of mass approach to route flow through the stream reach and it assumes that the water surface is not level. The Muskingum K is

essentially the travel time through the reach that is estimated from the knowledge of the cross-section properties and flow properties. The Muskingum X is the weighting between inflow and outflow influence.

We estimated the travel time using the Manning's equation as shown in equation B-7,

$$V = \frac{1.49 R^{\frac{2}{3}} S^{\frac{1}{2}}}{n}$$

Where,

V = Average flow velocity in fps that is usually determined for the bankfull elevation.

n = Manning's roughness

S = Average Channel Slope (%)

R = Hydraulic Radius of the channel in feet,

R = A/P, where A is Area in square feet and P is Wetted Parameter in feet

Travel time, K = l/V, l is the Flow length of the channel in feet

Sample Calculation: We assumed the channel as trapezoidal section as shown in Fig 9-5 and calculated width and depth from the DEM data using ArcGIS, a sample calculation is given below:
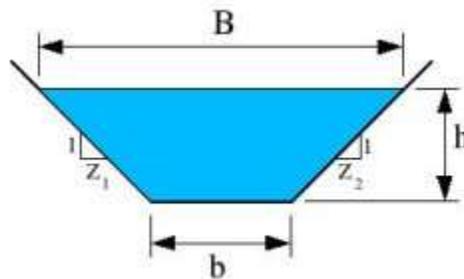

Figure 9-5 **An example of trapezoidal channel cross-section used in HEC-HMS routing calculation.**

We know from continuity equation,

Q = AV, where Q is the flow rate in cfs, A is Area and V is mean velocity, using the bankfull discharge for a storm event we calculated the hydraulic radius, R and used that R in the later calculation to determine V.

Assume, Q = 10000 cfs, A = (b+zh)h = (1000+2*20)20 = 20800 ft^2

n = 0.025, S = 0.0005

V = Q/A = 10000/(20800) = 0.48 fps

R = (V*n /1.49*S$^{0.5}$)$^{3/2}$ = (0.48*0.025/1.49*0.0005$^{0.5}$)$^{1.5}$ = 0.216 ft

Using this R we calculated the velocity from equation B-7 and calculated K as follows:

$$V = \frac{1.49 R^{\frac{2}{3}} S^{\frac{1}{2}}}{n} = \frac{1.49 (0.216)^{\frac{2}{3}} (0.0004)^{\frac{1}{2}}}{0.030} = 0.3577 \text{ ft/s}$$

K = l/V = 20300 / 0.3577 = 56740 seconds = 15 hrs

And we assumed X values as the average of min and max of the range of X value which is 0.25a and later fixed in the calibration experiment.

Estimation of ET Parameters:

In this study we used Penman-Monteith method for the calculation of Evapotranspiration and the inputs for this method are Temperature, Wind Speed at 2-m height, Relative Humidity and Sunshine hours. Moreover, this method needs coordinate of Meridian that passes over the study area. We calculated the basin average temperature, wind speed, relative humidity and sunshine hour using GIS, we made an automatic model using model builder in GIS to create a time series of the basin average data needed for ET module. We used zonal statistics tools available in ArcGIS 10.6 version to calculate basin average inputs from NLDAS gridded data as shown in the Fig. 9-6.
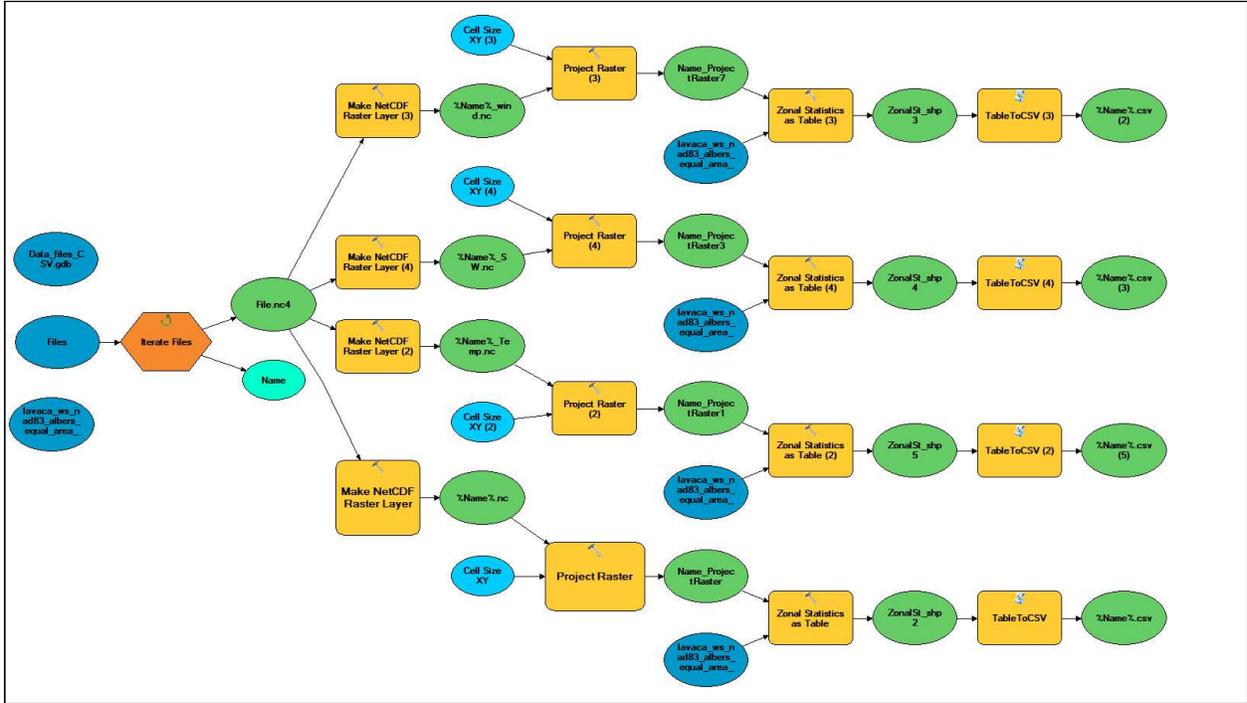
Figure 9-6   **Schematic of Model Builder tool in ArcGIS for computing basin average forcings from NLDAS gridded forcing data set**

After calculating the basin average, we used python code to make time series inputs for the ET Module. After taking inputs for all module, we specified the time window for our model as shown in Fig-B8, then we started calibration-validation experiment

104
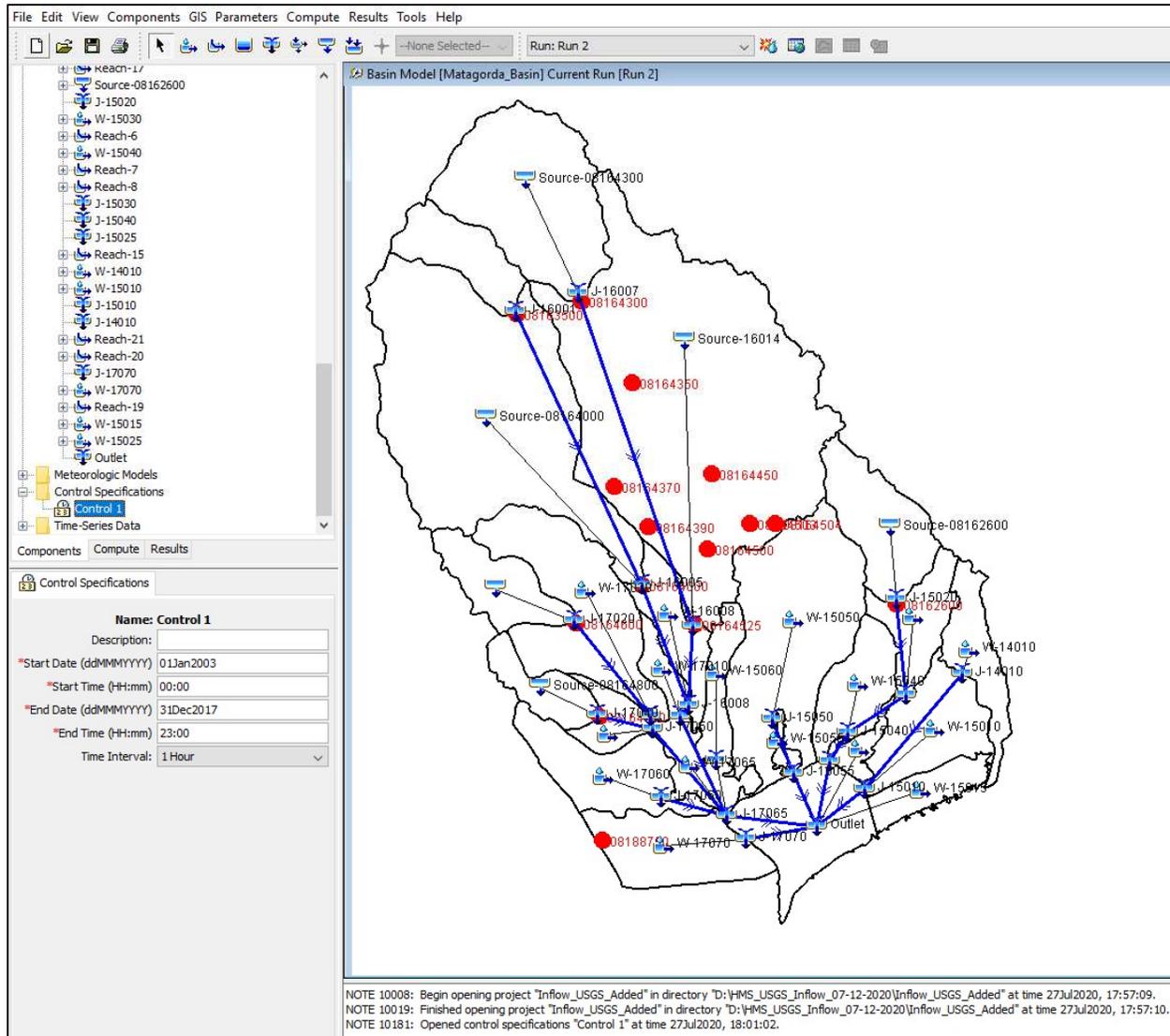
Figure 9-7   Control specification for HEC-HMS model.

Model calibration: Parameter adjustment for watershed 17040 (Outlet 08164800)

After calculating all the parameters, the monthly pan evapotranspiration data is added to meteorological models; precipitation and streamflow data from 2004-2012 are added to the time series data. The calibration session begins with running the model and examining the baseflow output. Initial values of the calibration-determined parameters, GW2 percolation rate, GW1 and GW2 baseflow coefficient and baseflow reservoir count, are set. For each calibration the canopy method, surface method has been fixed. However, the time of concentrations and storage coefficient has been changed a little bit. Mostly the loss parameters such as % impervious, maximum infiltration, soil storage and tension storage have been adjusted to match the observed discharge. These parameters have been found to be the most sensitive for the model calibration. After satisfactory model calibration, the validation process begins. Precipitation and streamflow

105

data from 2012 are added to the time series data. And validation experiments are performed. The final calibration model parameters are presented in the following Table 9-9.

Table 9-9   **SMA parameter values obtained from model calibration**

Model Parameters	Subbasin-15020	Subbasin-16005	Subbasin-16007	Subbasin-17020	Subbasin-17040
Time of Concentration (hr)	5	25	7.92	7.5	6.5
Storage Coefficient (hr)	50	40	25	17	11.5
Max. Canopy Storage (in)	0.02	0.02	0.02	0.02	0.02
Max. Surface Storage (in)	0.2	0.2	0.1	0.2	0.2
% Impervious	0.5	6	1	1	0.5
Max. Infiltration Rate (in/hr)	0.149	0.5	1.5	2.3	2
Soil Storage (in)	5	5	5.4	5.35	6
Tension Zone Storage (in)	4.85	4.8	4.5	4.35	3
Soil Percolation Rate (in/hr)	0.05	0.3	1.33	0.3	1.5
GW 1 Storage (in)	1.5	0.1	1	6.2	5.4
GW 1 Percolation Rate (in/hr)	0.347	0.2	0.1	0.254	0.8
GW 1 Coefficient (hr)	25	5	15.1	35	14
GW 2 Storage (in)	1.5	5	20	3.9	10
GW 2 Percolation Rate (in/hr)	0.00001	0.00005	0.00001	0.0005	0.0005
GW 2 Coefficient (hr)	1000	1500	1000	1500	2500
GW 1 Baseflow Coefficient (hr)	20	8	12	12	15
GW 1 Baseflow Reservoirs	1	1	1	1	1
GW 2 Baseflow Coefficient (hr)	200	20	200	200	20
GW 2 Baseflow Reservoirs	1	1	1	1	1

C. HL-RDHM model configuration and parameter estimation

The archives required for setting up and running HL-RDHM are summarized below.

Archive name	Content
RDHM-codes.tgz	HL-RDHM source code and documentation
RDHM-data.tgz	HL-RDHM configuration files for
	Examples of HL-RDHM output

These tools are best used in a unix/linux environment. The UTA project team performs HL-RDHM simulations on a Dell Workstation with 32GB memory and 15TB storage space. In order to run HL-RDHM in real time. It is recommended that a Linux workstation with at least 32GB memory and 8TB storage be set up to run the model for Matagorda Bay.

Below is a table summarizing the hardware, operating systems and software settings recommended for using the tools. Note all the compiles and utilities listed here can be obtained for free.

Hardware Requirements	Workstation with >32GB memory and >8TB storage
Operating systems	Linux with Kernel 4.x and above
Compilers	Gnu C, C++ and gfortran; or Intel C, C++ and Fortran compilers
Utilities	Gnu tar; shell; Gnu Make
	Python3, R
Libraries	C++ Boost, libz, libm

The HL-RDHM source codes are delivered in the RDHM-codes folder. To decompress the archive, issue the following command in a linux/unix shell.

```
[#####@#### TWDB-deliverables]$ cd RDHM-codes/
[#####@#### RDHM-codes]$ tar zxf hl-rdhm-release-3.5.12.1.tgz
[#####@#### RDHM]$ cd hl-rdhm-release-3.5.12.1/
[#####@#### RDHM]$ ./configure
```

This will generate makefiles that allow you to compile the code
```
[#####@#### RDHM]$ ./make
```

Compiling the code would yield executable "rdhm" under "driver" subfolder, and this executable can be moved to a location (say /usr/local/bin) where it can be easily accessed by all users.

Now decompress the RDHM-data.tgz.

```
[#####@#### TWDB-deliverables]$ tar zxf RDHM-data.tgz
[#####@#### TWDB-deliverables]$ cd RDHM-data
```

Under the folder RDHM-data, there are several folders where input decks, parameters and outputs are stored.

input-cards/: input files for running HL-RDHM
RDHM-domain-wide-routing-params/: routing parameters for all watersheds in the study domain
SAC-priori-ssurgo/: A priori SAC-SMA parameter grids
USGS-15min-observations/: 15-min USGS flow and state observations downloaded from USGS
USGS-hourly-card/: hourly USGS observations in data card format, converted from raw USGS rdb format
rdhm-runs/: outputs.

The input file for generating inflow across bay watersheds is rdhm_all_inlets.card under input-cards/. You may view this input deck using any editor

[#####@#### RDHM-data]$ cd input-cards/
[#####@#### input-cards]$ more rdhm_all_inlets.card

##RDHM input deck using upstream flow replacement

#simulaion time period
time-period = 20030101T00 20171231T23

#simulation time step in the format of HH:MM:SS.XXXX
time-step = 1

#the connectivity file
connectivity = /media/data1/TWDB-deliverables/RDHM-data/input-cards/cellarea_connectivity_12d.con

#HRAP grid/cell/pixel size
pixel-size-hrap = 1.0

#output path

#output-path = /media/data1/TWDB-deliverables/RDHM-data/rdhm-runs/upstream-flow-replacement/MTGA1
output-path = /media/data1/TWDB-deliverables/RDHM-data/rdhm-runs/upstream-flow-replacement/MTGA2

upstream-flow-replacement = EDNT2=/media/data1/TWDB-deliverables/RDHM-data/USGS-hourly-card/08164000.obs
upstream-flow-replacement = LTXT2=/media/data1/TWDB-deliverables/RDHM-data/USGS-hourly-card/08164525.obs
upstream-flow-replacement   = PLPT2=/media/data1/TWDB-deliverables/RDHM-data/USGS-hourly-card/08164800.obs
upstream-flow-replacement = NGCT2=/media/data1/TWDB-deliverables/RDHM-data/USGS-hourly-card/08164600.obs
upstream-flow-replacement = MTPT2=/media/data1/TWDB-deliverables/RDHM-data/USGS-hourly-card/08162600.obs

The descriptions for each of the variable can be found in the HL-RDHM manual (NWS, 2008). Note the upstream replacement is done at the five USGS gauging station locations

To run the model: first confirm that rdhm executable is on your path:

[#####@#### input-cards]$ which rdhm
/usr/local/bin/rdhm

If confirmed (as shown above), type the following after the prompt:

[#####@#### input-cards]$ rdhm rdhm_all_inlets.card

The output hydrographs can be found under "RDHM-data/rdhm-runs/hourly-simulated". These hourly data can be aggregated to daily accumulations through a script "RDHM-data/R-scripts/output_process.R".

To view the HL-RDHM output, first enter the directory "RDHM-data/rdhm-runs/hourly-simulated".

[#####@#### input-cards]$ cd RDHM-data/rdhm-runs/hourly-simulated; ls

08162600/ 08164525/ MTGA1/   MTGA2/ MTGA5/ MTGA8/
08164000/ 08164600/ MTGA10/ MTGA3/ MTGA6/ MTGA9/
08164300/ 08164800/ MTGA11/ MTGA4/ MTGA7/

The simulations for a specific outlet (or bay inlet) are stored underneath the directory named after the USGS ID or the "MG"ID. For example, the simulations for Lavaca River at Edna can be found under 08164000/

[#####@#### input-cards]$ cd 08164000/
[#####@#### input-cards]$ ls

asin.info0*   EDNT2_discharge_outlet.ts* EDNT2_xmrg_local.ts basin_info_after_loop0

The second and third files contain the discharge series and the basin averaged precipitation series. To view the content of the discharge series:

[#####@#### input-cards]$ more EDNT2_discharge_outlet.ts

$ RDHM OUTPUT AT 2020-Feb-15 20:04:28
$ Basin Area is 2130.32KM^2
$ Total Num of Pixels is 148
$ Pixel Size is 1 HRAP
$ Simulation Time Step is 01:00:00
$ NORMALIZE = 0
$ Par/St Name   Initial Value   Scaling Factor   grid(Y - from deck; N
- from grid)
$ sac_UZTWM   45.85   -0.8   Y
$ sac_UZFWM   19.49   -0.6   Y

109

$ sac_UZK	0.591	-1.2	Y
$ sac_PCTIM	0.01	0.01	Y
$ sac_ADIMP	0.1	0.1	Y
$ sac_RIVA	0.04	0.04	Y
$ sac_ZPERC	135.4	-0.8	Y
$ sac_REXP	2.235	-1	N
$ sac_LZTWM	287.2	-0.8	Y
$ sac_LZFSM	44.39	-1	N
$ sac_LZFPM	124.4	-1	N
$ sac_LZSK	0.1876	-1	N
$ sac_LZPK	0.03129	-1	N
$ sac_PFREE	0.2838	-1	N
$ sac_SIDE	0.1	0.1	Y
$ sac_RSERV	33.76	0.2	Y
$ sac_EFC	0	0	Y
$ pe_JAN	1.477	-1	N
$ pe_FEB	1.969	-1	N
$ pe_MAR	2.801	-1	N
$ pe_APR	3.91	-1	N
$ pe_MAY	4.938	-1	N
$ pe_JUN	5.611	-1	N
$ pe_JUL	5.744	-1	N
$ pe_AUG	5.295	-1	N
$ pe_SEP	4.398	-1	N
$ pe_OCT	3.287	-1	N
$ pe_NOV	2.262	-1	N
$ pe_DEC	1.6	-1	N
$ peadj_JAN	0.5997	-1	N
$ peadj_FEB	0.7135	-1	N

The header contains the information about the watershed, and basin-averaged parameter values used in the simulation. The discharge data look like the follows:

```
RDHM OUTPUTS  SQIN L3/T CMS  1    EDNT2
01  2003 12  2017 1   F13.4
EDNT2    010103  1      1.3770
EDNT2    010103  2      1.6785
EDNT2    010103  3      1.9350
EDNT2    010103  4      2.1610
EDNT2    010103  5      2.3969
EDNT2    010103  6      2.6818
EDNT2    010103  7      3.0419
EDNT2    010103  8      3.4889
EDNT2    010103  9      4.0233
EDNT2    010103  10      4.6395
EDNT2    010103  11      5.3308
```

EDNT2   010103 12   6.0918

where the second, third and fourth columns contain the date (DDMMYY), hour (1-24; 24 being 0z for the next day), and discharge in cms.

This remainder of this appendix offers a brief description of steps for establishing the connectivity and parameterization for the model. Note that the detailed steps can be found in an accompanying document and the HL-RDHM manual.

Deriving connectivity grid and hillslope slope parameter S_h
To perform hillslope routing in HL-RDHM it is necessary to derive accurate information about flow direction and the hillslope routing parameter, hillslope slope S_h at coarse resolution (e.g. full HRAP) based on DEM data of the study area of interest at fine resolution (e.g. 30 m). Flow direction data is used to derive cell-to-cell connectivity file. The connectivity for the delivered HL-RDHM implementation is

In the current study, we followed the procedure described by Seo et al. (2015) (shared as a supplement under RDHM-DATA). This routine is a customized version of NWS-OHD (Reed 2003) module to run for each of 18 CONUS sub-regions based on NHD-Plus Version2 data set (https://nhdplus.com/NHDPlus/index.php) shown in Fig. D-1. To derive cell-to-cell connectivity and hillslope slope parameter S_h the following inputs to the module are required 1) The elevation data file NHDPlusV21_TX_12_12d_NEDSnapshot_01.7z and 2) The flow direction and accumulation data file NHDPlusV21_TX_12_12d_FdrFac_01.7z both at ~30m resolution and downloadable at https://nhdplus.com/NHDPlus/NHDPlusV2_12.php. Required softwares to run the codes/scripts include 1) Windows 64-bit 2) Cygwin (http://www.cygwin.com/install.html) 3) ArcGIS license for spatial analyst extension and 4) Linux for running the scripts. The codes/shell scripts and derived cell-to-cell connectivity and hillslope slope files for the entire (12d) region are provided by the UTA.
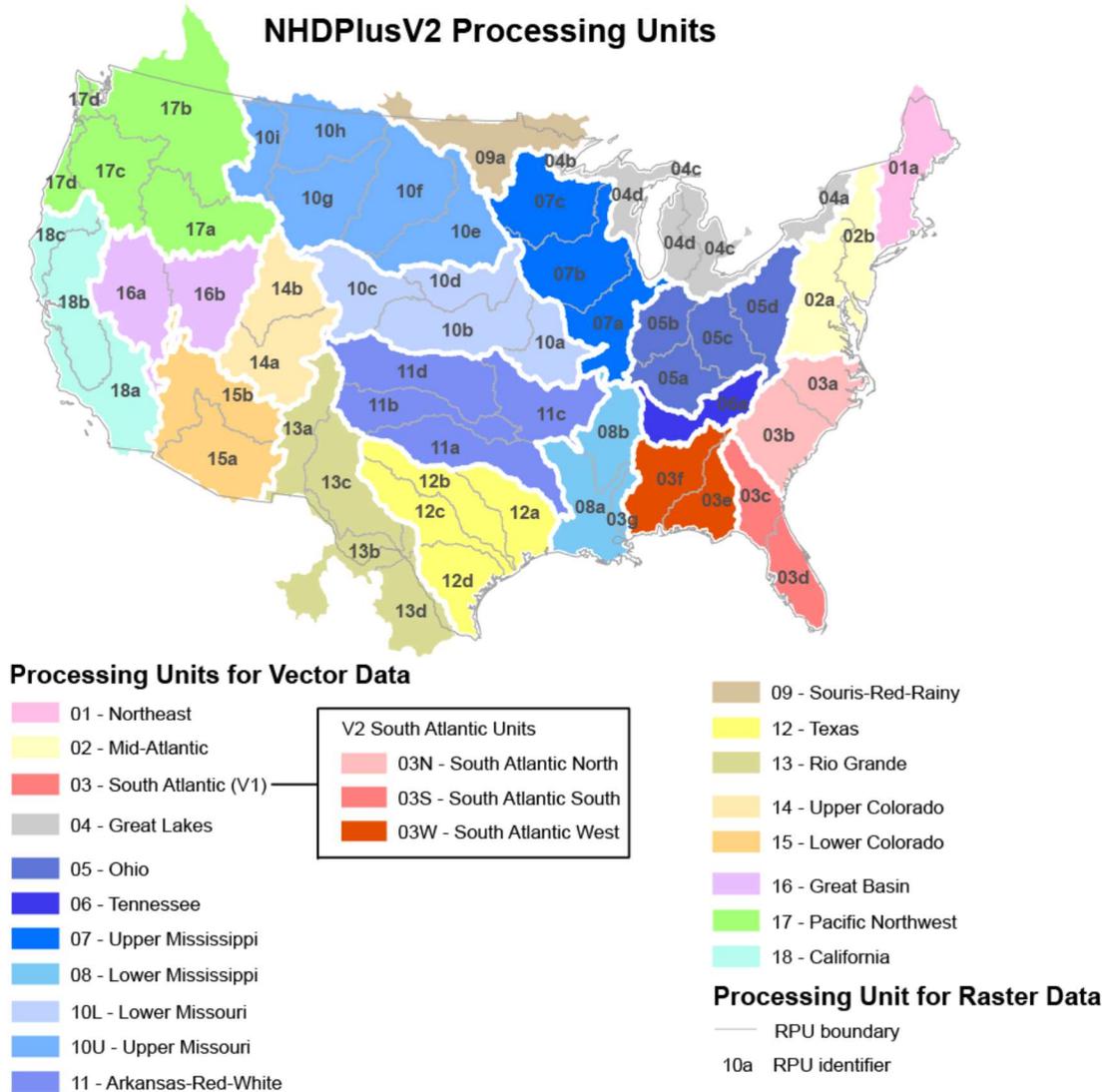
Figure 9-8   NHD-Plus V2 Processing Units (Source: https://nhdplus.com/NHDPlus/)

Adjusting the connectivity file

To convert rainfall-runoff depths to streamflow, HL-RDHM estimates the sum of overall areas of upstream cells based on the connectivity file. However, this area may differ from the actual upstream area of a USGS gauging station where verifying streamflow observations are available. The differences can be attributed to the coarse resolution of HRAP coordinate system leading to miscalculation in basin boundaries. To overcome this problem, we use a module named "cellarea". The "cellarea" is run with the help of a control file which specifies the basin name and the USGS area in sq. km and outputs a new connectivity file with adjusted cell areas. See the HL-RDHM user manual (NWS 2008) for further details.

Deriving and generating customized hillslope routing parameters

To derive discharge per unit area of hillslope q_{LH} in eq. 4-2, HL-RDHM requires input grid parameters: stream channel density (D) and hillslope roughness coefficient (n_h). In this work the default values $D = 2.5\ km^{-1}$ and n_h=0.15 were considered. To generate routing parameters for upstream cells of a given forecast point or USGS gauging station, we use a utility named "genpar". The "genpar" utility is run for each basin of interest and generates the specified parameters for its upstream determined by the connectivity file (NWS 2008).

Deriving and generating customized channel routing parameters

To derive channel routing parameters, we rely on rating curve method (rutpix9 in HL-RDHM) in which the channel discharge for each cell Q_c, is a power function of wetted cross section area A as follows: $Q_c = q_0 A^{q_m}$ (eq. 4-4) where q_0 is discharge per unit channel cross section area and q_m denotes the exponent in the formula. Channel routing parameters q_0, q_m are estimated using power law regression analysis based on observed USGS gaging stations measurements and extrapolated to the upstream cells using the "genpar" utility. Whereas q_m is kept constant, q_0 is adjusted for each upstream cell to reflect changes in cross-section area along a channel. (see, Koren et al. 2004; NWS 2008). For ungauged basins, and for the forecast points located along the major rivers where the USGS gauging station existed, we used the parameters estimated for the immediate upstream USGS gauging station. For ungauged points located elsewhere (not along the major rivers) the routing parameters calculated for the nearest USGS gauge were used.

HL-RDHM model calibration

To calibrate HL-RDHM against verifying USGS observations we adopted both automatic and manual calibration methods. In both techniques, a multiplication factor to previously determined a priori SAC-SMA parameter(s) was applied to minimize the simulation error. The automatic calibration is based on stepwise line search technique and a multi-scale objective function to optimize multiplication factors (SLS, see Kuzmin et al. 2008 for further details) in multiple time steps. To perform automatic calibration, USGS 1-hourly streamflow timeseries are downloaded and processed to be ingestible by the HL-RDHM input deck. In this work we used 240h and 720h time scale and adjusted the three SAC parameters UZTWM, UZFWM and UZK. These parameters were further calibrated manually, in particular for large basins where automatic calibration yielded unreliable simulated hydrographs. For ungauged forecast points, calibrated SAC parameters of upstream USGS gauging station or the nearest calibrated parameters were adopted if the forecasts point was not located along the major river.

Replacing simulated flow by USGS observations

In order for HL-RDHM to mimic TxRR operation, the simulated flow at upstream USGS station locations is replaced by the observations to reduce errors associated with the former. To perform flow replacement analysis, USGS 1-hourly streamflow timeseries are downloaded and converted into the NWS Datacard format. Here is an example of the latter format:

```
ORMS OUTPUTS  QIN  L3/T CMS  1    LTXT2
 1 2003 12  2017  1   F13.2
LTXT2    010103  1      43.84
LTXT2    010103  2      43.84
LTXT2    010103  3      43.84
LTXT2    010103  4      43.84
```

```
LTXT2   010103  5      43.84
LTXT2   010103  6      43.84
LTXT2   010103  7      94.10
LTXT2   010103  8      94.10
LTXT2   010103  9      94.10
LTXT2   010103  10     94.10
```

Note the flow rate is converted to cubic meters per second (CMS) to be consistent with HL-RDHM setup.

The flow replacement is done in the input deck in the following manner:

upstream-flow-replacement = EDNT2=/media/data1/TWDB-deliverables/RDHM-data/USGS-hourly-card/08164000.obs
upstream-flow-replacement = LTXT2=/media/data1/TWDB-deliverables/RDHM-data/USGS-hourly-card/08164525.obs
…

where "EDNT2" and "LTXT2" are the SHEF code for outlets where the replacement is done, and the ".obs" files are the USGS observations that are used to replace the simulations at these oulets. For USGS station 08164525 (Lk Texana nr Edna, TX), only daily release data were available, and this daily data is disaggregated to hourly increments by assuming that release is constant for each day (defined in zulu time). The script for converting the USGS rdb formatted streamflow to HL-RDHM compatible format is RDHM-data/R-scripts/rdb2card.revised.R, and the script for performing the temporal disaggregation is RDHM-data/R-scripts/texana.release.process.R.

D. Retrieving and processing NWM streamflow reanalysis

The archive with information on setting up and retrieving NWM streamflow reanalysis is provided in NWM.tgz.

Archive name	Content
NWM.tgz	Files for extracting streamflow for selected segments from NWM reanalysis (or real-time analysis); example outputs; and bias table

Below is a table summarizing the hardware, operating systems and software settings recommended for using the tools. Note one can also set up and run the python and R scripts in a Windows environment. But since the project team uses Linux only, only the procedures tested in a Linux platform are described here.

Hardware requirement	Workstation with >16GB memory and >8TB storage
Operating systems	Linux with Kernel 4.x and above
Compilers	Gnu C, C++ and gfortran; or Intel C, C++ and Fortran compilers
Utilities	Gnu tar; shell; Gnu Make, Amazon Web Service (aws)
	Python3, R
Libraries	Netcdf,

For this project we download the NWM 1.2 reanalysis hosted at amazon cloud server, though it should be noted the real-time analysis should be downloaded from a different site (ftp://ftp.ncep.noaa.gov/pub/data/nccf/com/nwm/prod). The tools developed for decoding the channel routing data from reanalysis can be applied to the real-time analysis without modification.

First, un-archive the archive NWM.tgz through the following command:

[#####@#### TWDB-deliverables]$ tar zxvf NWM.tgz

This will create directory "NWM". Now enter this directory

[#####@#### TWDB-deliverables]$ cd NWM
[#####@#### NWM]$ ls
201701011400.CHRTOUT_DOMAIN1.comp NWM-08164300_Full.csv*
Bias_Corrected-plots.docx*   NWM-08164600_Full.csv*
BiasCorrection-NWM.xlsx*   NWM-08164800_Full.csv*
extr.ncdf.R*   NWM_7843187_TWDB_16008.csv*
Flowlines_Matagorda.csv*   NWM_Bias_Corrected-Inflow.xlsx*
Inflow_NWM_Map.jpg*   RDHM_Inflows_Time_zone_corrected.csv*
NWM-08162600_Full.csv*   Tables/
NWM-08164000_Full.csv*

Among these files, "201701011400.CHRTOUT_DOMAIN1.comp" is the example channel

routing data. "Flowlines_Matagorda.csv" contains the segment IDs for all stream segments for Matagorda Bay watersheds. "extr.ncdf.R" is a R script that extracts the streamflow analysis for only the segments present in Flowlines_Matagorda.csv.

The method through which channel routing data are downloaded is briefly described here. In order to download the reanalysis data, one needs to first install aws. In a Linux shell, type

[#####@#### NWM]$ which aws
/usr/bin/aws

If aws is not installed, please refer to https://docs.aws.amazon.com/cli/latest/userguide/install-cliv2-linux.html on how to install aws utilities.

Once aws is installed, one should first read the documentation about NWM reanalysis at https://docs.opendata.aws/nwm-archive/readme.html before downloading the data. NWM produces four types of output files, namely RTOUT (surface routing), LAKEOUT (reservoir routing), CHRTOUT (channel routing), and LDASOUT (land surface variables). Among these files, streamflow data (discharge) is stored in channel "CHRTOUT". An example "201701011400.CHRTOUT_DOMAIN1.comp" is included in the deliverable (under NWM). This file contains the model outputs for Jan. 11, 1400z on 2017. The naming convention of the file format is identical for the reanalysis and real-time analysis. Downloading can be done through command line. Here is an example for downloading all CHRTOUT for the year of 2007:

```
aws s3 sync s3://nwm-archive/2007 ../2007 --no-sign-request --endpoint-url https://griffin-objstore.opensciencedatacloud.org
--no-verify-ssl --exclude "*" --include "2007*CHRTOUT*"
```

Or, if you know the specific date/time of interest, you may use the following command:

[#####@#### NWM]$ aws s3 cp s3://nwm-archive/2007/201701011400.CHRTOUT_DOMAIN1.comp --no-sign-request ./

A script can be developed to loop through the years of interest. The CHRTOUT files are in netcdf format, and each stores information including the streamflow (variable "streamflow") at each stream segment in the CONUS referenced by "feature_id" (ID of the segment), the lateral inflow through surface and subsurface contributions, and other variables. You may check the content of the files using the ncdump utility, which is part of Netcdf package. Let us look at one example.

To extract the streamflow for only those segments that drain Matagorda Bay, the team used ArcGIS to subset the NHD-Plus flowlines and saved in to "Flowlines_Matagorda.csv". Here is a segment of this file:

```
COMID,AvgAnnualQ
3763772,0
3763992,0
3764008,0
3765368,0
```

3765372,0

The first column stores the ID of the reach, and its heading "COMID" corresponds directly to the "feature_id" in the CHRTOUT file.

Now, let us view the script "extr.ncdf.R" that will be used to extract the streamflow from each CHRTOUT files into ascii table.

[#####@#### NWM]$ more archive/2007/201701011400.CHRTOUT_DOMAIN1.comp --no-sign-request ./

```
#----------------------------------------------
#R script for readhing netcdf format
#dishcarge/inflow reanalysis for each NHD+ reach
#Author: Yu Zhang (yu.zhang@uta.edu)
#----------------------------------------------

library(ncdf4)
file.cmid<-"Flowlines_Matagorda.csv"
data.cmid<-read.csv(file.cmid)

dir.out<-"Tables"

file.lst<-"201701011400.CHRTOUT_DOMAIN1.comp"

…
```

This script relies on "Flowlines_Matagorda.csv" to subset the segments for Matagorda Bay, and it processes only one file, i.e., "201701011400.CHRTOUT_DOMAIN1.comp" in the current directory. If needed, the "file.lst" variable can be expanded to include a list of files to be processed.

To run this script, make sure that ncdf4 library is installed in R. Once it is installed, issue the following command:

[#####@#### NWM]$ R -f extr.ncdf.R

 An example output "201701011400.csv" can be found under NWM/Tables:

[#####@#### NWM]$ more Tables/201701011400.csv

```
"","COMID","q.st","q.lat","q.ter"
"1",3765378,0,0,0
"2",3765402,0,0,0
"3",3766376,227.349994918332,0,0
```

117

```
"4",7840417,0,0,0
"5",7840419,0,0,0
"6",7840421,0,0,0
"7",7840423,0,0,0
"8",7840425,0,0,0
```

The second column is the streamflow (with heading of "q.st"). The output files for each hour can be combined to yield flow time series for all links of interest. In this project, streamflow was retrieved for the links with IDs listed in Table 4-11 with available reanalysis data (3nd column).